



Lawrence Berkeley Laboratory

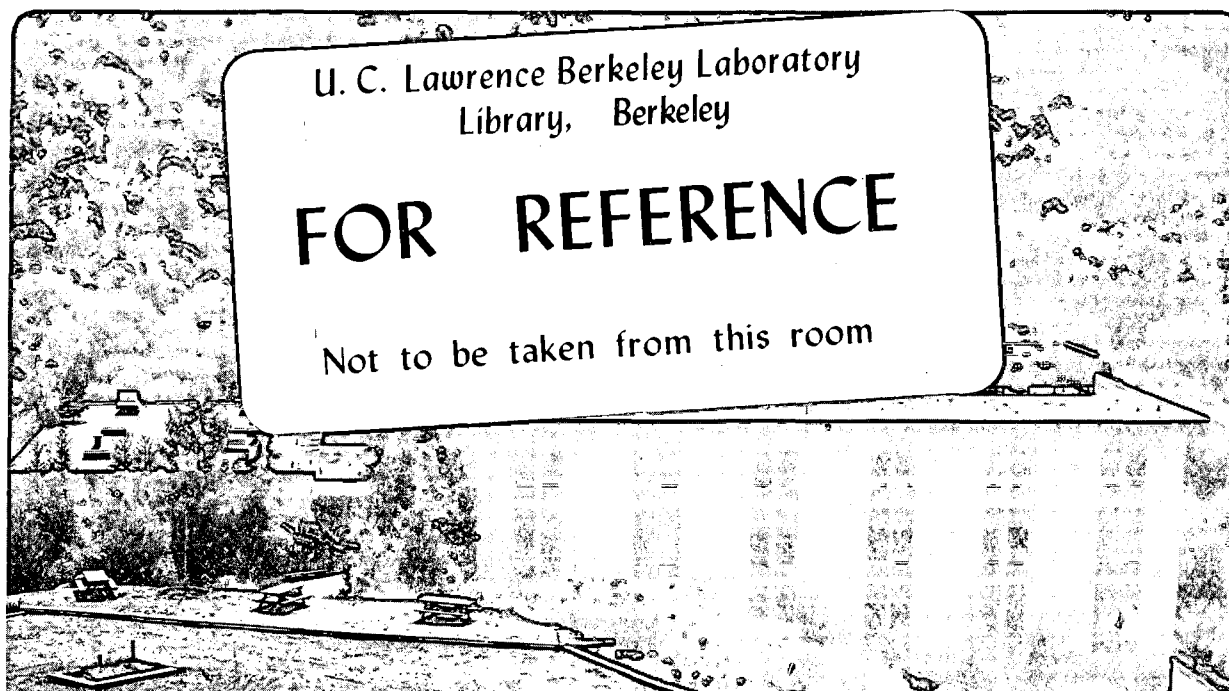
UNIVERSITY OF CALIFORNIA

Materials Sciences Division

AC Microcalorimetry of Adsorbates on Evaporated Metal Films: Orientational Ordering of H₂ Multilayers

R.B. Phelps
(Ph.D. Thesis)

November 1991



U. C. Lawrence Berkeley Laboratory
Library, Berkeley

FOR REFERENCE

Not to be taken from this room

Bldg. 50 Library.
Copy 1

LBL-31576

DISCLAIMER

This document was prepared as an account of work sponsored by the United States Government. While this document is believed to contain correct information, neither the United States Government nor any agency thereof, nor the Regents of the University of California, nor any of their employees, makes any warranty, express or implied, or assumes any legal responsibility for the accuracy, completeness, or usefulness of any information, apparatus, product, or process disclosed, or represents that its use would not infringe privately owned rights. Reference herein to any specific commercial product, process, or service by its trade name, trademark, manufacturer, or otherwise, does not necessarily constitute or imply its endorsement, recommendation, or favoring by the United States Government or any agency thereof, or the Regents of the University of California. The views and opinions of authors expressed herein do not necessarily state or reflect those of the United States Government or any agency thereof or the Regents of the University of California.

**AC Microcalorimetry of Adsorbates on Evaporated Metal Films:
Orientational Ordering of H₂ Multilayers**

R. B. Phelps
Ph.D. Thesis

Physics Department
University of California

and

Materials Sciences Division
Lawrence Berkeley Laboratory
University of California
Berkeley, CA 94720

November 1991

This report has been reproduced directly from the best available copy.

This work was supported in part by the Director, Office of Energy Research,
Office of Basic Energy Sciences, Materials Sciences Division, of the U. S.
Department of Energy under Contract No. DE-AC03-76SF00098.

**AC Microcalorimetry of Adsorbates on Evaporated Metal Films:
Orientational Ordering of Hydrogen Multilayers**

Copyright © 1991

by

Robert Bloss Phelps

The U.S. Department of Energy has the right to use this thesis
for any purpose whatsoever including the right to reproduce
all or any part thereof

AC Microcalorimetry of Adsorbates on Evaporated Metal Films: Orientational Ordering of Hydrogen Multilayers

by
Robert Bloss Phelps

Abstract

We have improved and extended a novel ac calorimetric technique for measuring the heat capacity of adsorbates on evaporated metal films. Metallic substrates are of particular interest in current studies of the thermodynamics of adsorbed molecules. The method described in the present work is the only calorimetric technique which allows measurements of molecules on simple metallic surfaces. Among other improvements, we have achieved significant progress in the preparation and characterization of the evaporated metal film.

We have applied this novel technique to a study of hydrogen multilayers on gold and sapphire substrates. We have shown that samples of normal-hydrogen with a nominal coverage n of approximately 25 monolayers (ML) undergo a bulk-like orientational ordering transition. The transition is suppressed as the coverage is decreased, and no sign of the transition remains above 1.6 K for $n \approx 1$ ML. For $n \lesssim 8$ ML, the peak in the heat capacity exhibits signs of finite-size effects. At higher coverages, finite-size effects are not observed, and the shape of the peak depends strongly on the substrate. We conclude that the peak is inhomogeneously broadened for $n \gtrsim 8$ ML. This work represents the first measurements of the heat capacity due to orientational ordering in adsorbed hydrogen.

The results of an earlier experiment involving vibrational spectroscopy of adsorbed molecules are included in the Appendix. In this work, we have used infrared emission spectroscopy to study the spectral region in the vicinity of the C=O stretch vibration of bridge-bonded CO on Pt(111). Our results, which have been confirmed by subsequent measurements, show a single line only at 1849 cm^{-1} . These results are in qualitative disagreement with those from an earlier study by Hayden and Bradshaw, who observed two lines in this region. The results of the present work strongly suggest that the double line observed by Hayden and Bradshaw was due to residual defects in their substrate.

To my parents, Warren Phelps, Sr. and Patricia Phelps

1. Introduction and Survey.....	1
1.1 Introduction.....	1
1.2 Conventional Methods for Measuring Heat Capacity of Adsorbates	1
1.3 Monolayers Adsorbed on Graphite.....	5
1.4 Multilayers	10
1.5 Metallic Substrates--Motivation for Present Work.....	12
References.....	18
2. Apparatus and Procedures.....	21
2.1 Introduction.....	21
2.2 Calorimeter	21
2.3 UHV System and Cryostat	30
2.4 Measurement Electronics.....	36
2.5 Constraints of the Method.....	38
References.....	40
3. Results for H ₂ Multilayers	41
3.1 Introduction.....	41
3.2 Previous Work.....	41
3.3 Results.....	44
3.4 Discussion.....	52
3.5 Conclusions.....	61
References.....	62
4. Preparation and Characterization of Evaporated Metal Films	64
4.1 Introduction.....	64
4.2 Structure	64
4.3 Cleanliness	70
References.....	78
5. Future Work.....	79
5.1 Introduction.....	79
5.2 Further Measurements Using the Existing Apparatus.....	79
5.3 Extension to Lower Temperatures.....	84
5.4 Monolithic Si Calorimeters.....	87
References.....	91
6. Conclusions.....	93
Appendix	
Infrared Emission Spectroscopy of CO on Pt(111).....	94

Abstract.....	94
A.1 Introduction.....	94
A.2 Experimental	97
A.3 Results and Discussion.....	97
A.4 Summary.....	107
References.....	109

Acknowledgements

The people who have contributed to this work, directly or indirectly, are many. It is a pleasure to acknowledge them here. I feel grateful that I have been able to benefit from the wisdom, experience, friendship and love of so many people. To each of them, I extend my heartfelt thanks.

First and foremost, I would like to thank my thesis advisor, Professor Paul Richards. His patience and persistence outlasted the difficulties and delays. His talent for pulling useful gadgets out of obscure drawers in the laboratory provided an escape from many a tight spot. Finally, his buoyant optimism transformed my occasional mood of despair into one of ordinary gloom.

My predecessors, Dr. Roger Tobin and Dr. Thomas Kenny, were responsible for my day-to-day training. Roger served as my UHV yoda. His ability to pierce confusion with logic and impose order through organization set an excellent example for me. The work in the Appendix was directed by him and reflects the distinctive clarity of his approach. Tom took over where Roger left off, introducing me to his apparatus for measuring the heat capacity of adsorbates. I've never known anyone quite as cheerful or good-natured as Tom. Glasses which looked half empty to me seemed, well, at least three-quarters full to him. When he left town, he bequeathed to me not only his experiment, but also his luxurious apartment and his tropical fish. Fortunately for both of us, he took with him his taste for bad movies and monster trucks.

My other labmates kept me company and helped me keep my perspective after Roger and Tom had left. Dr. Carl Mears deserves credit for pushing me to push myself, in the lab, up Mt. Shasta, and under the hood of my '84 Rabbit. Mike Nahum kept my excess food supplies from going to waste and showed me how to act tough in weight rooms. Simon Verghese (who is undoubtedly the Dale Carnegie of the 90's) saved me numerous hours and headaches by showing me how to use Kermit. John Birmingham infused the heat capacity project with his twin gifts, Vigor of Youth and Wryness of Wit. Through their exhortation and (less frequently) their example, André Clapp and David Miller reminded me to remain Calm in the face of Great Difficulties. I'd also like to thank Warren Holmes, Dr. Chris Hagmann, and Dominick Benford for their support.

I would like to thank the staff of the low temperature laboratory for producing the para-hydrogen used in the work of Chapter 3, and Jim Ames for performing the Raman spectroscopy. I am also grateful to the staff of the mechanical and electronics shops in the Physics Department, especially Al Daft, Brian Nunn, and Andy Brocato.

My housemates from the Ward Street house, where I lived for four years, deserve thanks for countless pep talks. Ruth Ellen Thomson deserves special credit for her recruitment efforts, which played a major role in my decision to come to Berkeley. She was always willing to listen to my problems before helping me to see that they weren't *really* problems. Like Carl and another housemate, Mats Gustafsson, she served on my Rabbit is Sick Advisory Panel. All three also made great company on many outdoor adventures and bike rides.

My current and former housemates on Orchard Lane, Mary Greene, Dr. Tom Pollard, Maria Laso, Dr. Reinhard Hehl and Janie Lee, helped me make it through the home stretch. Thanks go to them for walks, talks, and dinners without equal.

The members of the UC Ballroom Dance group gave me a gift I'll always treasure: the joy of dancing. I would especially like to thank Karin Ericsson and Genevieve Fong, my companions in many West Coast Swing lessons. I would also like to thank the members of the 9:00 choir and the Young Catholics group and Newman Hall for their support and friendship. Thanks also to Sharon Anderson for her gifts of wisdom and grace.

For making graduation seem more attractive than ever before, and for her steady and sure support, I thank my fiancée, Marie Clark. Lastly, I would like to thank my parents and family. Their encouragement and sense of humor have seen me through from beginning to end. (Finally!) The lessons I have learned from them are the ones I will remember the longest.

I am grateful to the National Science Foundation, which provided me with a Fellowship during my first three years of graduate school.

This work was supported by the Director, Office of Energy Research, Office of Basic Energy Sciences, Materials Sciences Division of the U. S. Department of Energy under Contract No. DE-AC03-76SF00098.

1. Introduction and Survey

1.1 Introduction

Interest in the thermodynamics of physisorbed molecules has greatly expanded in recent years. The growth of the field has been stimulated by significant improvements in experimental techniques, and by wide-spread interest in the properties of two-dimensional (2D) systems. Physisorbed monolayers represent an important testing ground for recent theories of ordering in 2D systems, while multilayers provide opportunities for exploring the transition from 2D to 3D behavior. Finally, studies of physisorbed systems complement those on chemisorbed systems. The relatively simple van der Waals bonding in the former is somewhat easier to model theoretically, while an understanding of the stronger, chemical bonds of the latter forms the foundation of applied fields such as catalysis.

To present the motivation for the present work, we will begin with a survey of previous measurements of the heat capacity of physisorbed systems. The aim of the survey will be to introduce the reader to the traditional techniques for making such measurements and to highlight important issues in the field through the use of selected examples, rather than to provide a comprehensive review. Following an introduction to the conventional experimental methods, we will discuss previous measurements of monolayers and multilayers adsorbed on graphite, the substrate for which the greatest amount of data is available. Next, we will discuss the need for alternative substrates. We will demonstrate that the present ac calorimetric technique, which allows surface heat capacity measurements on evaporated metal films for the first time, provides a means for separating out of the large body of past results those which are specific to a particular substrate from those which have a more universal character. Finally, to illustrate the power of the new technique, we will discuss measurements of the heat capacity of $^4\text{He}/\text{Ag}$.

1.2 Conventional Methods for Measuring Heat Capacity of Adsorbates

The great majority of all measurements on physisorbed systems have been performed on exfoliated graphite. The primary reason for the popularity of graphite is its outstanding homogeneity.¹ An ideal (i.e., perfectly homogeneous) substrate would have only one type of site to which adsorbates

could bind. On real substrates, some fraction of the total number of sites will have special characteristics because of their proximity to various defects: edges of crystallites, steps, vacancies, chemical impurities, etc. Often, the binding energy of such sites will be higher than at other locations on the surface. Heterogeneity is expected, therefore, to be particularly problematic at low coverages when adsorption at special sites may dominate the system. Yet, it often has a profound impact at higher coverages as well; sharp phase transitions are broadened when defects interfere with the interactions of neighboring adsorbates, thereby breaking the adsorbed layer into a patchwork of smaller, locally coherent regions.² It has even been suggested that the growth of multilayers is influenced by heterogeneity of the substrate.³

The figure of merit used to characterize the homogeneity of the substrate is the average, linear dimension of the domains within which adsorption is observed to be uniform. Domains can be determined by steps as small as a single atom in height. Hence, they tend to be smaller than the size of a typical crystallite. Thermodynamic measurements, especially adsorption isotherms,⁴ are frequently used as qualitative, yet sensitive gauges of substrate homogeneity.⁵ Early measurements demonstrated that a commercially available, recompressed form of exfoliated graphite known as Grafoil possessed homogeneity which was clearly superior to that of several other types of substrates which had been investigated. It was later discovered that exfoliated graphite which was carefully prepared and not recompressed had domains which were larger than those of Grafoil by an order of magnitude or more. Direct measurements of domain size are made by means of x-ray or neutron diffraction from an adsorbed monolayer. Typical values for various types of exfoliated graphite range from 150 Å for Grafoil to 2000 Å for ZYX graphite.⁶ The availability of products with such superior homogeneity gave rise to the current position of graphite as the standard substrate for measurements of physisorbed systems. Phase diagrams for many adsorbates on graphite, including all the noble gases, have been mapped in great detail. Interesting new phases and phase transitions have been discovered, some of which will be discussed in the following section. The first observation of an ideal 2D classical gas (with a temperature-independent specific heat $C/Nk_B = 1$) was in the system He/graphite. The observation of this phase was attributed to the homogeneity of the physisorption potential of this system.⁷

Despite the many successes achieved with graphite, considerable effort has been directed toward the development of alternative substrates. The motivation for this effort is based on the observation that the strength and unusually large corrugation of the adsorption potential on graphite have a significant (and sometimes dominant) effect on the properties of the adsorbed system. The term corrugation refers to the periodic variation of the physisorption potential as a function of lateral displacement along the surface. (It is the corrugation which gives rise to commensurate or registered phases.) We will return to these issues in sections 1.3 and 1.5.

Before discussing the heat capacity results which have been obtained with graphite substrates, we present a brief outline of the typical experimental procedures used for these measurements.⁷ Fig. 1.1 shows a schematic diagram of the experimental apparatus. Grafoil sheets are first baked in vacuum at temperatures near 750°C for several hours and purged with pure helium gas to remove impurities. Disks cut from these sheets are coated with a thin Cu film and stacked in a Cu container separated by fine Cu powder. The total surface area of the graphite is ~200 m². The cell is then heated to ~1000°C in vacuum to sinter the disks to each other and to the wall of the container. This procedure is necessary to compensate for graphite's poor thermal conductivity. The container is sealed, fitted with a filling line, and mounted above a cryostat. The filling line leads to a gas handling system equipped with calibrated volumes and a capacitance manometer for measuring the pressure of the vapor above the adsorbed film.

The heat capacity of the empty cell is measured by adding a known amount of heat in a single pulse and measuring the increase in the temperature. Gas is then added incrementally, and the cell is left to equilibrate overnight. After re-measurement and subtraction, the heat capacity of the adsorbate is obtained. Coverages can be calculated from a knowledge of the volume of gas admitted to the cell and the value of the residual pressure of the vapor after adsorption is completed. Adsorption isotherms are performed by measuring the quantity of gas adsorbed as a function of the 3D vapor pressure. The pressure is measured at room temperature after the cell has reached internal thermal equilibrium. For further details of the procedure, we refer the reader to Ref. 7.

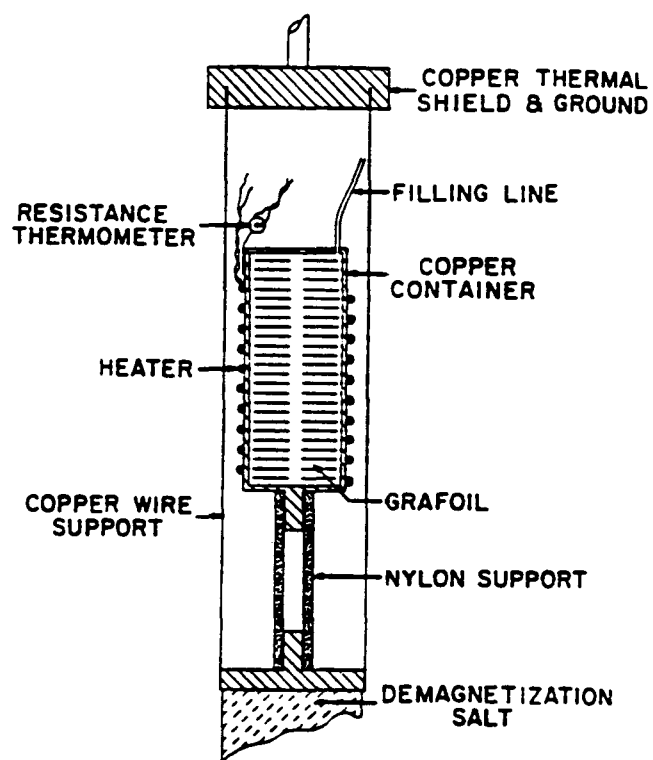


Figure 1.1 Schematic diagram of a typical cell used in adiabatic measurements of the heat capacity of adsorbed molecules. (From Bretz *et al.*⁷)

1.3 Monolayers Adsorbed on Graphite

In this section we discuss phenomena of particular interest in the monolayer and submonolayer regimes, using previous data for noble gases adsorbed on graphite to clarify the central concepts. We begin with the phase diagram for $^4\text{He}/\text{graphite}$ shown in Fig. 1.2a and the contour plot of specific heat measurements for the same system shown in Fig. 1.2b.⁸⁻¹⁰ Similar phase diagrams are observed for the other adsorbates for which quantum mechanical zero-point energy is important (H_2 , D_2 , etc.). The broad plateau in Fig. 1.2b for which $C/Nk_B \approx 1$ corresponds to the nearly ideal 2D gas mentioned in the previous section. For coverages between 0.025 and 0.048 \AA^{-2} and temperatures above 2 K, the upward deviations of the data from the ideal gas result agree with predictions of a theory based on quantum virial coefficient effects.¹¹ The agreement between theory and experiment breaks down at lower temperatures. Near 1.5 K, the theory predicts a divergence in the specific heat, but the ^4He data exhibit rounded peaks. The peaks are due to condensation of the gas into a commensurate phase which coexists with the gas at low temperature.¹² The data for ^3He , which are otherwise similar to those of ^4He above 1 K, exhibit different behavior in this coverage range. The quantum virial coefficient corrections for fermions cause the heat capacity to deviate downwards from $C = Nk_B$. The ^3He data agree well with these calculations at temperatures as low as 1 K.

Subsequent analysis showed that three other effects contribute to the specific heat of the 2D gas: heterogeneity of the substrate, band structure in the energy levels of the adsorbate, and excitation of vibrations perpendicular to the surface.¹³ The effects of heterogeneity were first removed from the data by means of a model for the distribution of binding energies on the surface. The data were then compared with a model for the band structure effects. The latter arise from the motion of the adatom through the periodically varying adsorption potential. Hence, they reflect the large corrugation of this potential for $^4\text{He}/\text{graphite}$. The vibrations normal to the substrate contribute to the specific heat at temperatures above ~ 5 K.⁹

The most dramatic consequence of the corrugation is the commensurate ($\sqrt{3} \times \sqrt{3}$) phase observed at coverages from ~ 0.05 to ~ 0.07 \AA^{-2} . This phase, identified as a commensurate solid (CS) in Fig. 1.2a, is also known as a lattice-gas or registered phase.¹⁰ The ^4He atoms are localized on top of hexagons formed by the graphite lattice, as shown in Fig. 1.3. The CS phase

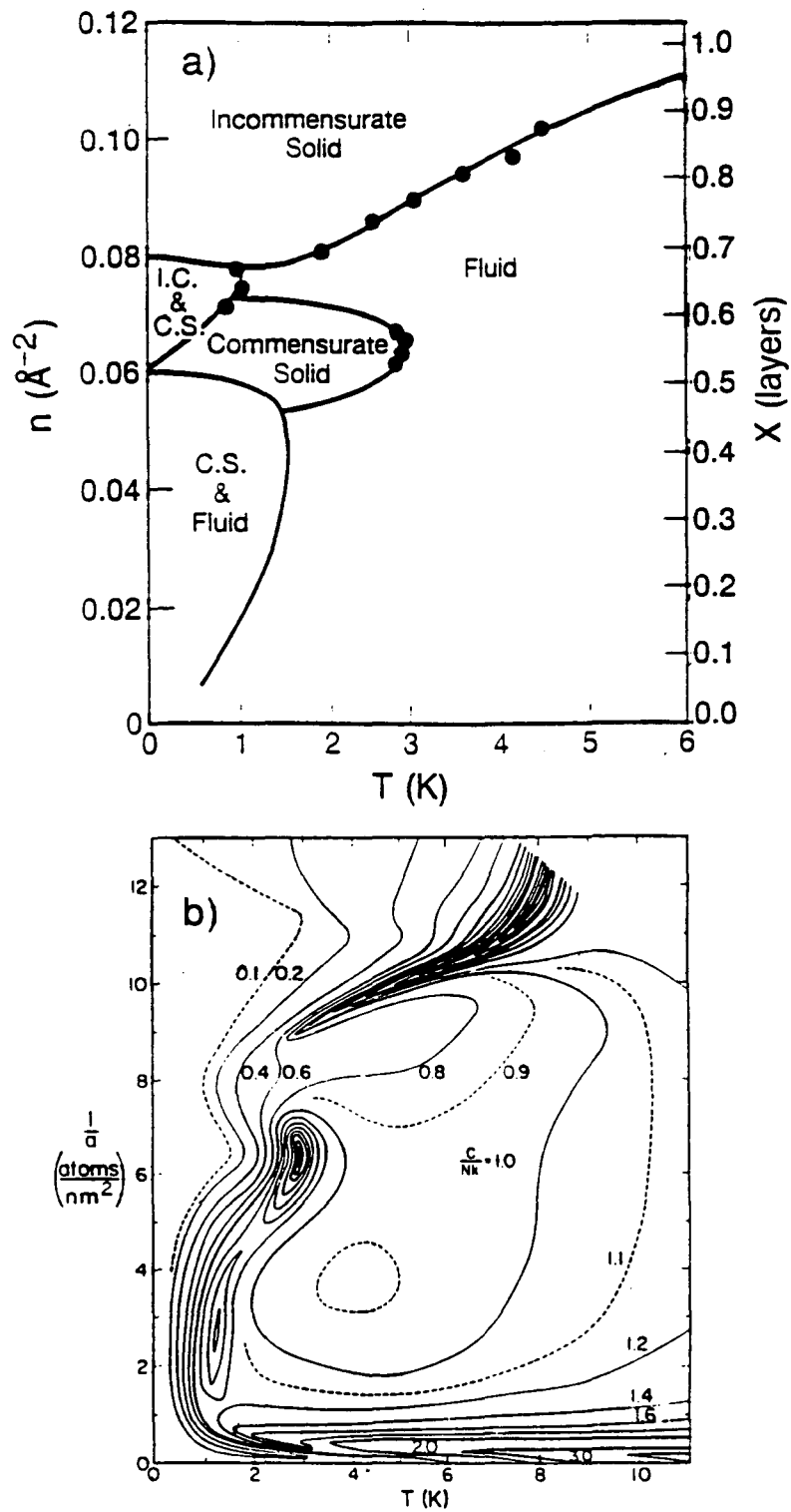


Figure 1.2 a) Phase diagram of $^4\text{He}/\text{graphite}$ for coverages up to one monolayer. (From Campbell and Bretz.⁸) b) Contours of constant specific heat for $^4\text{He}/\text{graphite}$ in a comparable range of coverage and temperature. (From Elgin and Goodstein.⁹)

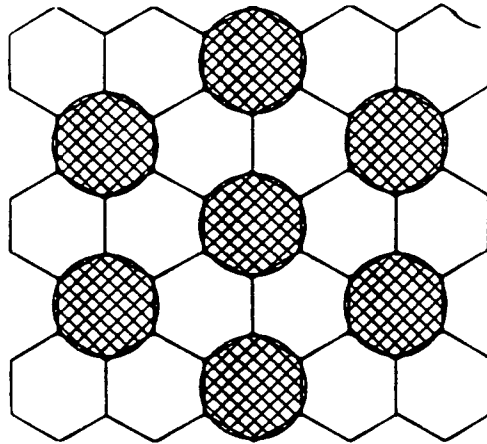


Figure 1.3 The $\sqrt{3} \times \sqrt{3}$ structure of ^4He /graphite. (From Dash.¹⁷)

undergoes an order–disorder transition near 3 K, yielding sharp, strong peaks in the specific heat.² The critical exponent α for these peaks is found to be in good agreement with the predictions of three–state Potts models.^{14, 15}

At still higher coverages, the number of ^4He atoms exceeds the number of sites available in the $\sqrt{3} \times \sqrt{3}$ structure, and an incommensurate solid (IC) phase is formed. The melting line of this phase gives rise to the prominent ridge running along the top of the contour plot in Fig. 1.2b. The formation of this phase indicates that the dominant interactions in this coverage range are those between the atoms in the adsorbed layer, and this observation has prompted comparisons of the specific heat data with recent novel predictions for the melting of 2D solids.

Theories of 2D melting can be divided into two groups: those which predict a first–order transition (as is seen in 3D melting), and those which are based on the work of Kosterlitz, Thouless, Halperin, Nelson, and Young (KTHNY).¹⁶ The latter predict a two–stage melting process consisting of two continuous transitions with an intermediate, hexatic phase. At the first transition ($T = T_m$), positional order is lost but bond–orientational order is maintained. In the hexatic phase, the system has six–fold symmetry and behaves like an anisotropic liquid. At the second transition ($T = T_i$), bond–orientational order is also destroyed, and the liquid becomes isotropic. The transitions are marked by abrupt changes in certain elastic constants, and by changes in the positional and bond–orientational correlations of the adsorbed molecules. The latter are observable with x–ray diffraction.

The specific heat is expected to be smooth at T_m and T_i , but will have a maximum above each of these transition temperatures. It was originally thought that these maxima would be rounded, reflecting a gradual loss of order. It has recently been shown that the width and height of the maxima can vary considerably depending on the details of the model.¹⁶ For this reason, it is believed to be difficult to distinguish between a first–order transition and certain types of continuous transitions predicted by KTHNY on the basis of specific heat data alone. The challenge becomes even greater if the first–order transition is broadened by the effects of heterogeneity.

The case of ^4He /graphite provides a clear example of the sort of difficulty just described. Hurlbut and Dash¹⁸ (HD) studied the melting transition of ^4He submonolayers in the IC phase through measurements of the 2D pressure ϕ . The 2D pressure, also known as the spreading pressure, is

defined as $-(\partial F/\partial A)_{T,V}$. This definition is in analogy with that of the usual 3D pressure, $P = -(\partial F/\partial V)_{T,A}$. In these definitions, F , T , V , and A represent the free energy, temperature, volume, and area, respectively, of the adsorbed film in equilibrium with its 3D vapor.¹⁹ The derivative $(\partial\phi/\partial T)$ at constant density is equivalent to the specific heat,¹⁸ making it possible to draw comparisons between the work of HD and models of 2D melting.

Hurlbut and Dash found the transition to be broadened by effects due to heterogeneity. Through deconvolution of these effects, the intrinsic width $\Delta T/T$ was determined to be less than or equal to 0.04. The authors concluded that this width was too narrow to be explained by theories of continuous melting. Strandburg *et al.*²⁰ argued, however, that simulations of the Laplacian roughening model of continuous melting yield widths as narrow as 0.02. They concluded (and HD subsequently agreed²¹) that the data of HD are consistent with a continuous transition.

The melting of Xe monolayers has also attracted considerable attention. Thermodynamic measurements^{22, 23} and several x-ray diffraction studies²⁴⁻²⁹ of Xe/graphite provided evidence of a crossover from first-order to continuous melting near a coverage of one monolayer. The x-ray diffraction measurements also detected six-fold symmetry in the overlayer above the melting temperature. The observation of six-fold symmetry was consistent with the hexatic phase predicted by KTHNY, but it was also consistent with the six-fold symmetry of the corrugation of the substrate. Rosenbaum *et al.*²⁸ analyzed the diffraction data and determined that the corrugation needed to explain the data is three orders of magnitude larger than the accepted value. Hence, they concluded that the hexatic phase had been observed.

Measurements by Greiser *et al.*³⁰ confirmed the conclusions reached in the previous studies. They repeated the x-ray diffraction measurements using Ag(111) as the substrate. The corrugation for Xe/Ag(111) is predicted to be an order of magnitude smaller than that of Xe/graphite. (See, however, the discussion of corrugation in section 1.5.) Despite the difference in corrugation, the diffraction results were essentially the same as those in the earlier work. The similarity of the results on two very different substrates was interpreted as providing strong evidence for the existence of an hexatic phase in melted Xe monolayers.

Recently, these conclusions have been called into question by the precise thermodynamic measurements of Jin *et al.*³¹ These authors measured the isothermal compressibility K_T , where $K_T = (1/n^2)(\partial n/\partial \mu)$. Both the coverage n and the chemical potential μ can be determined from the known quantity of gas admitted to the cell and the resulting pressure of the 3D vapor in equilibrium.⁹ They found peaks in K_T much sharper than those measured previously, and they also observed very sharp peaks in the specific heat ($\Delta T/T \lesssim 0.01$). These results were found to be incompatible with the predictions of KTHNY, and the authors concluded that the melting transition is first-order at all Xe coverages. They also cited a series of computer simulations which support their conclusions.

In summary, we have seen that the phases observed in adsorbed monolayers are quite varied, including nearly ideal 2D gases, commensurate solids, and incommensurate solids. The melting transition of the incommensurate solids is still highly controversial, but the experimental evidence against KTHNY seems to outweigh that in its favor.³² Finally, we note that important information about the influence of corrugation can be gained through the use of weakly corrugated, metallic substrates.

1.4 Multilayers

Adsorbed multilayers constitute the transition between monolayers and bulk matter. We shall consider three topics of interest in the study of physisorbed multilayers: wetting, surface melting, and surface roughening.

Wetting refers to the manner in which the multilayer covers the substrate as it grows in thickness. If a uniform film covers the substrate, coexisting with the bulk phase only at infinite thickness, the film is said to be completely wet. This behavior is also known as "type-1," or Frank-van der Merwe growth. If coexistence with the bulk occurs at a finite thickness of the film, the wetting is said to be incomplete. This mode is known as "type-2," or Stranski-Krastanov growth.^{33, 34} Wetting has been studied by several experimental techniques, including electron diffraction,^{35, 36} ellipsometry,^{37, 38} and microbalance techniques.^{39, 40} Type-2 growth is usually observed for solid multilayers.

The reason for the prevalence of type-2 growth is understood as follows.³⁹ If the adsorbate-substrate binding energy u_1 is weak compared to the cohesive energy of the bulk adsorbate h_0 , the growth of the bulk phase

will be favored. If $u_1/h_0 \gg 1$, the first few monolayers adsorbed on the calorimeter are compressed to densities which are higher than that of the bulk. This compression causes structural mismatch between the first few monolayers and succeeding ones, which again yields incomplete wetting. Complete wetting occurs only for those few combinations of substrate and adsorbate for which $u_1/h_0 \approx 1$. The adsorbates known to wet graphite completely are Xe, Kr, and Ar.

Many adsorbates for which $u_1/h_0 \gg 1$ exhibit type-2 growth at low temperature but undergo a wetting transition to type-1 growth at a wetting temperature T_w . Frequently, this transition occurs at the triple point, and the film is said to display "triple-point wetting." The usual interpretation of this behavior is that the melting of the bulk phase at the triple point eliminates the structural mismatch between bulk and film which limits wetting at lower temperatures. Triple point wetting is observed for most adsorbates on Au, a relatively weak-binding substrate.³⁹ It has also been suggested that heterogeneity of the substrate may induce triple point wetting.³ In this case, the limit on wetting is imposed by polycrystalline growth of the adsorbate at nucleation sites on the substrate. Energy costs associated with grain boundaries rise as the film grows in thickness, ensuring a crossover to growth of the bulk phase at some finite thickness.

The wetting properties of ^4He and ^3He are not in accord with the simple picture described above.^{33, 40} Adsorbed He multilayers are always in the limit $u_1/h_0 \gg 1$, since the attractive interactions between He molecules are extremely weak. At the same time, the coexisting bulk phases are liquid, which excludes the possibility of structural mismatch. Thus, complete wetting is expected, but measurements of normal He films show the opposite behavior. Complete wetting is observed only for superfluid ^4He . The origin of this behavior has not been explained.

Surface melting and surface roughening are two distinct but related mechanisms by which the surface of bulk solids in thermal equilibrium can become disordered at temperatures below the bulk melting temperature T_M .^{37, 41} Surface melting involves the formation of a mobile "quasiliquid" layer whose thickness increases with temperature, diverging as T approaches T_M . Surface roughening occurs through a proliferation of vacancies and adatoms on an otherwise smooth atomic plane. As the temperature increases, clusters of defects form, increase in size, and acquire their own

adatoms and vacancies. As T approaches the roughening temperature T_R , the characteristic size of the clusters diverges, and the surface of the crystal no longer conforms to a particular crystalline plane.

Both of these processes are manifest in the behavior of uniform multilayer films. Fig. 1.4 shows a set of measurements of the specific heat of Ar/graphite.⁴² The curves (a) through (i) correspond to thicknesses from 10.4 to 3.6 monolayers (ML), respectively. The prominent peak in curve (a) corresponds to the melting of the film as a whole, and its temperature approaches the triple point temperature as the thickness increases. It is the equivalent of the usual bulk melting peak at infinite thickness. This peak is slightly asymmetric, with the approach from the low-temperature side being somewhat more gradual. (The asymmetry becomes obvious for still greater thicknesses.) This asymmetry is attributed to surface melting occurring at temperatures just below that of the main peak. The anomalies located near 68 K represent order-disorder transitions in the thin films which evolve to a roughening transition in the thick films. In films up to ~ 7 ML, the disordering is restricted to steps which are only a single layer in height. If the system is at the critical density for such a transition, a sharp, cusp-like anomaly is observed, as seen in curves (i) and (f). For thicker films, steps with varying heights may form, the anomalies become weaker and more rounded, and the transition tends toward the bulk roughening transition.

1.5 Metallic Substrates--Motivation for Present Work

The influence of the substrate on the behavior of physisorbed systems has been a persistent theme in the preceding sections. We have seen that parameters such as corrugation, binding energy, and heterogeneity play a key role in shaping the properties of the adsorbate. Effects due to the substrate must always be considered, even in the case of incommensurate overlayers.

In view of the significant influence of the substrate, measurements on different types of substrates are particularly valuable. Comparison of results on a variety of substrates allows substrate-induced effects to be distinguished from behavior intrinsic to the adsorbate. As discussed in section 1.3, a comparison of this type provided important support for arguments favoring KTHNY melting of Xe monolayers.³⁰

Metallic substrates have been recognized by many workers as an important alternative to graphite. One major difference between metals and

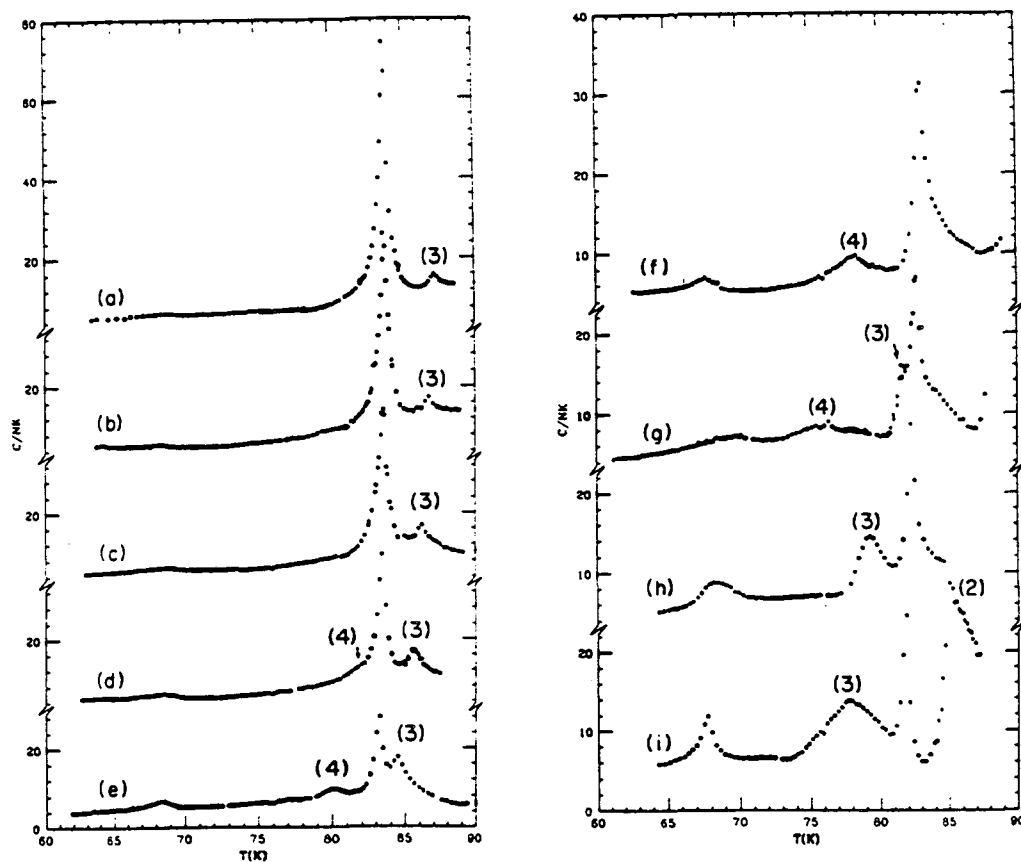


Figure 1.4 The specific heat of Ar/graphite for coverages from 10.4 ML for sample (a) to 3.6 ML for sample (i). The prominent peak near 83 K is due to the melting of the entire film. The features labelled by numbers (n) arise from the melting of the n^{th} monolayer. The anomaly near 68 K is due to an order-disorder transition, as discussed in the text. (From Zhu and Dash.⁴²)

graphite is the strength of the bond to the adsorbate. The binding energy of ^4He on transition metals is a factor 2–3 lower than that on graphite. On the alkali metals, the reduction is a factor of 10–100.⁴³ It has recently been proposed that ^4He may exhibit unusual properties on weak-binding substrates. The first 1–2 monolayers of ^4He are known to solidify on most substrates.³³ However, Cheng *et al.*⁴⁴ have predicted condensation into a liquid monolayer for adsorption on the alkali metals. Cheng and Cole⁴⁵ have also proposed a model in which weak binding energies result in delocalization of the ^4He atoms in the direction normal to the substrate. This delocalization weakens the $^4\text{He} - ^4\text{He}$ interactions. For very weak binding, they propose that a weakly interacting Bose gas may be formed.

The corrugation of the adsorption potential is also expected to be smaller on metals than on graphite. The corrugation for rare gases adsorbed on close-packed metal surfaces is estimated to be one-tenth as large as that on graphite on the basis of ^4He diffraction data. Kern has questioned the applicability of such estimates for heavier gases such as Xe.⁴⁶ He argues that the diffraction studies measure the corrugation of the repulsive part of the potential, not the corrugation of the bottom of the well, where the heavy gases are bound. His estimate for the corrugation of Xe/Ag(111) is considerably closer to that of Xe/graphite. The model he uses has been criticized, however, for failing to accurately predict experimental observations for Kr/graphite and N_2 /graphite.⁴⁷ Despite the disagreements concerning the heavy rare gases, there seems to be general agreement that the corrugation for adsorbates such as ^4He is much less on metals than on graphite.⁴⁸

There have been several experimental studies on metallic substrates, including x-ray diffraction,³⁰ quartz-crystal microbalance measurements,^{33, 39} and a study using a surface plasmon resonance technique.⁴⁹ Uniformity of the adsorption potential comparable to that of Grafoil has been achieved for evaporated metal films. Domains of uniform adsorption have been shown to be as large as 200 Å for polycrystalline Ag and Au films with (111) oriented crystallites.³³

Until the introduction of the present technique, however, surface heat capacity measurements on simple metallic surfaces were not possible. One obstacle to such measurements is the relatively large specific heat of metals at low temperatures. The heat capacity of all crystalline solids possesses a contribution C_{ph} due to excitation of phonons.⁵⁰ For temperatures $T \ll \Theta$,

where Θ is the Debye temperature, $C_{ph} \approx 234 Nk_B (T/\Theta)^3$. The value of Θ is typically of the order of 10^2 K. For nonmetals, C_{ph} is often the dominant contribution to the heat capacity, resulting in low heat capacities at LHe temperatures. The heat capacity of metals, however, also possesses an electronic contribution⁵¹ $C_{el} \approx (\pi^2/2) Nk_B (T/T_F)$, where T_F is the Fermi temperature and is of order 10^4 K. Because of its linear dependence on T , C_{el} becomes the dominant contribution to the total heat capacity at sufficiently low temperatures. For Ag, $C_{el} \approx C_{ph}$ at 4 K. Thus, the sensitivity of surface heat capacity measurements on metallic single crystals would be limited by the large heat capacity of the substrate. A possible solution to this problem is to use powdered metallic substrates with a large surface area-to-volume ratio, in imitation of the traditional techniques for graphite. Such substrates would very likely display considerable heterogeneity, however, due to the multiplicity of crystallite orientations exposed and the difficulty of cleaning the surface.

Our approach is to evaporate a metallic film with a thickness of 500–1000 Å on a dielectric substrate with low heat capacity. The heat capacity of such a structure is low enough that small fractions of a monolayer of ^4He or H_2 can be measured, yet the adsorption surface can be made smooth and relatively homogeneous. Any metal which can be evaporated in ultra-high vacuum can be used to coat the substrate. This technique allows us to measure the heat capacity of adsorbates on weak-binding, weakly corrugated substrates for the first time. As we have discussed, measurements on such substrates are likely to yield novel results, and to offer new perspectives on previous results.

The first measurements made with this new technique do, in fact, contrast sharply with previous results on graphite.⁵² Fig. 1.5 shows measurements of the heat capacity of various exposures of ^4He on Ag. The heat capacity is independent of temperature for low exposures. This result is consistent with the nearly ideal 2D gas which is observed on graphite over a broad range of temperature and coverage. For higher exposures, however, the data for $^4\text{He}/\text{Ag}$ decrease at low temperature. As Fig. 1.2b shows, the specific heat of $^4\text{He}/\text{graphite}$ *increases* at low temperature for most submonolayer coverages. The most prominent features of Fig. 1.2b, all of which are associated with various solid phases, do not appear in the data for

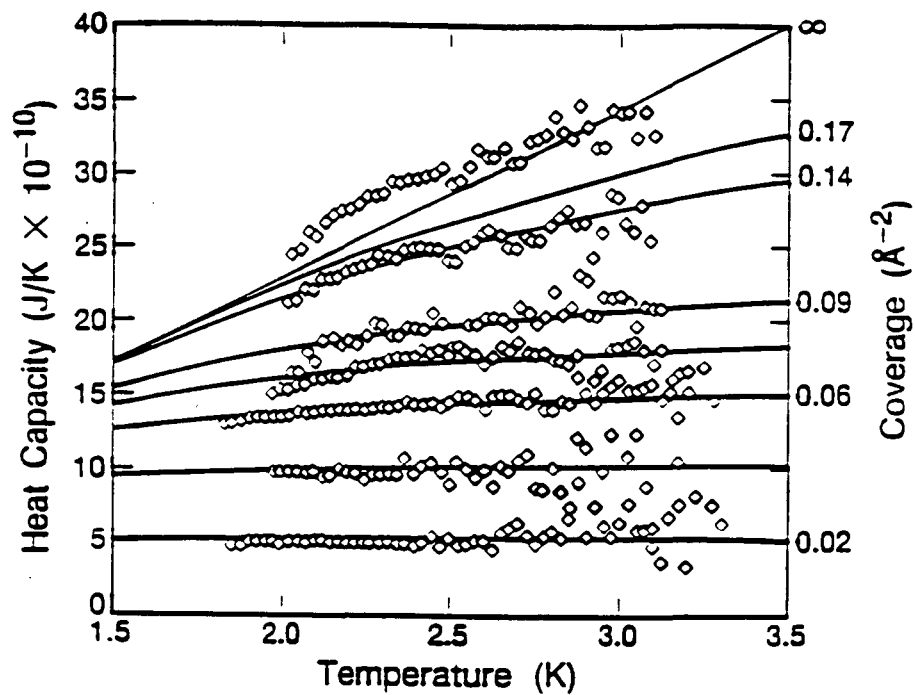


Figure 1.5 Heat capacity for several exposures of ^4He adsorbed on Ag. The solid lines show the heat capacity of a noninteracting 2D Bose gas for the coverages shown at right. (From Kenny and Richards.⁵²)

$^4\text{He}/\text{Ag}$. This absence of these features makes this study the first to demonstrate the absence of solidification for ^4He monolayers.

Furthermore, it was found that the $^4\text{He}/\text{Ag}$ data could be fit by a simple model of a non-interacting 2D Bose gas, as shown by the solid lines in Fig. 1.5. The coverage was the only adjustable parameter in the model. The high temperature limit of the solid curves is independent of temperature for all coverages. In this limit, the Bose gas behaves as an ideal classical 2D gas with $C/Nk_B = 1$. The success of this simple model confirms the expectation that metallic substrates offer opportunities for exploring fundamentally new areas of research.

Hydrogen was chosen as the next system for study. Results for H_2 form the focus of Chapter 3. Both ^4He and H_2 are light molecules. Hence, both exhibit large effects due to quantum mechanical zero point motion. There are two forms of H_2 which differ significantly in their thermodynamic behavior at low temperatures. Para- H_2 (p- H_2) is spherically symmetric and is more similar to ^4He . Ortho- H_2 (o- H_2) is asymmetric and possesses an electric quadrupole moment. The phase diagram for monolayers of p- H_2 is similar to that of ^4He , but the phase boundaries are scaled upward in temperature by a factor of four. It is clearly of significant interest to see whether the dramatic differences between $^4\text{He}/\text{Ag}$ and $^4\text{He}/\text{graphite}$ hold for H_2 as well.

References

- ¹J. G. Dash, Films on Solid Surfaces , (Academic Press, New York, 1975) p. 49.
- ²M. Bretz, Phys. Rev. Lett. **38**, 501 (1977).
- ³J. G. Dash, J. Cryst. Growth **100**, 268 (1990).
- ⁴Adsorption isotherms are measurements of the coverage on the surface as a function of vapor pressure in thermal equilibrium. Isotherms on highly uniform substrates have a "stepwise" structure which results from layer-by-layer growth of the adsorbed film. The sharpness of the steps is indicative of the uniformity of the substrate. See Ref. 1.
- ⁵J. G. Dash, Films on Solid Surfaces , (Academic Press, New York, 1975) p. 216.
- ⁶R. J. Birgeneau, P. A. Heiney and J. P. Pelz, Physica B **109 & 110**, 1785 (1982).
- ⁷M. Bretz, J. G. Dash, D. C. Hickernell, E. O. McLean and O. E. Vilches, Phys. Rev. A **8**, 1589 (1973).
- ⁸J. H. Campbell and M. Bretz, Phys. Rev. B **32**, 2861 (1985).
- ⁹R. L. Elgin and D. L. Goodstein, Phys. Rev. A **9**, 2657 (1974).
- ¹⁰M. Schick, in Phase Transitions in Surface Films , edited by J. G. Dash and J. Ruvalds (Plenum Press, New York, 1980), p. 65.
- ¹¹R. L. Siddon and M. Schick, Phys. Rev. A **9**, 907 (1974).
- ¹²R. E. Ecke, Q.-S. Shu, T. S. Sullivan and O. E. Vilches, Phys. Rev. B **31**, 448 (1985).
- ¹³M. W. Cole, D. R. Frankl and D. L. Goodstein, Rev. Mod. Phys. **53**, 199 (1981).
- ¹⁴R. J. Baxter, J. Phys. A **13**, L61 (1980).
- ¹⁵M. den Nijs, J. Phys. A **12**, 1857 (1979).
- ¹⁶K. J. Strandburg, Rev. Mod. Phys. **60**, 161 (1988).
- ¹⁷J. G. Dash, Films on Solid Surfaces , (Academic Press, New York, 1975) p. 196.

- ¹⁸S. B. Hurlbut and J. G. Dash, *Phys. Rev. Lett.* **53**, 1931 (1984).
- ¹⁹J. G. Dash, *Films on Solid Surfaces*, (Academic Press, New York, 1975) p. 63.
- ²⁰K. J. Strandburg, R. M. Suter, N. J. Colella, P. M. Horn, S. A. Solla, R. J. Birgeneau, S. G. J. Mochrie, E. D. Specht, K. L. D'Amico and D. E. Moncton, *Phys. Rev. Lett.* **55**, 2226 (1985).
- ²¹S. B. Hurlbut and J. G. Dash, *Phys. Rev. Lett.* **55**, 2227 (1985).
- ²²N. J. Colella and R. M. Suter, *Phys. Rev. B* **34**, 2052 (1986).
- ²³R. Gangwar, N. J. Colella and R. M. Suter, *Phys. Rev. B* **39**, 2459 (1989).
- ²⁴R. J. Birgeneau and P. M. Horn, *Science* **232**, 329 (1986).
- ²⁵P. Dimon, P. M. Horn, M. Sutton, R. J. Birgeneau and D. E. Moncton, *Phys. Rev. B* **31**, 437 (1984).
- ²⁶P. A. Heiney, R. J. Birgeneau, G. S. Brown, P. M. Horn, D. E. Moncton and P. W. Stephens, *Phys. Rev. Lett.* **48**, 104 (1982).
- ²⁷S. E. Nagler, P. M. Horn, T. F. Rosenbaum, R. J. Birgeneau, M. Sutton, S. G. J. Mochrie, D. E. Moncton and R. Clarke, *Phys. Rev. B* **32**, 7373 (1985).
- ²⁸T. F. Rosenbaum, S. E. Nagler, P. M. Horn and R. Clarke, *Phys. Rev. Lett.* **50**, 1791 (1983).
- ²⁹E. D. Specht, R. J. Birgeneau, K. L. D'Amico, D. E. Moncton, S. E. Nagler and P. M. Horn, *J. Phys. (Paris)*, *Lett.* **45**, L561 (1985).
- ³⁰N. Greiser, G. A. Held, R. Frahm, R. L. Greene, P. M. Horn and R. M. Suter, *Phys. Rev. Lett.* **59**, 1706 (1987).
- ³¹A. J. Jin, M. R. Bjurstrom and M. H. W. Chan, *Phys. Rev. Lett.* **62**, 1372 (1989).
- ³²A. J. Dahm, M. A. Stan and R. G. Petschek, *Phys. Rev. B* **40**, 9006 (1989).
- ³³A. D. Migone, J. Krim, J. G. Dash and J. Suzanne, *Phys. Rev. B* **31**, 7643 (1985).
- ³⁴S. Dietrich, in *Phase Transitions and Critical Phenomena*, edited by C. Domb and J. Lebowitz (Academic Press, New York, 1988), Vol. 12.

- ³⁵M. Bienfait, J. L. Seguin, J. Suzanne, E. Lerner, J. Krim and J. G. Dash, *Phys. Rev. B* **29**, 983 (1984).
- ³⁶J. Krim, J. M. Gay, J. Suzanne and E. Lerner, *J. Physique* **47**, 1757 (1986).
- ³⁷H. S. Youn and G. B. Hess, *Phys. Rev. Lett.* **64**, 918 (1990).
- ³⁸H. S. Youn and G. B. Hess, *Phys. Rev. Lett.* **64**, 443 (1990).
- ³⁹J. Krim, J. G. Dash and J. Suzanne, *Phys. Rev. Lett.* **52**, 640 (1984).
- ⁴⁰P. Taborek and L. Senator, *Phys. Rev. Lett.* **57**, 218 (1986).
- ⁴¹J. G. Dash, *Contemp. Phys.* **30**, 89 (1989).
- ⁴²D.-M. Zhu and J. G. Dash, *Phys. Rev. B* **38**, 11673 (1988).
- ⁴³G. Vidali, G. Ihm, H.-Y. Kim and M. W. Cole, *Surf. Sci. Reports* **12**, 133 (1991).
- ⁴⁴E. Cheng, G. Ihm and M. W. Cole, *J. Low Temp. Phys.* **14**, 519 (1989).
- ⁴⁵E. Cheng and M. W. Cole, *Phys. Rev. B* **42**, 3960 (1990).
- ⁴⁶K. Kern, *Vacuum* **41**, 389 (1990).
- ⁴⁷F. Y. Hansen, V. L. P. Frank, H. Taub, L. W. Bruch, H. J. Lauter and J. R. Dennison, *Phys. Rev. Lett.* **64**, 764 (1990).
- ⁴⁸L. W. Bruch, private communication.
- ⁴⁹X. Qian and M. Bretz, *Phys. Rev. Lett.* **61**, 1497 (1988).
- ⁵⁰C. Kittel, *Introduction to Solid State Physics* , (John Wiley and Sons, New York, 1976) p. 138.
- ⁵¹C. Kittel, *Introduction to Solid State Physics* , (John Wiley and Sons, New York, 1976) p. 165.
- ⁵²T. W. Kenny and P. L. Richards, *Phys. Rev. Lett.* **64**, 2386 (1990).

2. Apparatus and Procedures

2.1 Introduction

This chapter describes the apparatus and techniques used to measure the heat capacity of adsorbates on metal films with ac microcalorimetry. This chapter represents an extension of the work of Kenny *et al.*¹⁻³ The description of the electronics system is from Ref. 3. The principal change in procedures documented in this work concerns the implementation of a bake-out procedure, which is described here and discussed at greater length in Chapter 4.

The first section discusses the calorimeter itself. It includes a description of an ideal calorimeter, as well as details on the methods of construction and characteristics of real calorimeters. The second section discusses the cryostat and UHV system. The third section describes the electronics system, and the final section discusses the constraints of the method.

2.2 Calorimeter

Theory of Operation

The design for the ac calorimeters used in this work was adapted from that of the composite bolometer, the most sensitive detector of far-infrared radiation available. In the bolometer, a small heat capacity C at temperature T is coupled by a weak thermal link G to a cold stage at fixed temperature T_0 , as shown in Fig. 2.1. Incident radiation with power P is absorbed by the bolometer, causing its temperature to increase, and the rise in temperature is detected by a thermometer.

In the calorimeter, the thermal circuit is the same, but a resistive heater replaces the infrared radiation as the source of the power input. The heat capacity is then calculated from the power input and the change in temperature. Both devices achieve high sensitivity by making C and G small, and by utilizing sensitive thermometers.

A schematic diagram of the electrical circuit for the calorimeter is shown in Fig. 2.2. The power input is supplied by an ac voltage $V_H \cos(\omega t/2)$ across a heater with resistance R_H . This ac bias adds a small oscillatory component $T_{AC} \cos(\omega t)$ to the temperature of the calorimeter. The thermometer has a calibrated resistance $R(T) \equiv R_T$ and is biased with a direct

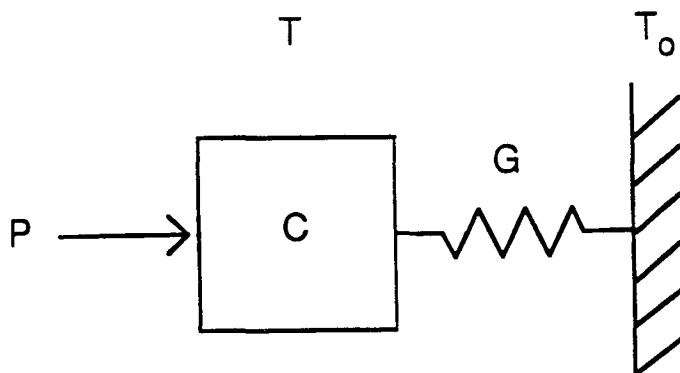


Figure 2.1 Schematic thermal circuit of the calorimeter. The labelled quantities are defined in the text.

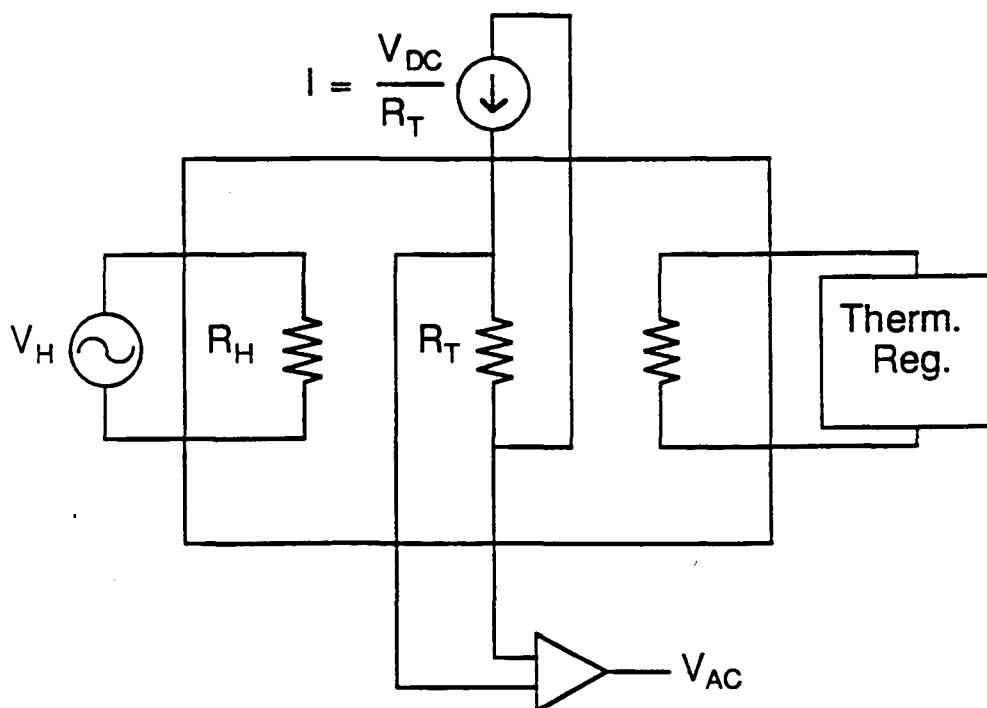


Figure 2.2 Schematic electrical circuit of the calorimeter. The ac bias, thermometer, and thermal regulation circuits are shown from left to right and are discussed in the text.

current $I = V_{DC}/R_T$. Because of the temperature dependence of R_T , the voltage across the thermometer also develops an oscillatory component with amplitude

$$V_{AC} = V_{DC} \alpha T_{AC} = \frac{V_{DC} \alpha V_H^2}{2R_H [(\omega C)^2 + G^2]^{1/2}} \quad (2.1)$$

where $\alpha \equiv (1/R) (dR/dT)$. In the limit $\omega C/G \gg 1$, the denominator in Eq. (2.1) can be approximated by $(2R_H \omega C)$. In this limit, the heat capacity of the calorimeter is given by

$$C \approx \frac{V_{DC} \alpha V_H^2}{2\omega R_H V_{AC}} \quad (2.2)$$

Kenny and Richards have analyzed the effects of noise due to energy fluctuations in the thermal conductance G and Johnson noise in the thermometer.³ For an ideal calorimeter limited only by these fundamental sources of noise, the signal-to-noise ratio is given by

$$\frac{V_{AC}}{V_N} = \left\{ \frac{G}{4k_B T} \left(\frac{1}{\alpha^2 T_{AC}^2 \Delta T_B} + \frac{T}{(\Delta T_H)^2} \right)^{-1} \right\}^{1/2} \quad (2.3)$$

where $\Delta T_B = V_{DC}^2/R_T G$ and $\Delta T_H = V_H^2/2R_H G$ are the contributions to the heating of the calorimeter due to the dc bias on the thermometer and the time average of the ac bias on the heater, respectively.

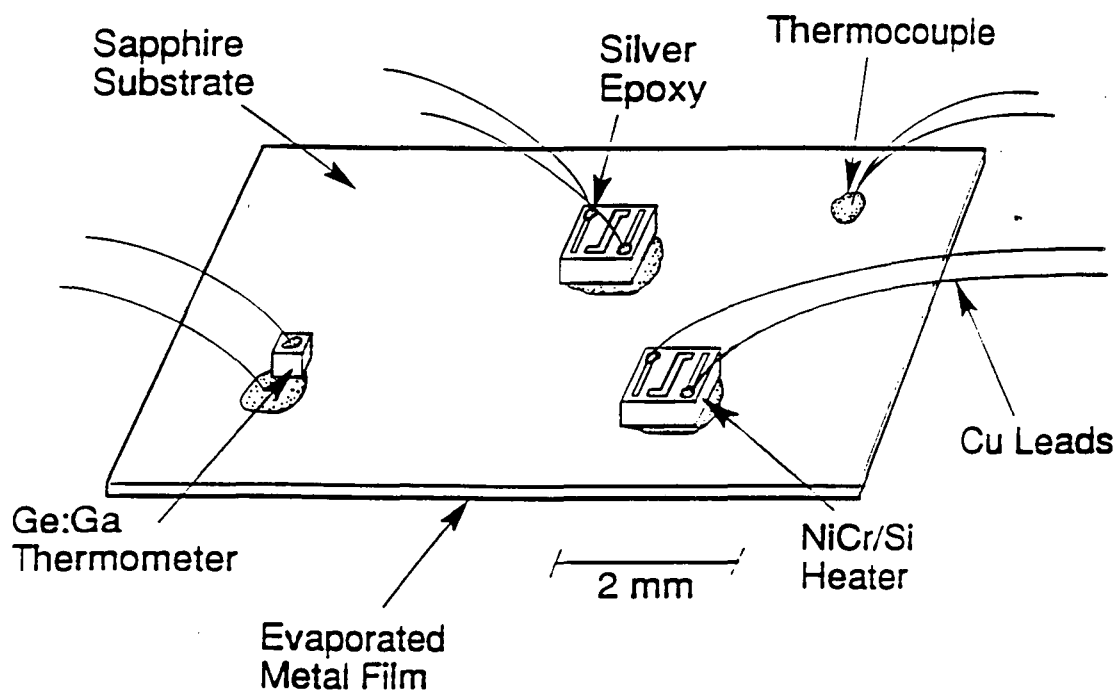
Increases in any of the four quantities ΔT_H , ΔT_B , α , or G will improve the signal-to-noise ratio; however, each of these quantities is constrained in real calorimeters. The quantities ΔT_H and ΔT_B limit the minimum operating temperature of the system according to $T_{min} = T_0 + (\Delta T_H + \Delta T_B)$. Extremely sensitive thermometers (i.e., those with values of $\alpha \gg 1 \text{ K}^{-1}$) are difficult to use over a broad temperature range. Lastly, Eq. (2.2) is valid only for $\omega C/G \gg 1$; hence, large values of G require either high frequencies or a more complicated analysis. However, the maximum frequency is limited to 2 kHz in the calorimeters presently used, because of an electrical time constant to be discussed below. Thus, the values of G which can be used are also limited.

In addition to the above constraints, real calorimeters are limited by drifts in the signal on long time scales. It takes at least fifteen minutes to make a typical measurement of the heat capacity as a function of temperature. To study an adsorbed film, two such measurements are needed, one before and one after the adsorbate is deposited. For diagnostic purposes, two successive measurements (without deposition of an adsorbate) can be compared. Drifts are found to be approximately 0.2% of the heat capacity of the calorimeter per hour. The amplifiers used to process the signals are a likely sources of such drifts. We have measured the stability of two lock-in amplifiers^{4, 5} and a preamplifier⁶ used in our measurements. We find drifts in the gain of the lock-in amplifiers of approximately 0.2% per hour. Such drifts are large enough to account for the drifts observed in the heat capacity. The stability of the preamplifier was better by a factor of three. Despite these limitations, the sensitivity of the calorimeter is more than adequate to measure submonolayer coverages of ^4He and H_2 .

Construction

A schematic diagram of the calorimeter is shown in Fig. 2.3. It consists of a 50 μm sapphire substrate, to which a neutron-transmutation-doped (NTD) resistive thermometer and two resistive heaters are attached with Ag-filled epoxy. One heater is used to regulate the average temperature of the calorimeter, and the other is ac biased to induce a small oscillation in the temperature. A chromel-alumel thermocouple epoxied to the substrate serves as a thermometer at temperatures above the useful range of the NTD thermometer. The thermocouple wires and Cu leads, all of which are 25 μm in diameter, provide the dominant thermal conductance to the cold stage, as will be discussed below.

Sapphire is used for the substrate because of its low heat capacity, high thermal conductivity, and high strength. Since the substrate provides the dominant contribution to the heat capacity of the calorimeter, increases in sensitivity can be achieved in two ways: 1) further reduction in the thickness, which will make the calorimeter more fragile, or 2) switching from sapphire to diamond, which has a higher Debye temperature. The heaters are commercially available packages, consisting of 1000 Ω NiCr films deposited on Si wafers.⁷ The Ag-filled epoxy⁸ is used for electrical and thermal contact as well as mechanical support. Its ease of application makes it technically convenient given the large number of contacts which must be made.



XBL 893-5074A

Figure 2.3 Schematic diagram of the calorimeter, as seen from the rear. The heaters and thermometer are attached to the substrate with conductive epoxy. The epoxy is also used for the electrical contacts. The metal film is evaporated on the opposite side.

Soldering is, by contrast, much more difficult: all the contacts must be soldered simultaneously due to the high thermal conductivity of the substrate. However, the outgassing properties of the epoxy have not been studied in UHV. We will present a discussion of the compatibility of the epoxy with the requirements of UHV in Chapter 4.

The NTD thermometers are made from single crystal, ultra-pure Ge. The Ge is doped with Ga acceptors and compensated with As and Se donors by means of neutron transmutation. The net concentration of carriers, $N_a - N_d$, ranges from 1.5×10^{15} to $8.4 \times 10^{16} \text{ cm}^{-3}$. Electrical contacts which contribute no excess noise are made by B^+ ion implantation and Au/Cr metallization. These thermometers are useful because of their low heat capacity and high sensitivity. Thermometers as small as $(100 \mu\text{m})^3$ have been fabricated with resistances which are compatible with the requirements of commercially available preamplifiers. Further details on the preparation of these thermometers have been published elsewhere.⁹

The resistivity as a function of temperature of NTD thermometers has been shown to agree with that predicted for systems with variable-range hopping in the presence of a Coulomb energy gap. The form predicted for the resistivity is²

$$\rho(E,T) = \rho_0 \exp[(T_0/T)^\alpha] \exp(-eEL/k_B T) \quad (2.4)$$

where E is the electric field, and L is the characteristic length for the hopping process. For temperatures small in comparison with the Coulomb gap, the value expected for α is 0.5. For fields $E \ll k_B T/eL$, the resistivity becomes independent of the field. In these limits, Eq. (2.4) simplifies to

$$\rho(0,T) = \rho_0 \exp[(T_0/T)^{1/2}]. \quad (2.5)$$

This behavior has been observed for NTD thermometers at temperatures below $\sim 2.8 \text{ K}$. At higher temperatures, a better fit to Eq. (2.4) is obtained for $\alpha = 1$. This temperature dependence is believed to be due to ionization of bound carriers. The field below which the resistivity is independent of E has been found to depend on the value of $N_a - N_d$. For the thermometers used in the present work (NTD#5), $N_a - N_d = 1.5 \times 10^{16} \text{ cm}^{-3}$. The low field limit for these thermometers is obtained for $E \lesssim 1.3 \text{ V/cm}$. All measurements

reported here were made with the bias across the thermometer in this low field limit.

Typical plots of the resistance as a function of temperature for the thermometers used in the present study are shown in Fig. 2.4. Similar measurements are made for each assembled calorimeter before it is installed in the UHV system. The calorimeter is submerged directly in a bath of liquid ^4He , which is gradually cooled from 4.2 K to 1.4 K by pumping on the vapor above the bath. The vapor pressure above the bath is monitored with a capacitance manometer. The resistance of the thermometer and the vapor pressure of the liquid ^4He are recorded manually throughout the above temperature range. The fit to $R(T) = R_0 \exp(A/\sqrt{T})$, the form expected from Eq. (2.5), is shown in Fig. 2.4a. A fit to $R(T) = R_0 \exp(B/T)$ is shown in Fig. 2.4b for comparison. The fit shown in a), compared to that in b), is better at low temperatures but worse at high temperatures, as expected. The two fits differ by 2% at 1.5 K. We have used the fit shown in a) in the present work. Repeated calibrations of NTD thermometers have shown that the calibration is unaffected by thermal cycling.¹

We noted earlier that the simple relation between C and V_{AC} given in Eq. (2.2) holds for $\omega C/G \gg 1$ in an ideal calorimeter. To determine the range of acceptable frequencies, V_{AC} is measured as a function of the frequency $f = \omega/2\pi$, and the product ($f \times V_{AC}$) is plotted as a function of f . According to Eq. (2.1), we expect a linear increase at low frequency, and a frequency-independent response at high frequency. Typical data for this measurement are shown in Fig. 2.5. The behavior is that expected from Eq. (2.1) up to a frequency of 2 kHz, where an additional time constant causes V_{AC} to decrease more rapidly than $1/f$. The range of acceptable frequencies in this plot is 800 Hz to 2 kHz. The additional time constant is thought to be electrical in origin, stemming from the capacitance of the heat sinks and the resistance of the thermometer.³

Time constants in excess of 10^{-2} s due to weak electron-phonon coupling have been observed in variable-range hopping systems.^{10, 11} Furthermore, measurements such as those shown in Fig. 2.5 have given evidence for an internal time constant of ~ 4 ms in lightly-doped NTD thermometers.² However, a more heavily-doped, NTD#4 thermometer showed no sign of this additional time constant. The NTD#5 thermometers used in the present study, which are still more heavily doped, show behavior

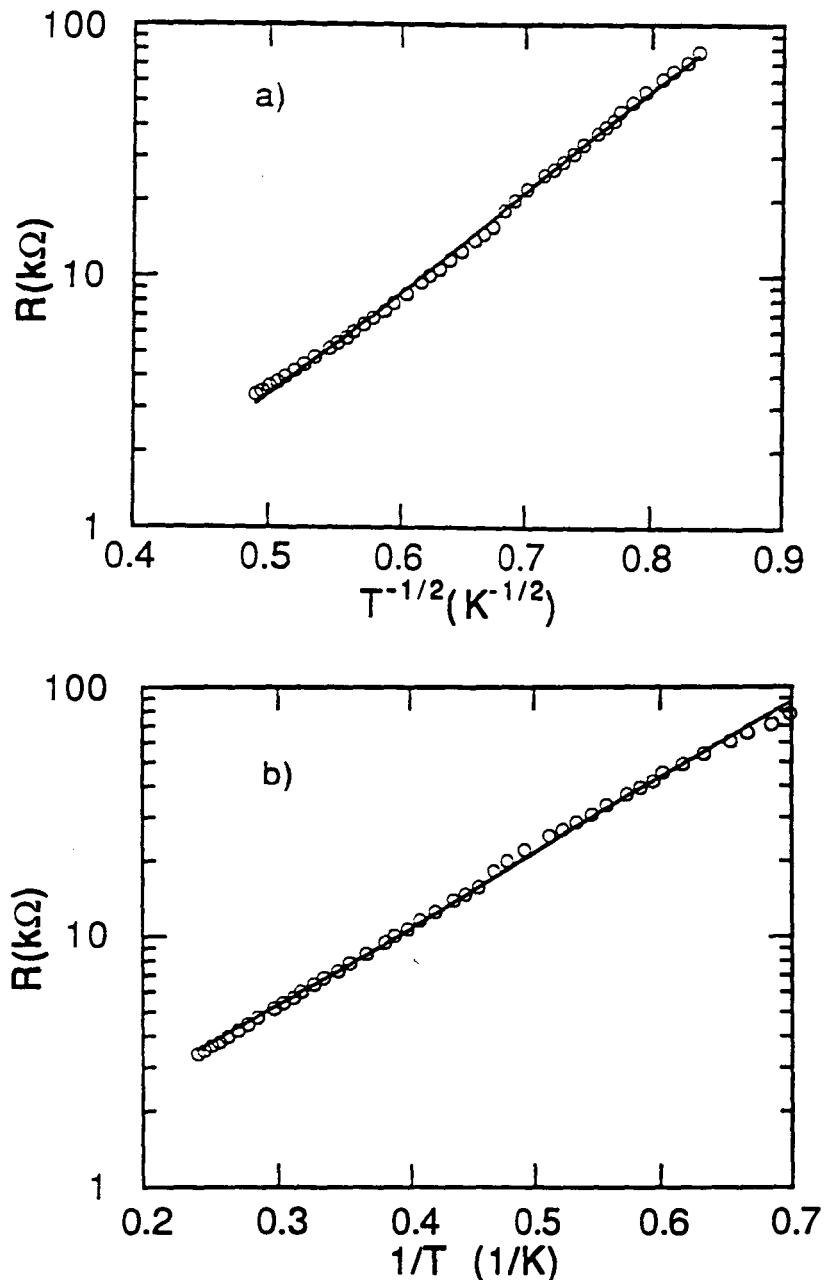


Figure 2.4 a) Resistance of the thermometer as a function of $T^{-1/2}$. The fit to $R = R_0 \exp(A/\sqrt{T})$, the behavior expected from the model of variable range hopping, is shown by the solid line. Fits to this function are used in the present work.

b) The data from a) plotted as a function of T^{-1} . The fit to $R = R_0 \exp(B/T)$, shown by the solid line, is slightly worse than the fit shown in a) at low temperatures.

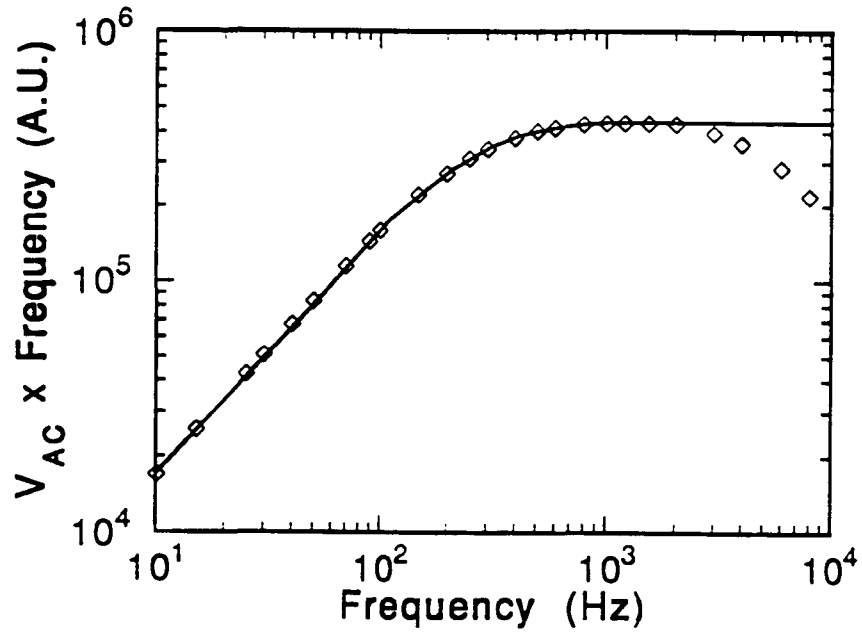


Figure 2.5 AC voltage across the thermometer multiplied by the frequency, as a function of frequency. The solid line shows the behavior expected for the thermal circuit shown in Fig. 2.1. The roll-off at high frequency is believed to be due to an electrical time constant.

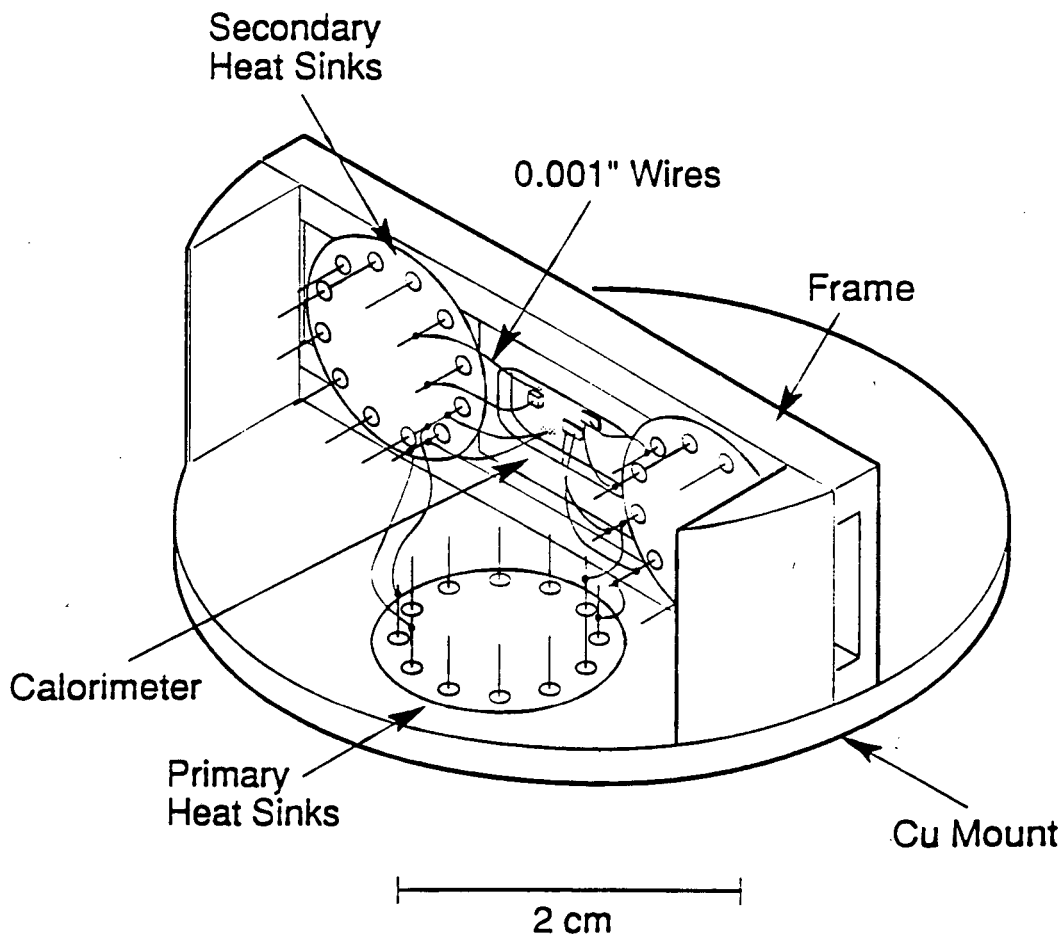
similar to that of the NTD#4 thermometer. Time constants due to the finite thermal conductance between the various components of the calorimeter (e.g., between the thermometer and the substrate) have been shown to be much smaller than those we have just considered. Measurements using far infrared picosecond pulses incident on bolometers similar to the calorimeters discussed here have shown these time constants to be of order $1 \mu\text{s}$.¹

The calorimeter is mounted on a stainless steel frame which constrains its motion with negligible thermal contact. Thin pieces of stainless steel serve both to hold the calorimeter against the frame and to mask the edges of the substrate during the evaporation of metallic films. This latter function is important: continuous metallic paths allow the possibility of migration of adsorbates off of or on to the calorimeter as it is heated and cooled during measurements.

After being mounted in its frame, the calorimeter is submerged in liquid ^4He for calibration, as described above. The frame is then screwed to posts on a Cu mount, as shown in Fig. 2.6. Transistor headers¹² soldered to the Cu mount and the stainless steel frame serve as UHV-compatible heat sinks for the electrical leads running to the calorimeter. Finally, this mount is attached to the end of a cold finger with stainless steel screws. To improve the thermal contact, a $12 \mu\text{m}$ Au foil is inserted between the mount and the cold finger. Under compression, the foil deforms and increases the effective area of contact between the mount and the cold finger. Indium foil, which is also highly malleable, is frequently used for this purpose. However, its thermal conductivity decreases rapidly below 3.4 K due to the onset of superconductivity. Since the temperature of the cold finger reaches 1.3 K, Au foil provides better thermal contact in this application.

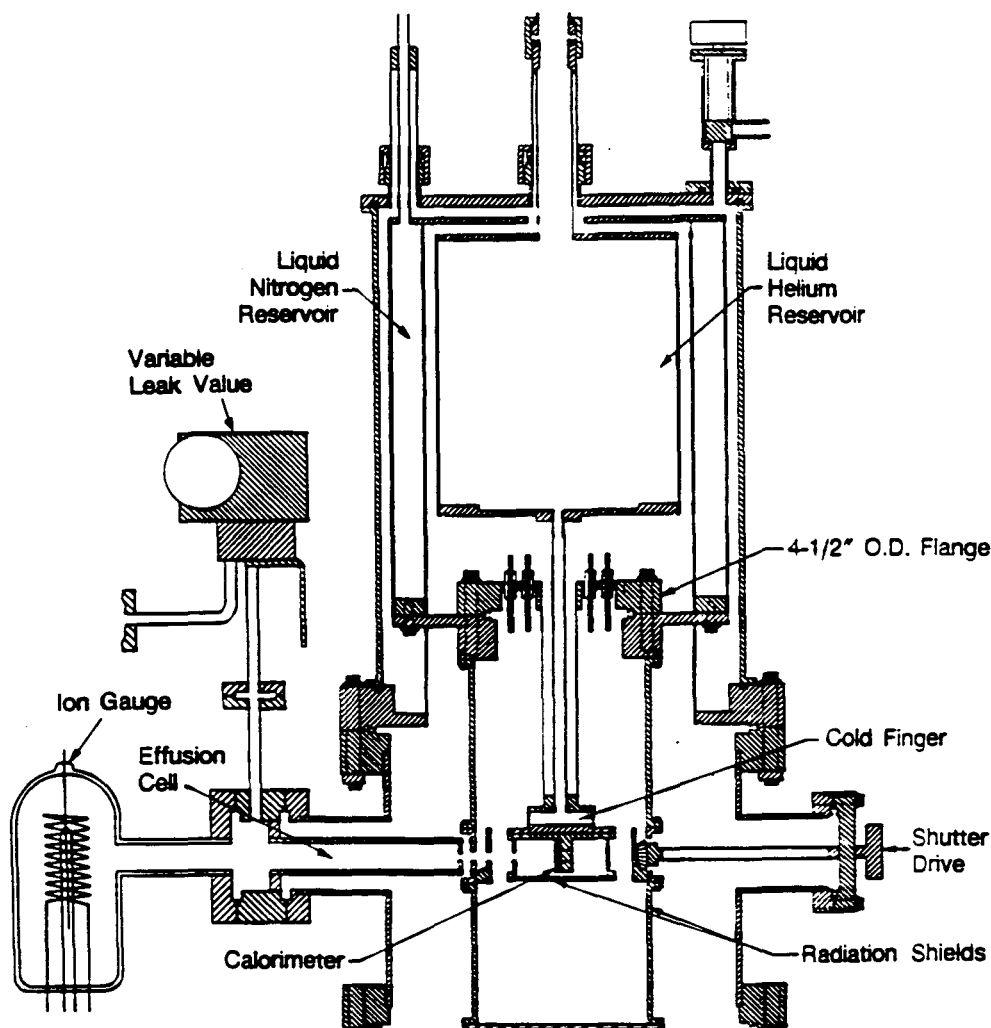
2.3 UHV System and Cryostat

Fig. 2.7 shows a cross-sectional view of the cryostat and the upper part of the UHV system. The cold finger, on which the calorimeter is directly mounted, is filled from the reservoir above with liquid ^4He (LHe) at a temperature of 1.3 K. The cryogenic vacuum surrounding the LHe reservoir is separated from the UHV system by the 4.5 inch (11.4 cm) Cu gasket-sealed flange, and by the thin-walled tubing extending downward from the flange. The cryogenic vacuum is maintained at the low 10^{-6} Torr level by cryopumping on the reservoir walls and by a 40 l/s turbomolecular pump.



XBL 8810-7636A

Figure 2.6 Rear view of the calorimeter mounted in its stainless steel frame. The transistor headers which serve as the heat sinks are soldered to the frame and the Cu mount. The frame is attached to the mount with stainless steel screws (not shown).



XBL 772-7512C

Figure 2.7 Cross-sectional view of the cryostat and the upper portion of the UHV system. The calorimeter is mounted at the end of the LHe cold finger. The system is equipped with an evaporation filament and a mass spectrometer, not shown in this view, at the same level as the effusion cell. Evaporation of metal films and dosing of adsorbates take place through holes in the radiation shields. The direct line-of-sight through these holes can be blocked by a rotating shutter to reduce heating due to thermal radiation.

The cryostat is made entirely of stainless steel. The LHe reservoir is wrapped in several layers of aluminum foil and surrounded by liquid N₂ (LN₂) shielding to reduce radiative heat flow into the bath. The hold time of the pumped LHe bath is approximately eight hours.

The minimum temperature of the pumped LHe bath is 1.3 K. To operate the calorimeter as close to this temperature as possible, the flow of heat to the calorimeter must be minimized. There are two sources of heat which are of concern: conduction down the electrical leads and thermal radiation. To reduce thermal conduction, the electrical leads chosen for their low thermal conductivity pass through three sets of heat sinks. The UHV feedthroughs on the 4.5 inch flange shown in Fig. 2.7 are the first set. This flange is cooled to approximately 100 K by the LN₂ reservoir. The other two sets employ the transistor headers located on the Cu mount, as shown in Fig. 2.6. The leads running between the 4.5 inch flange and the room are commercial coaxial conductors made of stainless steel.¹³ Initially, this coaxial product was also used to make the connection between the flange and the Cu mount. However, the jacket of a coaxial cable creates virtual leaks by trapping pockets of air. Thus, the coaxial conductors between the flange and the mount were replaced by tightly twisted pairs of teflon-coated manganin wire, 125 μm in diameter. The leads between the primary and secondary heat sinks on the Cu mount are bare Cu with a diameter of 75 μm.

Thermal radiation is reduced by two sets of shields, as shown in Fig. 2.7. There are holes in both shields to allow access to the calorimeter. The direct line-of-sight through the shields is blocked by a cooled rotatable shutter, except when access is needed to evaporate metal films or expose the calorimeter to the adsorbate to be studied. The outer shield and shutter, whose temperature is monitored by two chromel-alumel thermocouples, are cooled to approximately 100 K by conduction to the LN₂ reservoir. Indium foil is used to improve the thermal conductivity between the sections of the shield, as described above. The inner shield, which is attached directly to the cold finger, reaches temperatures in the LHe range.

The combined effects of the radiation shielding and the heat sinks allow the calorimeter to be operated as low as 1.6 K. Further reduction in the thermal loading of the calorimeter is possible and could conceivably reduce the minimum temperature by another 0.1–0.2 K. To reach still lower temperatures, a better refrigeration system (e.g., one using ³He) would be

required. A system using ^3He refrigeration has been constructed, and efforts to make heat capacity measurements below 1 K are currently under way.

The lower half of the apparatus is a commercial, 200 l/s ion-pumped UHV system. For most of the measurements presented here, the UHV system was baked to 120°C with the cold finger and cryostat removed and a blank 4.5 inch flange in the place of the cold finger. The system was subsequently vented and purged with dry nitrogen while the blank flange was removed and the cold finger quickly installed. This procedure was necessary because an epoxy¹⁴ which was incompatible with the bake-out had been used in several places on the cold finger and radiation shields. This epoxy is extremely useful in cryogenic applications because its thermal contraction matches that of metals, but it is expected to outgas heavily at the temperature required for the bake-out. It had been used to make heat sinks for electrical leads, to heat sink carbon resistors used for diagnostic thermometers on the LN_2 shields, and to attach charcoal to the LHe shields. Through suitable substitutions, the use of this epoxy has been eliminated in the course of this work. The epoxy-based heat sinks were replaced by transistor headers,¹² the carbon resistors by thermocouples, and the epoxy attaching the charcoal to the LHe shields by an UHV-compatible epoxy.¹⁵ Hence, bake-outs with the cold finger installed are now feasible. The importance of the baking procedure will be discussed in detail in Chapter 4.

After baking but before installing the cold finger, the pressure reaches 2×10^{-10} Torr, as measured by an ion gauge at the perimeter of the vacuum chamber. Following installation of the cold finger, the vacuum system is immediately pumped down, and the cryostat is also assembled and evacuated. As soon as possible, the cryostat is cooled with LN_2 . Cooling the cold finger serves both to greatly reduce the outgassing from its unbaked surface and, eventually, to provide cryopumping. When the cryostat reaches its minimum temperature, the pressure in the UHV system reaches 5×10^{-10} Torr (i.e, a factor of three higher than is obtained in the baked, room-temperature system before venting).

The pressure near the calorimeter is not directly measurable, but it is expected to be significantly lower than the pressure measured near the walls of the chamber. The cold radiation shields which surround the calorimeter function as a cryopump, trapping the molecules which collide against them. Most gases except He and H_2 can be pumped efficiently by cold metallic

surfaces. The charcoal attached to the LHe shields provides pumping for the light molecules.

The UHV system is also equipped with an evaporation filament for depositing metal films on the calorimeter *in situ*. The filament is thoroughly outgassed before the evaporation, and a water-cooled shroud helps reduce heating and outgassing during the evaporation. The pressure in the chamber rises to $\sim 5 \times 10^{-9}$ Torr during the evaporation. The thickness of the film is monitored by a commercial quartz oscillator located near the filament. Typical thicknesses are approximately 500 Å. The structure of the films and details on their growth will be discussed in Chapter 4. An effusion cell is used to expose the calorimeter to the gas to be adsorbed. This cell is filled with gas by opening a leak valve in a stainless steel gas line. The pressure in the cell is typically of the order of 10^{-5} Torr and is measured by an ion gauge. The rate of exposure is calculated from the dimensions of the cell's aperture, its distance from the calorimeter, and the pressure.

The procedures for measuring the heat capacity of adsorbates on metal films are as follows. First, the metal film is evaporated on the substrate. After the system has cooled, the calorimeter is momentarily heated to approximately room temperature to desorb molecules which have accumulated on the surface during cooling. At this point, two standard types of measurements are possible: fixed exposure and fixed temperature.

In a fixed exposure measurement, the heat capacity of the "bare" calorimeter is measured as a function of temperature. After dosing the calorimeter with the adsorbate to be studied, the combined heat capacity of the calorimeter and the adsorbate is measured. Subtraction of the two measurements yields the heat capacity of the adsorbate alone. This procedure is useful for measuring the heat capacity of the adsorbate as function of temperature for a fixed exposure.

In the other standard measurement, the temperature of the substrate is held constant. The heat capacity of the substrate and adsorbate are measured at roughly equal intervals of time as the calorimeter is exposed to the molecular beam from the effusion cell. The heat capacity of the bare calorimeter (recorded before the beginning of the dose) is subtracted from the data. This subtraction yields the heat capacity of the adsorbate as a function of exposure at a given temperature. These two standard measurements complement one another since they follow roughly orthogonal

thermodynamic paths in the coverage-temperature plane. Both types of measurements can be affected by desorption. The effects of desorption become more pronounced as the temperature and coverage are increased.

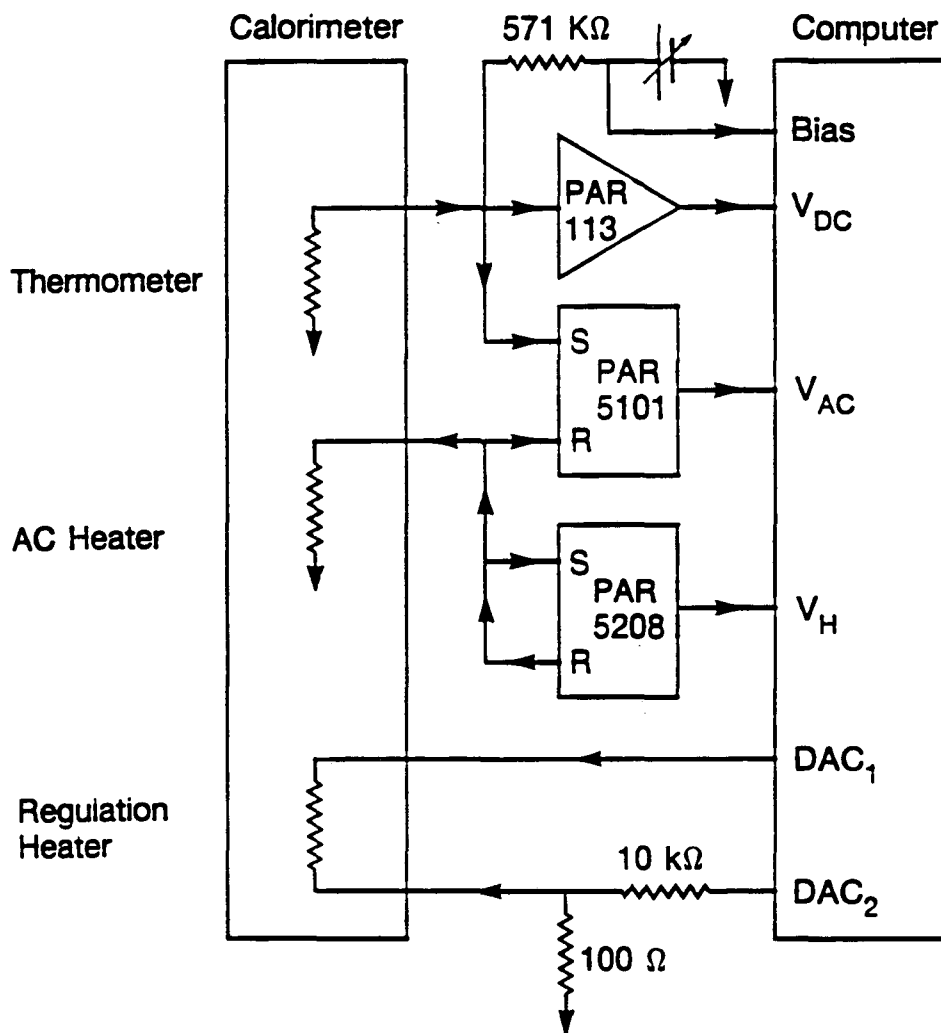
2.4 Measurement electronics

The electronic system used for this measurement can be described in three sections: the ac heater bias, the thermometer bias and readout, and the temperature regulation. A block diagram of the entire measurement circuit is shown in Fig. 2.8.

The ac heater bias voltage is generated by the reference output of a lock-in amplifier.⁵ This source was chosen for its excellent amplitude stability and ease of frequency and amplitude adjustment. The amplitude of this ac bias is measured by the same lock-in amplifier, allowing small amplitude drifts to be removed from the data. This voltage is applied to one of the heaters on the calorimeter and produces a temperature oscillation in the calorimeter.

The dc bias current for the thermometer is produced by two 9 V mercury batteries which are connected in series across a 500 k Ω 10-turn wire-wound potentiometer. The center terminal of the potentiometer is attached to a room temperature metal film load resistor in series with the cold thermometer. The resistance of the load resistor is much greater than that of the thermometer. When used to bias a resistance thermometer whose temperature is oscillating, this current source produces a voltage with both dc and ac components. The dc component is directly related to the average temperature of the calorimeter, while the ac component is used to calculate the heat capacity. The voltage from the thermometer is processed by both a dc preamplifier,⁶ which is low-pass filtered to remove the voltage oscillation, and by a second lock-in amplifier,⁴ which uses the ac heater bias as its reference signal.

An LSI-11 computer with an ADC-DAC board¹⁶ is used to record the measured voltages and to produce the thermal regulation voltage which is applied to one of the commercial NiCr films on the calorimeter. The resolution of the 12-bit DAC on this board is inadequate for the temperature regulation. An effective resolution of 18 bits is obtained by dividing one of the 12-bit DAC channels by 100 and adding it to the other. The voltages are



XBL 8810-7637

Figure 2.8 Schematic diagram of the electronics. The bias across the ac heater is generated by the internal reference of the PAR 5208. The ac and dc parts of the voltage across the thermometer are amplified separately. Thermal regulation and data acquisition are controlled by an LSI-11 computer.

generated by separate DAC channels with a common ground, and so neither of the wires leading to this heater can be externally grounded.

The computer program regulates the temperature and collects the data as follows. The total dc bias applied to the load resistor and thermometer is monitored by one channel of the ADC. Another channel monitors the output of the dc preamplifier. The computer program calculates the average resistance of the thermometer from these two voltages, and then calculates the temperature of the calorimeter. The regulation voltage is then adjusted by the computer so as to reduce the difference between the measured temperature and the specified temperature. Once the temperature of the calorimeter has been within 0.02% of the specified temperature for 10 lock-in time constants, the computer begins to record the outputs of the two lock-in amplifiers. The heat capacity is computed from Eq. (2.2). When the signals have been averaged for a specified length of time, a new temperature is selected and the process begins again. This continues until the temperature scan is completed. Typically, a 40-point scan takes less than 30 minutes to complete. This is important, as the experiments are limited to 8 hours by the hold-time of the cryostat.

2.5 Constraints of the Method

In contrast to conventional methods for measuring surface heat capacities, which employ a closed cell, the technique reported here is performed in UHV. An adsorbed film whose equilibrium vapor pressure is greater than the partial pressure of the adsorbed species in the vicinity of the calorimeter will desorb. For H₂ multilayers, such desorption becomes rapid on the time scale of the measurement near 3.7 K. Thus, desorption limits the range of coverage and temperature which can be studied using the ac calorimetric technique.

The absence of a gas phase in equilibrium with the film also makes the adsorption isotherm,¹⁷ a standard measurement in closed-cell systems, unsuitable for the present technique. In adsorption isotherms, the coverage of the adsorbate is measured as a function of the equilibrium vapor pressure P . The scale for P is set by the saturated vapor pressure P_0 , which is typically of the order of 10 Torr. In principle, the calorimeter could be contained within a closed cell filled with vapor. However, the thermal conductance of

the gas would become comparable to the $\sim 10^{-6}$ W/K conductance of the electrical leads of the calorimeter for vapor pressures greater than $\sim 10^{-7}$ Torr.

At present, the temperature range of the calorimeter is limited to 1.6 – 4.2 K. The lower limit is discussed above. The upper limit is imposed by the technique for calibrating the thermometers, which requires submersion in LHe. Thermometers like those used in this study can be calibrated above 4.2 K if they are heat sunk to a stage which can be heated above the temperature of the bath. Thermometers with significantly lower concentrations of dopants must be used for measurements above ~ 10 K. Also, the heat capacity of the substrate rises as T^3 as the temperature is increased, making the calorimeter less sensitive. Conversely, cooling the calorimeter to lower temperatures decreases the heat capacity of the substrate and makes the calorimeter more sensitive. Efforts to extend the lower limit of the temperature range to 300 mK are in progress and will be described in Chapter 5.

References

- ¹T. W. Kenny, Ph.D. thesis, University of California, Berkeley, 1989.
- ²T. W. Kenny, P. L. Richards, I. S. Park, E. E. Haller and J. W. Beeman, *Phys. Rev. B* **39**, 8476 (1989).
- ³T. W. Kenny and P. L. Richards, *Rev. Sci. Instrum.* **61**, 822 (1990).
- ⁴PAR 5101, Princeton Applied Research, Inc., Princeton, NJ.
- ⁵PAR 5208, Princeton Applied Research, Inc., Princeton, NJ.
- ⁶PAR 113, Princeton Applied Research, Inc., Princeton, NJ.
- ⁷MSTF-3-S-N-1K-02, Mini-Systems, Inc., North Attleboro, MA.
- ⁸Epo-Tek H20E, Epoxy Technology, Inc., Billerica, MA.
- ⁹E. E. Haller, *IR Phys.* **25**, 257 (1985).
- ¹⁰M. T. Loponen, R. C. Dynes, V. Narayanamurti and J. P. Garno, *Phys. Rev. B* **25**, 1161 (1982).
- ¹¹D. McCammon, S. H. Moseley, J. C. Mather and R. F. Mushotzky, *J. Appl. Phys.* **56**, 1263 (1984).
- ¹²A08-600-0010, Airpax Corp., Cambridge, MD.
- ¹³Ultra-Miniature Coaxial Cable, Type S1, Lake Shore Cryotronics, Inc., Westerville, OH.
- ¹⁴Stycast 2850-FT, Emerson and Cuming, Inc., Woburn, MA.
- ¹⁵Vac-Seal Epoxy, 288-6000, Perkin Elmer Vacuum Products Division, Eden Prairie, MN.
- ¹⁶DT2785-DI/5716-B-PGL, Data Translation, Inc., Marlboro, MA.
- ¹⁷J. G. Dash, Films on Solid Surfaces, (Academic Press, New York, 1975) pp. 215-218.

3. Results for H₂ Multilayers

3.1 Introduction

In this chapter, we discuss an application of the ac calorimetric technique to a study of orientational ordering in H₂ multilayers. The properties of this ordering transition have been thoroughly studied in the case of bulk H₂, but relatively little is known about this transition in H₂ adsorbed on surfaces. Our measurements show that a remnant of the bulk transition persists in films of H₂ as thin as 2–3 monolayers. The properties of phase transitions with a small number of particles N , where N is of order 10^2 or less in the case of first-order transitions, have recently received considerable attention. Such systems are said to exhibit finite-size effects.¹ Measurements of H₂ adsorbed on metallic surfaces are also of considerable interest following a recent report of extremely rapid ortho-to-para conversion on Ag(111).² In the present work, signs of finite-size effects are evident at the lowest exposures measured, and the rate of ortho-to-para conversion is comparable to that normally observed in bulk H₂.

We begin in section 3.2 by discussing previous work on the orientational ordering transition in H₂. The experimental apparatus and techniques were described in the previous chapter. Section 3.3 presents our measurements of the heat capacity of H₂ multilayers adsorbed on evaporated Au films and on sapphire. We defer a detailed consideration of the characterization of the Au films until Chapter 4, since an understanding of the heat capacity measurements themselves is necessary to properly assess the quality of the substrate. Section 3.5 presents the discussion of the data. Conclusions are drawn in the final section.

3.2 Previous Work

Hydrogen is known to occur in two states, which are designated ortho (o) and para (p).³ In o-H₂, the nuclear spins are aligned, yielding a symmetric nuclear wave function. Because the protons are indistinguishable fermions, the total molecular wave function must be antisymmetric. Thus, the rotational wave function is antisymmetric, and the rotational quantum number J is odd. In p-H₂, the nuclear and rotational symmetries are reversed, and J is even. For $T \lesssim 20$ K, only the $J = 0$ and $J = 1$ states are thermally populated. With reference to this limit of low temperature, we

designate the concentration of p-H₂ (including all states with even J) as c_0 and that of o-H₂ (including all states with odd J) as c_1 .

For H₂ in equilibrium at room temperature, known as normal-H₂ or n-H₂, c_1 exceeds c_0 by a ratio of 3 to 1. Because the $J = 0$ state is the ground state, the equilibrium value of c_0 rises as the temperature falls, reaching 0.998 at $T \approx 20$ K. Conversion from the ortho to the para state requires interaction with a magnetic field gradient and is normally quite slow. The intrinsic conversion rate in solid H₂ is 1.9% per hour. Samples with high concentrations of p-H₂ are prepared either by holding the sample at low temperature for many days, or through the use of catalysts.³

The rotational state of the molecule affects its interactions with other molecules. Ortho-H₂ molecules possess an electric quadrupole (EQ) moment and exhibit anisotropic interactions. For p-H₂ molecules, the EQ moment is zero and interactions with other molecules are isotropic. For simplicity, we may think of p-H₂ molecules as spheres, and o-H₂ molecules as ellipsoids.⁴ The EQ moment of the o-H₂ molecules drives an orientational ordering transition in solid H₂ at LHe temperatures.⁵ Fig. 3.1 shows a plot of the specific heat as a function of temperature for various concentrations of o-H₂. For $c_1 = 0.005$, there is no ordering, and the T^3 dependence of a Debye solid is observed. As c_1 is increased, Schottky anomalies due to the ordering of isolated pairs of $J = 1$ molecules become evident. Above a critical concentration $c_1 = 0.56$, the ordering becomes cooperative (i.e., there is a true phase transition.) For $c_1 = 0.74$, there is a first-order transition at $T_c = 1.6$ K. The specific heat exhibits a sharp peak at T_c and anomalous contributions at higher temperatures. The properties of this fascinating transition have been thoroughly studied and are reviewed by Silvera.³

Most studies of adsorbed H₂ have focused on p-H₂ because of its similarity to ⁴He.⁶⁻⁸ The phase diagram for monolayers of p-H₂/graphite is similar to that shown in Fig. 1.2 for ⁴He/graphite, except that the phase boundaries are scaled to higher temperatures by a factor of 5-10.^{7, 9} Measurements for monolayers and multilayers of p-H₂/MgO locate the phase boundaries for this system at 7-10 K.⁸ Thus, adsorbed H₂ is expected to solidify for all temperatures in the range of the present technique (1.6-4.2 K).

To our knowledge, there is only one set of measurements for adsorbed o-H₂. Kubik *et al.* have studied monolayers of o-H₂/graphite using nuclear magnetic resonance.¹⁰ They find an orientational ordering transition at 600

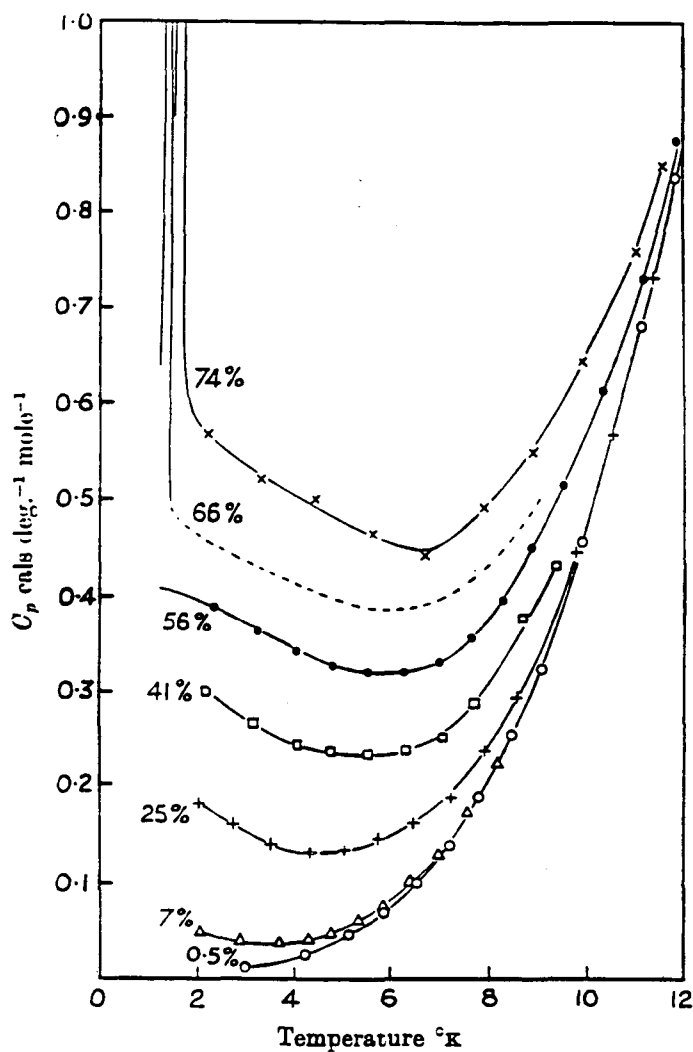


Figure 3.1 Specific heat as a function of temperature for bulk solid hydrogen. The concentration of ortho- H_2 for each measurement is shown beside the corresponding curve. The sharp peak near 1.6 K is due to the orientational ordering transition of the ortho molecules. From Hill and Ricketson.⁵

mK for $c_1 = 0.90$. For $c_1 = 0.77$, the transition temperature drops to 330 mK. No heat capacity measurements of this transition have been made, and the crossover between the monolayer and bulk transitions has not been studied.

The growth mode of H_2 multilayers has also been investigated. Migone *et al.* have shown that H_2/Ag exhibits triple-point wetting.¹¹ As explained in Section 1.4, this term applies to systems which show complete wetting above the triple point and incomplete wetting below it. The triple point of H_2 is 14 K. Thus, in the temperature range accessible to the present technique, H_2 is expected to form a very thin film of only one or two monolayers before the onset of coexistence with bulk-like islands.¹²

Finally, extremely rapid ortho-to-para conversion has been reported by Avouris *et al.* for H_2 adsorbed on Ag(111) and evaporated Ag films.² Coverages of approximately four monolayers of n- H_2 were found to be essentially completely converted to p- H_2 within one to two minutes after the exposure. This rate is much faster than that observed for bulk H_2 . It is also two orders of magnitude faster than the rate observed in similar measurements for $H_2/Cu(100)$.¹³ A recent theory attributes the rapid conversion observed by Avouris *et al.* to a novel mechanism involving the creation of electron-hole triplet pairs in the metal substrate.¹³ A special electronic surface state is found to enhance the rate expected from this mechanism by approximately two orders of magnitude. This special surface state is present on the (111) faces of all the noble metals, but not on faces with other orientations. Thus, the theory accounts for the large difference in rates observed in the experiments on Ag(111) and Cu(100).

3.3 Results

We have measured the heat capacity of H_2 adsorbed on evaporated Au films and on sapphire at temperatures from 1.6 to 3.7 K. Results obtained on both substrates were generally found to be similar. Most of our measurements were made using n- H_2 , but some measurements were also made using H_2 with $c_0 = 0.95$. The p- H_2 was prepared using techniques similar to those described by Silvera, and the ortho/para ratio was determined using Raman spectroscopy.³

Typical data for the heat capacity of H_2 multilayers as a function of temperature are shown in Fig. 3.2. The data in the figure are for H_2/Au ; similar data have been observed for $H_2/sapphire$. The two sets of data shown

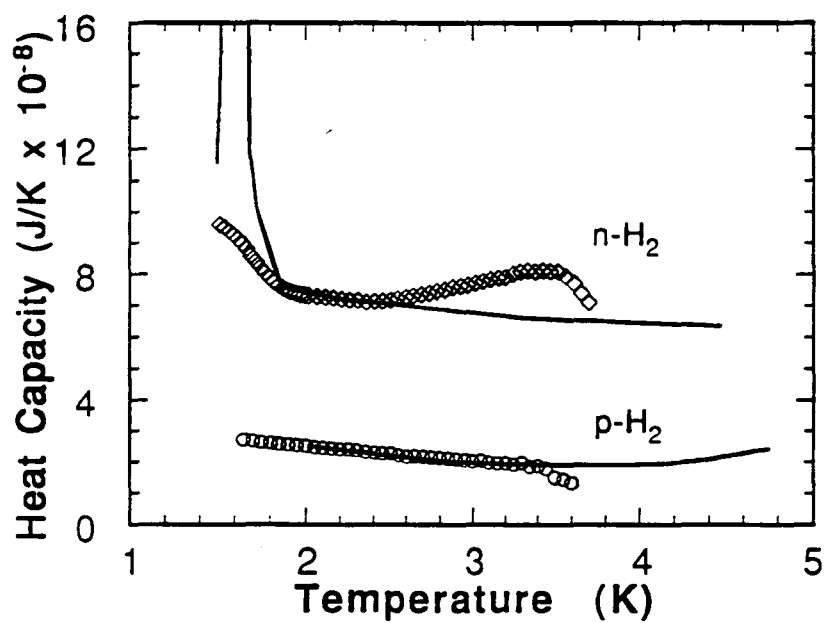


Figure 3.2 Typical results for the heat capacity of identical 3.3 \AA^{-2} exposures of n-H₂ and p-H₂ adsorbed on Au. The nominal coverage in monolayers for the n-H₂ sample is $n = 25$. The solid curves show the data for bulk H₂ with $c_1 = 0.74$ and $c_1 = 0.07$, separately scaled to match the corresponding multilayer data at 2.2 K.

correspond to 3.3 \AA^{-2} exposures of n-H₂ and p-H₂. Both sets of data exhibit a decrease in heat capacity near 3.6 K due to desorption of H₂ from the calorimeter. Apart from this decrease, the data for p-H₂ are nearly independent of temperature. However, the data for n-H₂ show two other features: an increase from 1.8 K to the lowest temperature measured, and a broad maximum at 3.5 K. The rise at 1.8 K is believed to be a portion of a peak located just below our minimum temperature. This interpretation is supported by the data shown in Fig. 3.3, in which the peak has evidently shifted up into our temperature range. For simplicity, we will refer to this feature as a "peak" throughout this work, even when the top of the peak is not observed. The lower limit on the temperature range of the present measurements is imposed by our method of refrigeration (i.e., pumping on liquid ⁴He). Measurements at lower temperatures are clearly desirable and are in progress.¹⁴

It is instructive to compare these data with previous measurements of the specific heat of bulk H₂. The solid curves in Fig. 3.2 represent the data of Hill and Ricketson⁵ for H₂ with $c_1 = 0.74$ and $c_1 = 0.07$, separately scaled to match the multilayer data at a temperature of 2.2 K. We note that there is qualitative agreement between the multilayer and bulk measurements. The low temperature peak seen in multilayers of n-H₂ appears to be a broadened remnant of the sharp peak observed in the bulk due to orientational ordering of the o-H₂ molecules. There is no feature in the bulk data corresponding to the maximum at 3.5 K in the multilayer data.

Results for n-H₂ multilayers on some surfaces showed behavior which was in considerably closer agreement with that of bulk H₂. Figs. 3.3 and 3.4 show results for H₂/sapphire and H₂/Au, respectively. Each figure shows data corresponding to four different exposures of H₂. The topmost curve in each figure corresponds to the exposure of the data shown in Fig. 3.2. As before, the solid curves show the data for bulk H₂ with $c_1 = 0.74$, scaled to match the multilayer data at 2.2 K. We see that the peak in Fig. 3.3 is sharper than that of Fig. 3.2. As mentioned earlier, it has shifted up into our temperature range. The high temperature peak is absent. In Fig. 3.4, the increase near 1.9 K is the sharpest we have observed. The results on this Au film were reproducible in a set of measurements lasting over a week.

In all measurements of n-H₂ multilayers, the low temperature peak was suppressed as the exposure was decreased. This effect is shown in Figs.

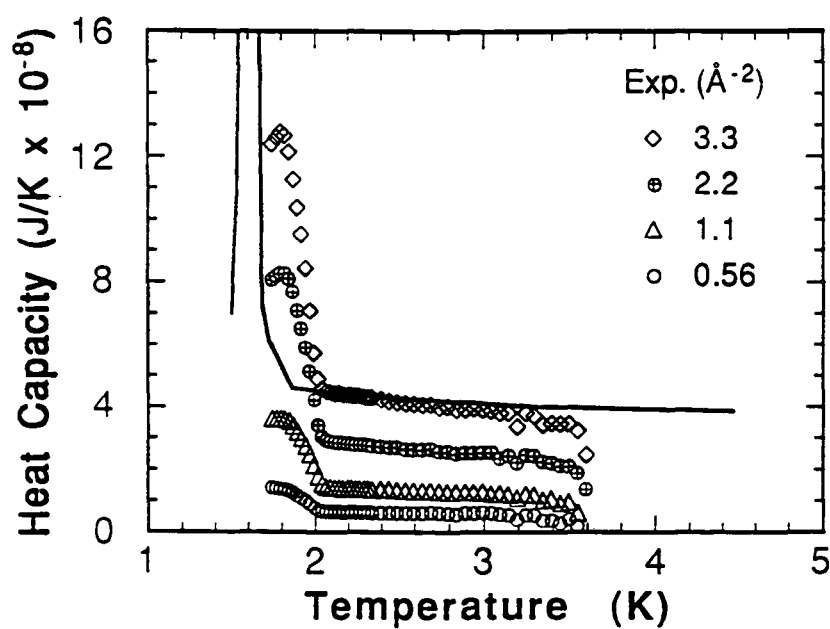


Figure 3.3 Heat capacity as a function of temperature for four exposures of n-H₂/sapphire. Nominal coverages n in monolayers are \diamond , 25; \oplus , 16; Δ , 8; \circ , 3. The solid curve shows the data for bulk H₂ with $c_1 = 0.74$, scaled to match the topmost multilayer curve at 2.2 K.

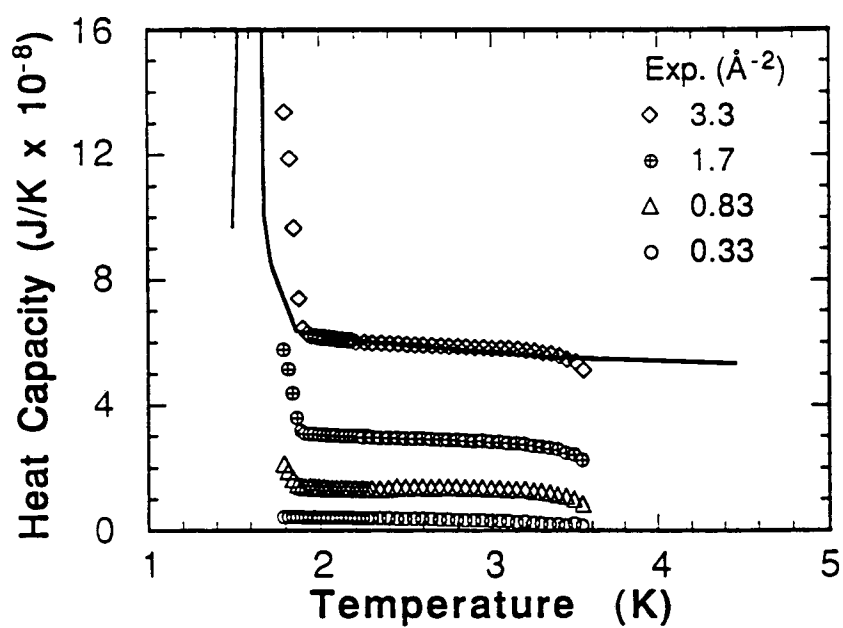


Figure 3.4 Measurements similar to those described in Fig. 3.3 with an evaporated Au film as the substrate. Nominal coverages n in monolayers are \diamond , 25; \oplus , 12; Δ , 5; \circ , 1. The solid curve shows the data for bulk H_2 , as described in Fig. 3.3.

3.3 and 3.4. The behavior of the peak for low exposures is shown in greater detail in Fig. 3.5. For all exposures except the lowest, some sign of the peak is still evident above 1.7 K.

The sticking coefficient for n-H₂ incident on a 3 K Si bolometer has been measured by Govers *et al.*¹⁵ Using their results, we can compute a nominal coverage n . We report n in monolayers (ML), where 1 ML is defined to be 0.1 Å⁻². The values of n for the measurements shown in Figs. 3.3 and 3.4 range from 1 to 25 ML, and the range for Fig. 3.5 is 1 to 2 ML. Thus, anomalous contributions to the heat capacity are obtained for all values of n greater than one.

The heat capacity of H₂ multilayers has also been measured as a function of exposure at fixed temperatures for exposures up to 0.8 Å⁻². As can be seen in Fig. 3.6, the data exhibit two linear segments at low exposure, with abrupt changes in slope or "kinks" at 0.05 and 0.21 Å⁻². At higher exposures, the data measured at 2.1 K show a slight downward curvature. The data measured at 2.4 K are unchanged up to the second kink, but beyond this point the rise in the heat capacity is less rapid than at the lower temperature.

For comparison, we have superimposed a plot of the binding energy as a function of exposure from the work of Govers *et al.* The binding energy is high initially, when H₂ molecules stick directly to the substrate, but by an exposure of ~0.3 Å⁻², it falls to a limiting value of 103 K, the energy of sublimation of a H₂ molecule bound to the surface of bulk H₂. We note that the kinks in the heat capacity data coincide with similarly abrupt changes observed in the binding energy. The arrow marked "1 ML" indicates the exposure at which monolayer completion was thought to occur in the sticking study.

We have also observed a decrease in the heat capacity of H₂ multilayers as a function of time. We attribute this decrease to desorption. For a n-H₂ multilayer with $n \approx 14$, the rate of decrease dC/dt was $(-7.4 \pm 1.1) \times 10^{-13}$ JK⁻¹s⁻¹, or 5.8% of the heat capacity of the multilayer per hour. To convert dC/dt to a rate of desorption, we again make use of the sticking coefficient results of Govers *et al.* Furthermore, we approximate dC/dn by $\Delta C/\Delta n$, where ΔC and Δn are the total heat capacity and coverage of the multilayer, respectively. We find the desorption rate dn/dt to be $(-2.1 \pm 0.3) \times 10^{-4}$ s⁻¹. The temperature dependence of this rate is strong. At 3.6 K, the rate was

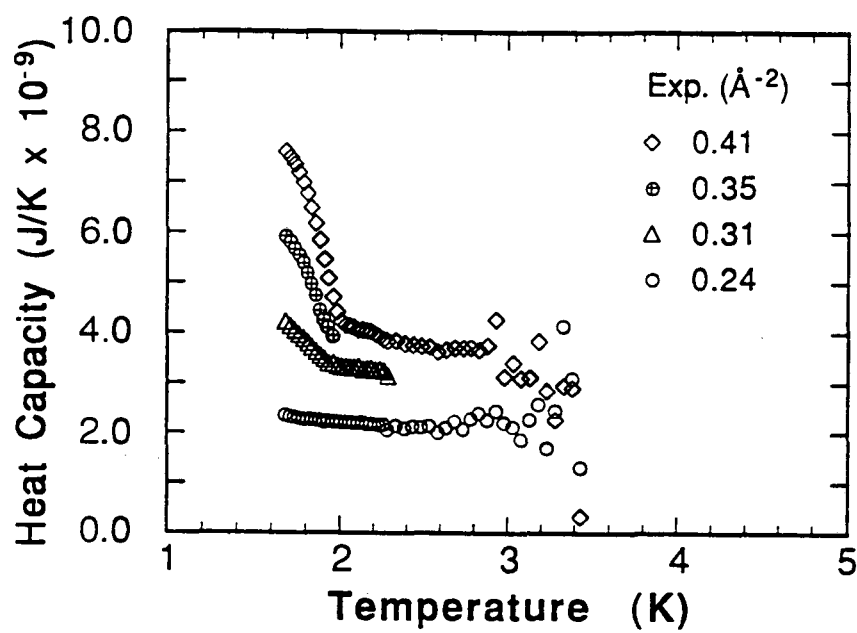


Figure 3.5 Heat capacity as a function of temperature for low exposures of n-H₂ on sapphire. Nominal coverages n in monolayers are \diamond , 1.9; \oplus , 1.5; Δ , 1.2; \circ , 0.7. The uncertainty in n is ± 0.2 .

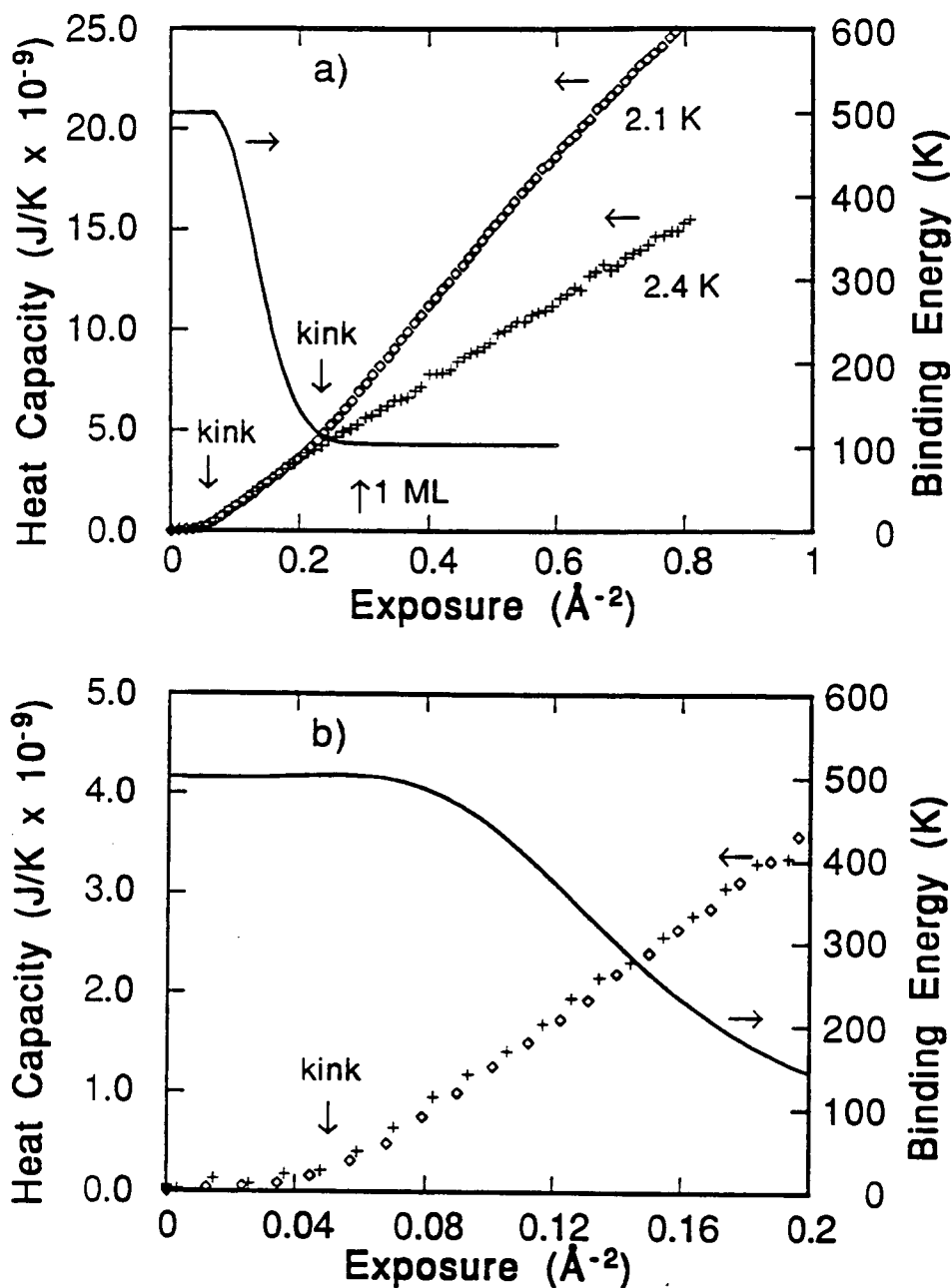


Figure 3.6 a) Heat capacity as a function of exposure for n-H₂/sapphire at two substrate temperatures. The solid curve shows the binding energy as a function of exposure for n-H₂ on a 3 K Si bolometer, from the work of Govers *et al.*¹⁵ The arrow marked "1 ML" shows the exposure at which monolayer completion was thought to occur in Govers *et al.*

b) The data for the lowest exposures in a) plotted on an expanded scale.

observed to be approximately -0.1 s^{-1} . Since this rate is rapid on the time scale of our measurements, it causes sharp, irreversible drops in the heat capacity near 3.6 K. These drops are evident in Figs. 3.2–3.4. Repeated measurements on the same H_2 multilayer produce a family of curves which are similar in appearance to those in Figs. 3.3 and 3.4, confirming that the time dependence of the heat capacity is due to desorption.

Finally, we have made repeated measurements on one sample of $n\text{-H}_2$ to look for changes in the peak as a function of time. Fig. 3.7 shows two successive measurements, each of which lasted ~ 20 minutes. The heat capacity is slightly lower in the second measurement, which is probably due to desorption. It is possible that there is a slight shift of the peak to lower temperatures. If so, the shift is less than 25 mK.

3.4 Discussion

On the basis of the qualitative agreement between the present measurements for H_2 multilayers and previous measurements for bulk H_2 , we assign the peak observed in the heat capacity as a function of temperature of $n\text{-H}_2$ multilayers to a bulk-like orientational ordering transition. The observation of signs of this peak for n as low as two indicates that the growth of the bulk phase begins after the completion of only one to two uniform monolayers. These results are consistent with those of Migone *et al.*, who showed that H_2 wets Ag incompletely below its triple point T_t , where $T_t = 14 \text{ K}$.¹¹ They observe growth of as many as 23 ML just below T_t , but in the temperature range of the present measurements, formation of only one or two uniform monolayers is expected.¹²

The data for the heat capacity as a function of exposure are also consistent with the expected structure: the linear regions and kinks at low exposure give evidence of the formation of a tightly bound monolayer, while the temperature dependence and the absence of kinks in the region beyond 0.21 \AA^{-2} are consistent with the growth of a less tightly bound, bulk-like phase.

As was shown in Figs. 3.3 and 3.4, the orientational ordering peak is suppressed as the exposure is decreased. We have replotted the data for several exposures of $n\text{-H}_2$ on sapphire in Fig. 3.8. A linear fit to the data above the peak has been subtracted, and the sticking measurements of Govers *et al.* have again been used to obtain the nominal coverages and to normalize

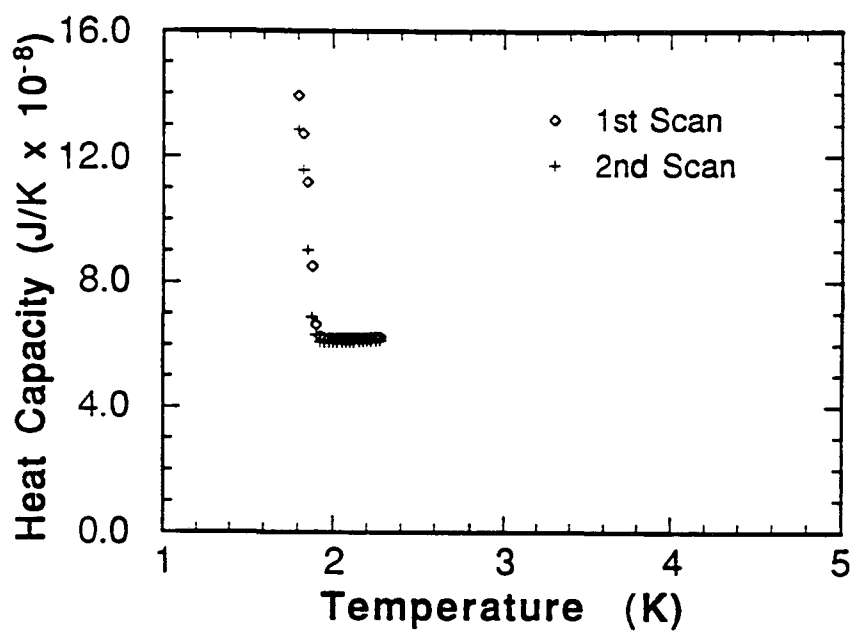


Figure 3.7 Two successive measurements of the heat capacity as a function of temperature for the same sample of n-H₂/Au. The exposure for this measurement was 3.3 Å⁻².

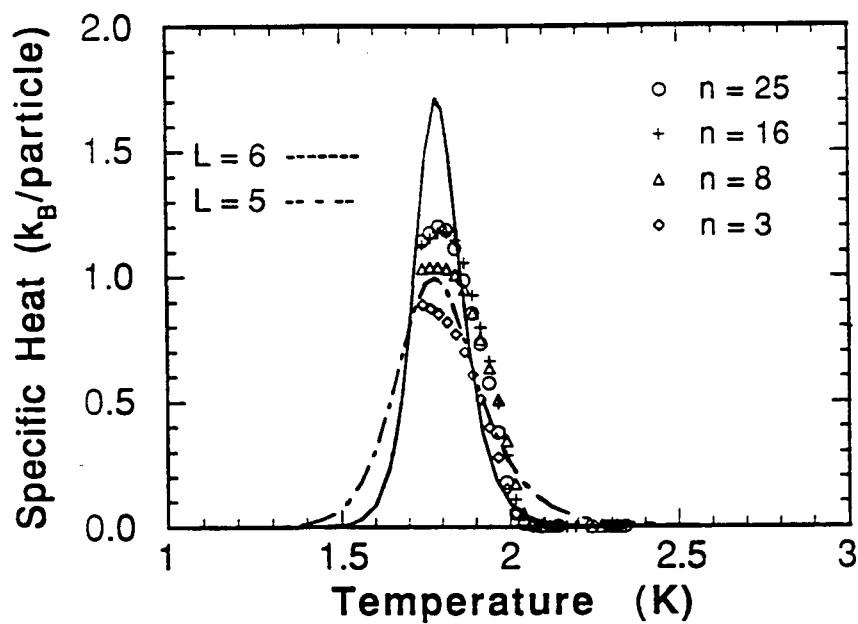


Figure 3.8 The results from Fig. 3.3, normalized according to the nominal coverage n . A linear fit to the data above the peak has been subtracted from the data. The solid and dashed curves show the prediction of the model of Challa *et al.*¹⁶ for a first-order transition broadened by finite-size effects, as described in the text.

the data to specific heats in k_B per particle. The peak shifts to higher temperature and grows in height with increasing exposure.

In view of this exposure dependence, we have analyzed our data for evidence of finite-size effects. The orientational ordering transition is known to be first-order in bulk H_2 . The theory of finite-size effects in first-order transitions has recently attracted considerable attention.^{1, 16-20} Agreement with theory has been demonstrated in both simulations¹⁶ and experiments.¹⁸⁻²⁰ However, there are few experimental studies in this area.

The qualitative behavior of a first-order transition broadened by finite-size effects can be demonstrated through a simple calculation due to Imry.¹ The temperature fluctuations in a small system are given by the well-known result^{1, 21}

$$\langle(\Delta T)^2\rangle = \frac{k_B T^2}{N c_v} \quad (3.1)$$

where N is the number of particles and c_v is the heat capacity per particle. We assume that the latent heat per particle A is the same in the finite system as in an infinite system. We denote the transition temperature by T_c and the broadened width of the transition by ΔT_c . The order of magnitude of c_v is then given by $A/\Delta T_c$. We also assume that the temperature fluctuations given by Eq. (3.1) correspond to the broadened width ΔT_c . With these substitutions, we obtain

$$\frac{\Delta T_c}{T_c} \sim \frac{k_B T_c}{NA} \quad (3.2)$$

The primary result is that the fractional width of the transition is inversely proportional to N .

A detailed theory of these effects by Challa, Landau and Binder (CLB)¹⁶ makes quantitative predictions for the peak in the specific heat in a form which facilitates comparison with experimental data. They approximate the distribution function for the energy of a finite system by a superposition of weighted Gaussian functions corresponding to the ordered and disordered phases. Their results are expressed as a function of the system size L in units of the lattice constant. For a system in d dimensions, the width of the peak is

found to be proportional to L^{-d} , in agreement with the $1/N$ dependence of Eq. (3.2).

We have analyzed the data of Fig. 3.8 in terms of the model of CLB. Several quantities derived from the experimental data are used as parameters in the model: these include the specific heats C_+ and C_- , the latent heat $E_+ - E_-$, and the transition temperature T_c of the infinite system. The subscripts + and - refer to the phases above and below the transition, respectively. Since our temperature range does not extend to sufficiently low temperature to allow measurement of all the relevant parameters, we assume for the sake of the analysis that $C_+ = C_-$. We denote the experimental value for the transition temperature as T_c^{exp} . When T_c^{exp} falls within our temperature range, we approximate $E_+ - E_-$ by doubling the appropriate integral over the half of the peak above T_c^{exp} . The value of $E_+ - E_-$ computed in this way fluctuates by approximately 10% for the different exposures shown in Fig. 3.8. Since the predictions of the theory are far more sensitive to L than to $E_+ - E_-$, we have used the average of the values for $E_+ - E_-$ calculated for the different exposures. Lastly, in our model of the system, we consider the islands of H_2 to be three-dimensional, with equal size L in each dimension.

The results obtained for three values of L from the model of CLB are shown by the curves in Fig. 3.8. Widths comparable to those observed in the experimental data are obtained for values of L between 5 and 6. However, the height and width of the peaks predicted by the model vary rapidly with L , whereas the peaks observed in the experimental data exhibit a very weak dependence on coverage for $n > 3$. This discrepancy is shown more clearly in the plot of fractional width (FWHM/ T_c) as a function of coverage shown in Fig. 3.9. The straight line in the figure shows the prediction of the model, assuming $L = n$.

The theory of CLB also predicts shifts in the temperature of the specific heat maximum as a function of L , denoted as $T_c(L)$. Quantitative estimates of these shifts requires the values of both C_+ and C_- . Therefore, such estimates are not possible for the present system without measurements at lower temperatures. However, the order of magnitude expected for the fractional shift is given by

$$\frac{\delta T_c}{T_c} \equiv \frac{T_c(L) - T_c}{T_c} \sim L^{-d}. \quad (3.3)$$

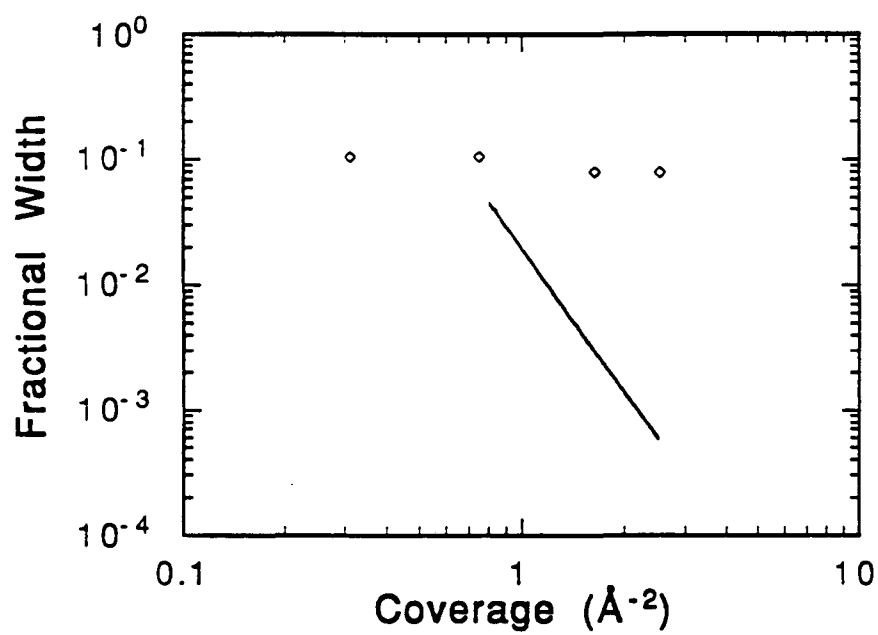


Figure 3.9 The fractional width as a function of coverage for the data shown in Fig. 3.8. The solid line shows the predictions of the model of Challa *et al.*¹⁶

Assuming $L = 3$, we find $\delta T_c/T_c \sim 0.04$. In comparison, we observe that $\delta T_c^{\text{exp}}/T_c^{\text{exp}} \geq 0.04$ for $n = 3$, in qualitative agreement with the expected shift. The high coverage limit of T_c^{exp} for the data shown in Fig. 3.8 is $1.80 \pm .01$ K. The measured value for T_c in bulk H_2 is 1.60 K, hence the high coverage limit of T_c^{exp} is 0.2 K higher than expected. We note, however, that T_c^{exp} depended on the substrate used and was below our temperature range (i.e., below 1.7 K) for all coverages on most substrates. In summary, qualitative agreement with a model of finite-size effects is observed in the present work for coverages $n \lesssim 8$. At higher coverages, finite-size effects are not observed.

We have noted that finite-size effects do not explain the behavior observed at coverages $n > 8$. Furthermore, the width and position of the peak are observed to vary on different substrates. Hence, we conclude that disorder in the adsorbed H_2 and/or heterogeneity of the substrate dominate the behavior of the peak in the specific heat. Disorder in the adsorbed multilayers is likely since they are grown by means of quench-condensation, a non-equilibrium process. Recent surface plasmon measurements by Albrecht *et al.*²² provide evidence of considerable disorder in quench-condensed H_2 films. Furthermore, these authors report that annealing for several minutes at 2.5 K produces irreversible changes in the structure of their films. We have also observed effects due to annealing in some of our thinnest films ($n < 1$). We have attempted to anneal thick films ($n \sim 25$) by heating them to temperatures near the desorption temperature for several seconds. However, such annealing results in significant reduction in the measured heat capacity without significant changes in the width or location of the peak. Finally, annealing of thick H_2 films is expected to be problematic on the basis of measurements of thermal diffusion in bulk H_2 . Diffusion becomes important in the bulk at $T \approx 10$ K,³ but desorption of our H_2 films occurs at ~ 3.7 K. Thus, the quench-condensed H_2 is likely to be disordered, and this disorder is a potential source of broadening.

Heterogeneity of the substrate is another potential source of broadening. Heterogeneity usually arises from structural defects or chemical contamination. The sapphire substrates employed in this study are atomically rough and are exposed to air prior to installation in the vacuum system. Hence, heterogeneity is expected for these substrates.

The homogeneity of the Au films is expected to be superior to that of the sapphire substrates, but our measurements indicate that heterogeneity still plays a significant role. The Au films are evaporated *in situ*. During evaporation, the cryostat is at LHe temperature, but the sapphire is heated to approximately room temperature. The rate of deposition is 1–2 Å/s, and the incidence of the Au flux is within 30° of normal. The thickness of the films used in this work was ~100 Å to ~500 Å. We have also deposited Ag films using similar parameters. These procedures are expected to produce a relatively smooth polycrystalline film with crystallites ~300 Å in size.²³⁻²⁵ Scanning electron and scanning tunneling micrographs of our films are consistent with the structure which is expected from the literature. Grain boundaries and lesser defects such as steps are known to be sources of heterogeneity, and it is likely that the structural defects in our Au films have contributed to the broadening of the orientational ordering peak. It is possible that variations in these defects from calorimeter to calorimeter contribute to the differences in the peak evident in Figs. 3.2–3.4.

Krim²⁵ and other workers²⁴ have shown that the homogeneity of evaporated Au films can be improved by using higher substrate temperatures (100 – 200°C) during evaporation. Increasing the temperature of the substrate produces crystallites which are larger and which exhibit a stronger preference for (111) orientation. This observation may explain the sharp peaks shown in Fig. 3.4. The film used for the measurements shown in that figure is believed to have been heated to a temperature significantly greater than that of our other Au films. Clearly, measurements on films deposited on substrates heated to higher temperatures are of interest and will be carried out.¹⁴

To protect against contamination, our Au films are evaporated *in situ*. Prior to evaporation, the Au-covered filament is outgassed. During evaporation, a shroud which surrounds the filament is water-cooled to further reduce outgassing, and the pressure in the chamber rises to $\sim 1 \times 10^{-9}$ Torr. Furthermore, the calorimeter is surrounded by LHe-cooled radiation shields which act as a cryopump. Despite these precautions, it is possible that local outgassing occurs in the vicinity of the filament or the calorimeter during deposition of the film. Hence, the Au film may exhibit heterogeneity due either to its structure or to residual impurities. We will consider these issues in greater detail in Chapter 4.

It is of interest to relate the desorption results reported in Section 3.3 to previous measurements. Benvenuti *et al.*²⁶ have measured the equilibrium pressure P^* as a function of coverage and temperature for H_2 adsorbed on stainless steel and other surfaces. To facilitate comparison with their work, a relationship between the desorption rate and P^* is needed. Using simple arguments from kinetic theory, it can be shown²⁷ that $|dn/dt| = (\alpha P^*/N_0) (2\pi k_B T m)^{-1/2}$, where dn/dt is the rate of desorption from an adsorbed film in s^{-1} , α is the sticking coefficient, P^* is the equilibrium pressure in the gas phase, N_0 is the number of molecules in one monolayer, and m is the mass of the adsorbate. Using $\alpha = 0.8$ and $N_0 = 1 \times 10^{15} \text{ cm}^{-2}$, we find $P^* = 3.56 \times 10^{-8} (TM)^{1/2} |dn/dt|$, where P^* is in Torr, T is in K, and M is the molecular weight. Thus, from the desorption rates reported in Section 3.3, we find $P^*(2.5K) = (1.7 \pm 0.2) \times 10^{-11} \text{ Torr}$, and $P^*(3.6K) \sim 8 \times 10^{-9} \text{ Torr}$. These values are in good agreement with those reported by Benvenuti *et al.* for adsorbed H_2 at a coverage of 10 ML: $P^*(2.5K) = 2.2 \times 10^{-11} \text{ Torr}$ and $P^*(3.6K) = 2.0 \times 10^{-8} \text{ Torr}$.

Benvenuti *et al.* have shown that their data for thick H_2 multilayers are consistent with the predictions of the Clausius–Clapeyron equation at temperatures $\geq 3 \text{ K}$. At lower temperatures, P^* becomes independent of temperature because of infrared–induced desorption (IRID). At 2.5 K, their desorption rate is two orders of magnitude higher than that expected from the extrapolation of the behavior above 3 K. Since our rates agree with theirs, it is possible that IRID is relevant to the present work. Measurements with control of the infrared flux and a more complete study of the temperature dependence of dn/dt are needed to address this issue. Recent results for hydrogen isotopes on graphite also show evidence of IRID.^{28, 29}

Finally, we consider the topic of ortho–to–para conversion. As can be seen from Fig. 3.1, the position of the sharp peak in the specific heat in bulk H_2 is sensitive to changes in the o– H_2 concentration. By estimating limits on the shift in the peak of our adsorbed H_2 multilayers, we can calculate an approximate limit on the rate of ortho–to–para conversion. Based on the data of Fig. 3.7, we estimate that the conversion rate for our highest coverages of H_2/Au is $< 2.8\%$ per hour. The limit for $H_2/\text{sapphire}$ is comparable. At low coverages, we have no information about the ortho/para content due to the suppression of the peak. This rate is comparable to that due to intrinsic conversion in bulk H_2 (1.9% per hour),³ which implies that conversion at the

substrate is either not enhanced, or, if enhanced, is unable to propagate away from the substrate. As mentioned earlier, classical diffusion is negligible in our temperature range. A mechanism does exist which allows diffusion of the quantum rotational state even when the molecules themselves are immobile. However, this form of diffusion causes isolated o-H₂ molecules to cluster together.³ Rather than enhance the spreading of a layer near the surface with an enhanced p-H₂ concentration, it would tend to confine it.

Thus, we have no evidence for enhanced ortho-to-para conversion, but we cannot exclude the possibility of rapid conversion which is confined to the first one or two monolayers. Comparison of our results with those of Avouris *et al.* is complicated by the above considerations, as well as by possible differences in the substrate. The rapid conversion rates in the latter study are thought to depend sensitively on both the distance from the substrate and the orientation of the crystallites.¹³ The presence of impurities would dramatically reduce the conversion rate. A similar decrease in the rate would occur if the fraction of the crystallites with (111) orientation and the mobility of the H₂ were both small.

3.5 Conclusions

In conclusion, we have observed orientational ordering in multilayers of H₂ adsorbed on sapphire and evaporated Au films. These results represent the first heat capacity measurements of this transition in adsorbed H₂. At high exposures, the heat capacity as a function of temperature is in qualitative agreement with that of bulk H₂, but is broadened by disorder in the H₂ and heterogeneity of the substrate. At low exposure, the peak decreases in size and shifts to lower temperature, in qualitative agreement with behavior expected from models of finite-size effects. The estimated ortho-to-para conversion rate appears to be comparable to the intrinsic rate of bulk H₂.

References

- ¹Y. Imry, *Phys. Rev. B* **21**, 2042 (1980).
- ²P. Avouris, D. Schmeisser and J. E. Demuth, *Phys. Rev. Lett.* **48**, 199 (1982).
- ³I. F. Silvera, *Rev. Mod. Phys.* **52**, 393 (1980).
- ⁴In the frame of the molecule, both p-H₂ and o-H₂ have the same, nearly spherical charge distribution. The distinction is that the orientational distribution of the molecular axis is spherical for p-H₂, but not for o-H₂. See Ref. 3 for a complete description.
- ⁵R. W. Hill and B. W. A. Ricketson, *Philos. Mag.* **45**, 277 (1954).
- ⁶F. A. B. Chaves, M. E. B. P. Cortez, R. E. Rapp and E. Lerner, *Surf. Sci.* **150**, 80 (1985).
- ⁷F. C. Motteler and J. G. Dash, *Phys. Rev. B* **31**, 346 (1985).
- ⁸J. Ma, D. L. Kingsbury, F.-C. Liu and O. E. Vilches, *Phys. Rev. Lett.* **61**, 2348 (1988).
- ⁹M. Nielsen, J. P. McTague and W. Ellenson, *J. Phys. (Orsay, Fr.)* **38**, C4 (1977).
- ¹⁰P. R. Kubik, W. N. Hardy and H. Glattli, *Can. J. Phys.* **63**, 605 (1985).
- ¹¹A. D. Migone, A. Hofmann, J. G. Dash and O. E. Vilches, *Phys. Rev. B* **37**, 5440 (1988).
- ¹²A. Migone, private communication.
- ¹³E. Ilisca, *Phys. Rev. Lett.* **66**, 667 (1991).
- ¹⁴J. T. Birmingham and P. L. Richards, to be published.
- ¹⁵T. R. Govers, L. Mattera and G. Scoles, *J. Chem. Phys.* **72**, 5446 (1980).
- ¹⁶M. S. S. Challa, D. P. Landau and K. Binder, *Phys. Rev. B* **34**, 1841 (1986).
- ¹⁷M. E. Fisher and A. N. Berker, *Phys. Rev. B* **26**, 2507 (1982).
- ¹⁸R. Marx, *Phys. Rev. B* **40**, 2585 (1989).

- ¹⁹H. Shechter, J. Suzanne and J. G. Dash, *Phys. Rev. Lett.* **37**, 706 (1976).
- ²⁰P. Sheng, R. W. Cohen and J. R. Schrieffer, *J. Phys. C: Solid State Phys.* **14**, L565 (1981).
- ²¹C. Kittel and H. Kroemer, *Thermal Physics*, (W. H. Freeman and Co., New York, 1980) pp. 83–84. These authors point out that, strictly speaking, the temperature of an object in thermal equilibrium does not fluctuate. It is the energy of the object which fluctuates, and these fluctuations can be expressed in terms of temperature through the relation $\Delta U = C_V k_B \Delta T$. This distinction does not affect the conclusion of the present argument. Hence, we retain Imry's notation.
- ²²U. Albrecht, P. Evers, H. Dilger, and P. Leiderer, to be published.
- ²³K. K. Kakati and H. Wilman, *J. Phys. D: Appl. Phys.* **6**, 1307 (1973).
- ²⁴T. Jach, G. Hembree and L. B. Holdeman, *Thin Solid Films* **187**, 133 (1990).
- ²⁵J. Krim, *Thin Solid Films* **137**, 297 (1986).
- ²⁶C. Benvenuti, R. S. Calder and G. Passardi, *J. Vac. Sci. Technol.* **13**, 1172 (1976).
- ²⁷D. P. Woodruff and T. A. Delchar, *Modern Techniques of Surface Science*, (Cambridge University Press, Cambridge, 1986) p. 4.
- ²⁸J. Cui, S. C. Fain and W. Liu, *J. Vac. Sci. Technol. A* **7**, 1850 (1989).
- ²⁹W. Liu and S. C. Fain, Jr., to be published.

4. Preparation and Characterization of Evaporated Metal Films

4.1 Introduction

In the measurements of H_2 multilayers reported in the previous chapter, it was found that the data were reproducible on a given calorimeter but varied substantially from one calorimeter to the next. This lack of reproducibility is illustrated in Fig. 4.1, which shows results for nominally identical samples of H_2 on three different Au films. We focus on the results for H_2/Au because characterization and control of the bare sapphire surface is more difficult. We note, however, that a similar range of behavior has been observed on sapphire, which suggests that the sources of the nonreproducibility may be similar on these substrates.

Measurement a) in Fig. 4.1 is significantly different from measurements b) and c) in two ways: the orientational ordering peak near 1.6 K is much sharper, and there is no sign of the rounded maximum observed near 3.5 K in the other two measurements. These differences indicate that parameters which are important in the preparation of the substrate have not yet been adequately controlled. This chapter focuses on the methods for preparing and characterizing evaporated metal films. The parameters which are important in preparing such films are identified. The films used in the present study are compared with those described in the literature. Finally, we discuss methods for improving both the reproducibility and the quality of the metal films used in ac calorimetry. We include a description of the limits to the quality of optimized films. The discussion is divided into two sections: structure and cleanliness.

4.2 Structure

An ideal substrate for studies of 2D phase transitions would be perfectly flat and infinite in extent. Grain boundaries, steps, and other structural defects are always present on real substrates to a greater or lesser degree. As discussed in Chapter 1, these defects divide the surface into a patchwork of domains such that the adsorbate is coherent within a domain but loses coherence between domains. These domains cause sharp peaks in the heat capacity to be broadened and shifted through finite-size effects, as can be seen from comparisons of data from substrates with different domain sizes.¹ Hence, changes in domain size due to variations in structure are a possible

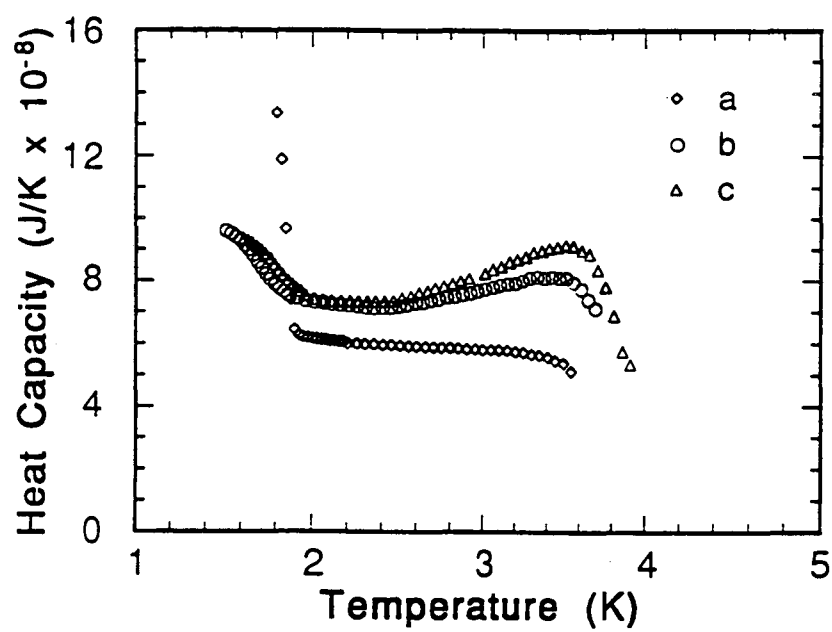


Figure 4.1 Heat capacity as a function of temperature for nominally identical 3.3 \AA^{-2} exposures of $n\text{-H}_2$ on three different Au films.

explanation for the differences in the orientational ordering peak shown in Fig. 4.1. The nature of the maximum at 3.5 K is unclear. Since its appearance correlates with a broadening of the orientational ordering peak, it is possible that it also arises from structural defects in the metal film.

Evaporated metal films display a wide variety of structures, depending on the parameters of the evaporation. A key parameter for many metals is the temperature of the substrate during deposition relative to the melting temperature of the metal. Systematic studies have been conducted for copper, silver, and gold.²⁻⁴ We will discuss the case of gold, the subject of an excellent, recent study by Jach, Hembree, and Holdeman (JHH).³

The gold films of JHH were evaporated on float glass substrates in a chamber with a base pressure of 5×10^{-9} Torr. They were deposited at a rate of 1–4 Å/s to a thickness of 2000 Å, and the gold flux at the substrate was close to normal incidence. The films were examined with reflection electron microscopy, which is performed at grazing incidence. This technique can thus resolve features normal to the plane of the film which are difficult to observe with normal incidence electron microscopy. Electron diffraction measurements were also made. Two substrate temperatures were used: room temperature and 420°C. The findings of JHH are as follows. Films deposited on room temperature substrates consist of crystallites which are 300 Å in diameter and 100 Å high. The diffraction measurements show that the crystallites show a slight preference for (111) orientation, but that the orientation of neighboring crystal planes rotates by large angles about axes normal to the substrate and parallel to it. Films deposited on substrates at 420°C consist of flat-topped columns of nearly equal heights. The columnar crystals have strong (111) orientation and are 3000 Å in diameter.

The development of larger, flatter crystallites on substrates at higher temperatures is attributed to a difference in free energy which favors the (111) surface relative to other orientations and to surface diffusion which is rapid compared with the deposition rate. The temperature at which columnar growth begins to dominate is approximately 320°C for gold. For other metals, columnar growth is expected for temperatures above $0.3 T_m$, where T_m is the melting temperature in °C.

Parameters other than the rate of deposition and the temperature of the substrate are thought to be of lesser importance. Results similar to those described by JHH are reported for thicknesses as small as 300 Å and pressures

during the evaporation as high as 5×10^{-8} Torr. The structure of the underlying substrate is believed to be unimportant.²

Using parameters similar to those of JHH, we have deposited gold and silver films on sapphire at temperatures near room temperature and have obtained films comparable to their room temperature films. Fig. 4.2 shows a scanning tunneling microscopy (STM) image of one of our silver films. This image was produced by workers under the direction of Professor Jacqueline Krim of Northeastern University. The silver crystallites have a lateral size of 1000 Å and are 200 Å in height. Relative tilting of adjacent crystallites is evident. Fig. 4.3 shows a scanning electron microscopy (SEM) image of a different silver film which was similarly prepared. The image shows crystallites which are 3000 Å in diameter and is typical of our silver films. These crystallites are comparable in diameter to the columnar crystals observed by JHH, but the STM image of Fig. 4.2 indicates that the structure is otherwise similar to that reported by JHH for films deposited on room temperature substrates.

No STM images are available for our gold films, and SEM images of these films failed to resolve any structure on three out of four films examined. The fourth film showed faint structures similar in appearance to those of Fig. 4.3, but one-tenth as large in diameter. The failure of normal incidence SEM to resolve structures on such films has been noted by JHH. The reason for the greater prominence of structure in the images of the silver films is unclear.

Since SEM was unable to resolve the structure of most of our gold films, it is not possible to directly correlate differences in film structure with the differences in the heat capacity measurements shown in Fig. 4.1. However, the preparation of film A corresponding to measurement a) in the figure is known to have been different from that of the other two films B and C in two ways: 1) it was significantly thinner (~ 100 Å vs. ~ 500 Å), and 2) it was probably heated to significantly higher temperatures. The latter statement is tentative because the use of a thermocouple for monitoring the temperature of the substrate during evaporations had not yet been implemented when film A was deposited. It is known, however, that the power used to heat substrate of film A during the evaporation was a factor of ~ 1.6 greater than that used to heat substrate of film C. Films B and C were deposited on substrates held at 10°C and 50°C, respectively. It is possible,

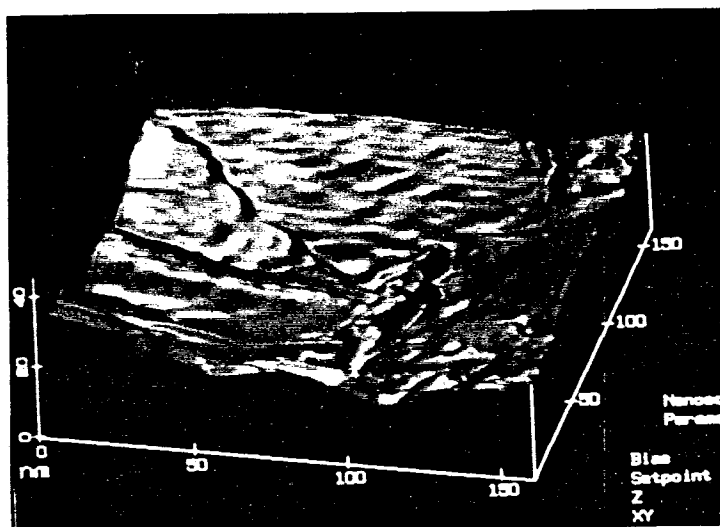


Figure 4.2 Scanning tunneling microscopy image of a silver film evaporated on sapphire heated to room temperature.

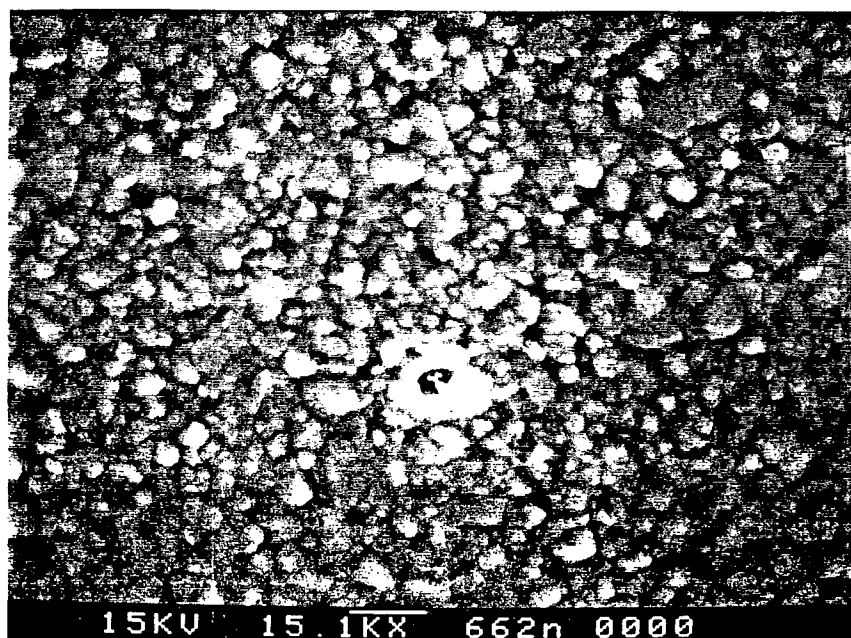


Figure 4.3 Scanning electron microscopy image of a typical silver film evaporated on sapphire heated to room temperature.

therefore, that the crystallites formed in A were larger and better oriented than those of the other films, and that this improvement yielded a sharper peak in the heat capacity. Further measurements on Au films deposited at higher temperatures and better characterization of these films (e.g., with STM) are clearly of interest.

In summary, differences in the structure of the Au films may be responsible for the lack of reproducibility in the measurements on different substrates. This observation emphasizes the need for better control of the parameters of the evaporation, especially the temperature of the substrate. Better control of these parameters is expected to yield greater reproducibility, both in the structure of the evaporated film, and in the heat capacity data as well.

It is also likely that the homogeneity of our metal films can be substantially improved by heating the substrate to higher temperatures during the evaporation. The current calorimeters can probably withstand temperatures as high as 350°C, which is above the onset temperature for columnar growth as reported by JHH. This temperature limit is imposed by several components. The NTD thermometers have Au contact pads which form a eutectic with Ge at 361°C.⁵ The shear strength of the conductive epoxy is uncertain beyond 340°C.⁶ Finally, the resistive heaters are stabilized at approximately 325°C during manufacture. If used at higher temperatures, the resistance of these heaters becomes unstable.⁷ Opportunities also exist for constructing calorimeters out of Si using microfabrication techniques. Such structures can withstand temperatures as high as 450°C. We will discuss the concept of Si calorimeters further in Chapter 5.

Finally, we note that the homogeneity of Au films has been studied by means of adsorption isotherms. On an ideal substrate (i.e., one with infinite domain size), the adsorption isotherm of an adsorbed film exhibiting layer-by-layer growth would display a series of vertical steps. On real substrates, nonvertical steps are observed. The slope of these steps can be used to estimate the mean domain size for the substrate. The domain size for Au films deposited at 200°C is 140–200 Å.^{2, 8} Because adsorption isotherms are sensitive to the presence of steps and other defects, these domains are smaller than the crystallites in these films by a factor of ~30. The homogeneity of structures like the columnar crystallites described by JHH has not been measured but is certainly of interest. Films of Au deposited on mica at

approximately 350°C are believed to have domain sizes as large as 500 Å.⁹ At present, this is believed to be the best homogeneity available from evaporated metal films.

4.3 Cleanliness

The other potential source of substrate heterogeneity is chemical contamination. Like defects in the structure of the metal film, chemical impurities present special binding sites which help create domains within the adsorbate. Different levels of contamination on different substrates could be a cause of the nonreproducibility shown in Fig. 4.1.

Direct measurements of surface cleanliness in UHV are often made using Auger electron spectroscopy (AES). This technique is both element-specific and surface-sensitive. It is well suited to studies of single crystals or evaporated metal films. It is not useful for studies of porous substrates such as graphite because it can probe only the outermost atomic layers of the substrate. *In situ* measurements with AES are both difficult and unusual in systems operated at LHe temperatures. The technique requires access to the sample over a rather large solid angle, which conflicts with the need for radiation shielding. We have therefore used the heat capacity measurements themselves as a gauge of cleanliness, much as adsorption isotherms are used to characterize graphite substrates.

Some information can be obtained by transferring substrates to a separate UHV chamber equipped for AES.² We have done so with one of our Au films. The composition of the surface was found to be 25 at. % C and 75 at. % Au. The exposure to air during the transfer itself is thought to induce contamination of approximately this magnitude.² Thus, AES in a separate chamber can only be used to check for gross contamination due to carbon or lower levels of other contaminants.

The clearest evidence of contamination was observed in measurements of the heat capacity of H₂/Ag prior to the implementation of the bake-out procedure. Fig. 4.4 shows measurements for nominally identical, 3.3 Å⁻² exposures of n-H₂ on a single calorimeter. We will refer to this exposure of n-H₂ as a "standard" exposure. Fig. 4.5 shows similar measurements for a different calorimeter. The first measurement in each figure was made on a freshly evaporated Ag film. Successive measurements

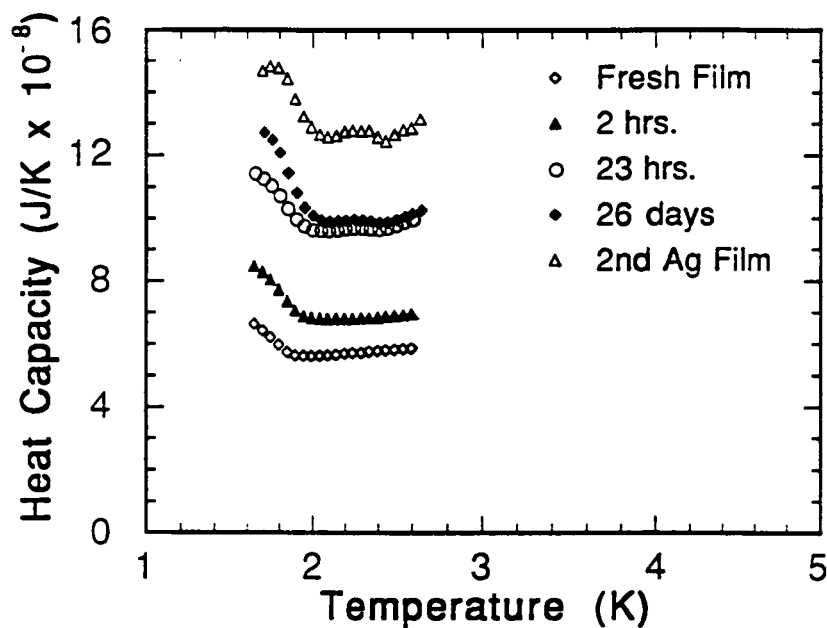


Figure 4.4 Heat capacity as a function of temperature for nominally identical samples of $n\text{-H}_2$ measured at several intervals following the deposition of a fresh Ag film.

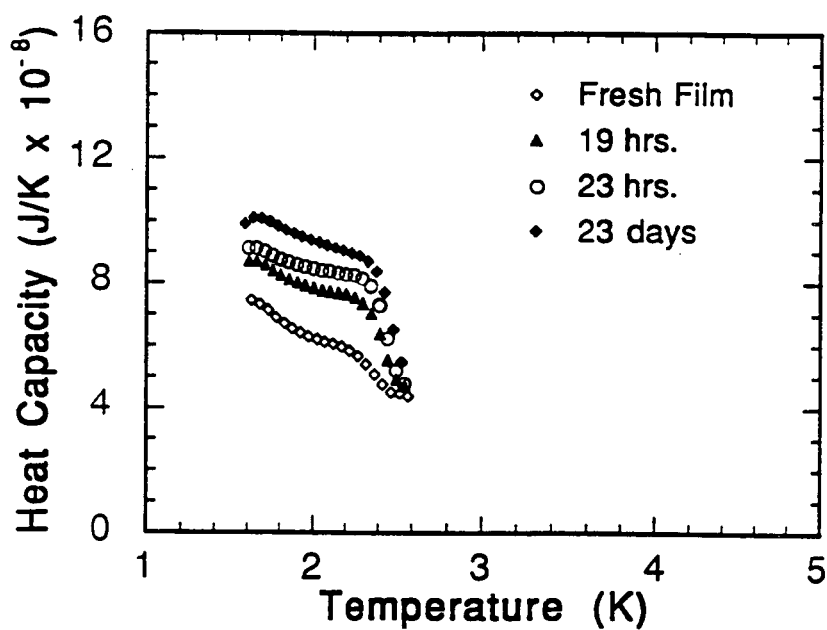


Figure 4.5 Measurements similar to those of Fig. 4.4 for a different Ag film.

were made at various intervals, as shown in the figure. The gas line was filled with fresh H₂ at the beginning of each day.

Before each measurement, the calorimeter was heated to a temperature T_d to desorb H₂ from the previous dose, if any, and to remove adsorbed gases accumulated through background dosing. For the measurements shown in Fig. 4.5, T_d ≈ 10–15 K, which is high enough to desorb H₂ and ⁴He. For the measurements in Fig. 4.4, T_d was close to room temperature. To determine which gases are likely to be desorbed at ~300 K, we note that the simplest rate equation for thermal desorption is of the form¹⁰ $R_d = N k_0 \exp(-E/k_B T)$, where R_d is the desorption rate, N is the number of molecules, k₀ is the pre-exponential factor, and E is the activation energy per atom. A typical value for k₀ is 10¹³ s⁻¹ (i.e., the adsorbate-substrate vibration frequency).¹⁰ If we set R_d/N = 1 s⁻¹ and T ≤ 300 K, we find that molecules with E ≤ 9000 K per atom (i.e., E ≤ 18 kcal/mole) will be desorbed. On a polycrystalline Au substrate, adsorbates likely to satisfy this criterion include¹¹ CO, CO₂, and N₂ (in addition to H₂ and the noble gases). Molecular oxygen has a higher desorption energy and, on the basis of this simple model, would not be expected to desorb below ~400°C.

The measurement on the fresh film in Fig. 4.4 resembles the results obtained after bake-outs had been implemented, as shown in Figs. 3.2–3.4. It also bears the greatest similarity to the data for bulk H₂. In both figures, the data evolve monotonically over time toward larger heat capacity and a more complex dependence on the temperature. Particularly noticeable is the feature near 2.3 K which appears either as a small bump or as a prominent shoulder on a larger feature near 1.6 K. Before the final (i.e., topmost) measurement in Fig. 4.4, a second Ag film was evaporated on top of the original one. The new film failed to restore the original behavior of the H₂ samples; in fact, it appears to have reinforced the trend which had been previously established.

These measurements strongly suggest that the calorimeters operated in the unbaked UHV system became contaminated through exposure to residual gases in the chamber on a scale of hours. The pressure in the UHV system, as measured by an ion gauge located at the wall of the chamber, was ≥ 3 × 10⁻⁹ Torr. At this pressure, surfaces are exposed to a flux of molecules equivalent to one monolayer every five minutes. The pressure near the calorimeter is expected to be considerably lower due to the cryopumping of the LHe

temperature radiation shields. However, the data of Figs. 4.4 and 4.5 show that the cryopumping was unable to adequately compensate for the relatively high residual pressure in the system as a whole.

Replacement of several materials thought to be sources of excessive outgassing and the implementation of bake-outs, as described in Chapter 2, led to dramatic improvements in reproducibility. Fig. 4.6 shows a series of measurements of standard samples on one Au film which lasted over a period of nine days. The shape of these data agrees well with that for bulk H₂, as explained in Chapter 3. The reproducibility is excellent in comparison with that of the data shown above. We note that the pressure of the UHV system (as measured at the wall of the chamber) is $\sim 5 \times 10^{-10}$ Torr, a factor of six lower than before the bake-outs.

Despite the significant improvement in reproducibility described above, measurements on different substrates are still not reproducible, as we have already discussed. The structure of the Au film and the effects of different structures on the behavior of the adsorbate were discussed in the previous section. The remainder of this section focuses on possible sources of contamination of the Au film. For each possible source, we discuss measures taken to guard against contamination. We also indicate areas of potential improvement in these safeguards.

The residual pressure during evaporation in the baked UHV system is $\leq 5 \times 10^{-9}$ Torr, which is low enough to make it an unlikely source of contamination. However, any part of the system which is heated during the evaporation may outgas and become a potential source of contamination. The areas heated include the gold wire, the tungsten filament, the surroundings of the filament, the surroundings of the calorimeter, and the calorimeter itself. We will consider these sources one by one.

The gold wire and filament are handled only with gloves and clean tweezers when being installed. After they have been installed in the UHV system and the system has been baked, the wire, the filament, and their surroundings are thoroughly outgassed. The current is gradually increased to heat the gold just to the point where evaporation begins, as monitored by the quartz-crystal oscillator. The pressure increases sharply at first, reaches a maximum, and eventually begins to slowly decrease. Outgassing is continued for at least one half hour to ensure that the surroundings are thoroughly heated. If the chamber is vented, the outgassing must be repeated. Some

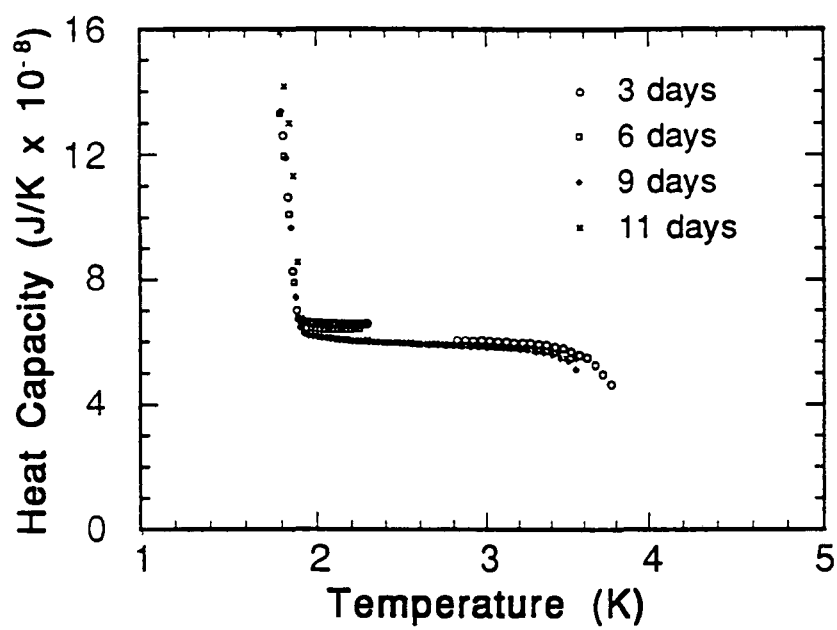


Figure 4.6 Measurements similar to those of Fig. 4.4 for an Au film. The UHV system was baked prior to this set of measurements.

additional outgassing occurs when the filament is heated for the actual evaporation. For this reason, the shutter between the sample and the filament is left closed until the evaporation rate reaches $\sim 1 \text{ \AA/s}$, and it is closed again at the end of the evaporation before the current to the filament is turned off. The filament is equipped with a water-cooled shroud and water-cooled electrodes. The water-cooling is used during the evaporation to reduce the outgassing from surfaces near the filament. The shroud also absorbs much of the thermal radiation emitted by the filament, thereby reducing the heating of other near-by surfaces.

The calorimeter is surrounded by radiation shields as shown in Fig. 2.7. The shields and the charcoal epoxied to them are cooled by contact with the LHe cold finger. The shields are warmed by radiation from the filament during evaporation. The charcoal does not view the filament directly, but it is also heated through its contact with the shields. The increase in temperature is unknown but may be large enough to desorb some of the gases which have been cryopumped. To determine the temperatures at which desorption is expected to occur, we must consider the metal surfaces of the shields and the charcoal as separate cases.

Desorption from the metallic surfaces of the shields is governed by the equilibrium vapor pressures of the gases cryopumped on these surfaces. For example, the vapor pressure of H_2 would rise to 10^{-9} Torr at a temperature of ~ 3.5 K. The corresponding temperature for CO is ~ 25 K. Heavier molecules would desorb at still higher temperatures. Because the vapor pressure of ^4He is high (~ 6 Torr) even at 1.6 K, it is not effectively cryopumped by the metallic surfaces. Hence, desorption of ^4He from the metallic surfaces is expected to be small.

Desorption from the charcoal depends not only on the temperature, but also on the condition of the charcoal surface and the quantity of gas adsorbed. Adsorption isotherms are used to measure the pressure in the gas phase as a function of temperature and the quantity of gas adsorbed for a given substrate-adsorbate combination. Using an estimate of the amount of ^4He in the UHV system prior to the cooling of the cryostat and published isotherms for ^4He on activated charcoal,¹² we find that a ^4He pressure of 10^{-9} Torr is expected at ~ 17 K. The corresponding temperature for H_2 is greater than 40 K. However, the charcoal used in the present work is not baked and is presumed to be covered with an unknown amount of adsorbed water.

Therefore, it is possible that significant desorption from the charcoal occurs at lower temperatures than those expected from isotherms for activated charcoal.

Finally, we consider the calorimeter itself. The sapphire substrate is ultrasonically cleaned in organic solvents before construction of the calorimeter. It is also wiped with methanol just before installation into the UHV system. Before the evaporation, the calorimeter is heated to approximately room temperature, as determined by the thermocouple shown in Fig. 2.3. It is held at this temperature during the evaporation, and for several minutes afterward, and is then allowed to gradually cool. Heating the calorimeter helps to produce smooth metal films, as described in the previous section, and to drive off gases adsorbed on its surface. The vapor pressure of common molecular adsorbates such as H_2O , N_2 , and CO are large enough at room temperature that thick layers of adsorbates are quickly pumped away. Thin layers may remain, depending on the binding energy to the substrate. The vapor pressure of the conductive epoxy on the back of the sapphire is unknown. The calorimeter is baked in air at temperatures of 50–100°C to cure the epoxy, and the smallest amounts of epoxy needed to make reliable contacts are used.

Measures which could be employed to further decrease the possibility of contamination from these sources are as follows. The gold wire and filament should be thoroughly cleaned before installation in the vacuum system. A recommended procedure is to use trichloroethylene, acetone, and methanol in that order, for 15 minutes each, in an ultrasonic cleaner. Krim has reported that tungsten evaporation baskets, even when cleaned, can be significant sources of contamination.^{2, 13} She reports that preliminary outgassing of the bare basket results in films which are substantially cleaner, as determined by AES. A feedthrough for dropping a gold pellet into the evaporation basket is required for this preliminary outgassing. Such a feedthrough would require a substantial modification of the existing apparatus, and it should be pursued only after less complicated measures directed at other potential sources of contamination have been implemented.

The surroundings of the evaporation filament could be separately baked following the system bake-out. To do so, it would be necessary only to wrap the evaporation port with a heating tape. The water-cooling of the

shroud could be changed to LN₂-cooling, which provides a significant level of cryopumping.

The temperature of the LHe radiation shields should be measured during an evaporation to determine whether or not desorption from these surfaces is a significant problem. If so, improvement of the thermal contact to the cold finger could be investigated.

Bake-outs with the cold finger installed could provide an important improvement in the cleanliness of the system as a whole. Baking the system in this manner would eliminate the need for venting the system. It would also render the cryosorption of the charcoal considerably more effective.

The calorimeter could be heated to substantially higher temperature during the evaporation. This would help to drive off molecules which are adsorbed at room temperature, and produce higher quality Au films as well. Construction of calorimeters without the use of conductive epoxy or commercial heaters is possible and will be discussed in the following chapter.

In summary, significant progress has been made in improving the cleanliness of the UHV system. The bake-out procedure we have implemented provides good reproducibility for many days in measurements on a given Au film. The reproducibility of measurements on different calorimeters needs to be improved. We have identified two likely sources of this nonreproducibility. The first is the structure of the Au film, which depends sensitively on parameters such as the temperature of the substrate during evaporation. The second is the cleanliness of the substrate, which can be degraded by local outgassing near the calorimeter or the evaporation filament. Straightforward solutions exist for these problems, making it very likely that good calorimeter-to-calorimeter reproducibility can also be achieved. Lastly, the homogeneity of the evaporated metal films can be significantly improved by heating the calorimeter to higher temperatures during the evaporation.

References

- ¹M. Bretz, Phys. Rev. Lett. **38**, 501 (1977).
- ²J. Krim, Thin Solid Films **137**, 297 (1986).
- ³T. Jach, G. Hembree and L. B. Holdeman, Thin Solid Films **187**, 133 (1990).
- ⁴K. K. Kakati and H. Wilman, J. Phys. D **6**, 1307 (1973).
- ⁵J. Beeman, private communication.
- ⁶Epo-Tek H20E Specifications, Epoxy Technology, Inc., Billerica, MA.
- ⁷B. LeMar, Technical Assistance, Mini-Systems, Inc., North Attleboro, MA, private communication.
- ⁸J. Krim, J. G. Dash and J. Suzanne, Phys. Rev. Lett. **52**, 640 (1984).
- ⁹J. Krim, private communication.
- ¹⁰D. Menzel, in Interactions on Metal Surfaces , edited by R. Gomer (Springer-Verlag, New York, 1975), p. 102.
- ¹¹G. A. Somorjai, Chemistry in Two Dimensions: Surfaces , (Cornell University Press, Ithaca, New York, 1981), pp. 283-330.
- ¹²P. Roubreau, G. D. Nigohossian and O. Avenel, in Colloque International Vide et Froid , (SFITV, Grenoble, 1969), p. 27.
- ¹³J. Krim, Ph.D. thesis, University of Washington, 1984.

5. Future Work

5.1 Introduction

The ac calorimetric technique which we are developing has demonstrated its value as an alternative to traditional techniques for measuring the heat capacity of adsorbates. Measurements of $^4\text{He}/\text{Ag}$ indicate an absence of solidification in sharp contrast with results for $^4\text{He}/\text{graphite}$. This result emphasizes the importance of parameters such as the binding energy and the corrugation of the substrate, which are known to be weaker on metals than on graphite. In the study of $n\text{-H}_2$, the ~ 2 ms time constant of the ac technique allowed measurements to be made on a time scale which is rapid in comparison with the ortho-to-para conversion rate. This situation contrasts with that for traditional, adiabatic techniques, which have time constants of ~ 20 mins. The data for $n\text{-H}_2$ illustrate the suppression of the orientational ordering transition as the coverage is decreased.

In this chapter, we discuss avenues for further research. We first consider additional measurements which can be made using the apparatus in its current form. Secondly, we briefly describe current efforts to reduce the minimum operating temperature of the technique from 1.6 K to ~ 300 mK. We propose measurements of particular interest which can be made at these lower temperatures. A second effort which is currently in progress is the construction of a quartz-crystal microbalance. The microbalance will provide measurements of the coverage of adsorbed films. Such measurements are valuable in their own right, and they assist in the interpretation of heat capacity measurements as well. Finally, we discuss methods which can be used to build monolithic Si calorimeters which can withstand temperatures as high as 450°C . Such calorimeters provide opportunities for further improving the preparation and cleaning of metal films evaporated for use as substrates.

5.2 Further Measurements Using the Existing Apparatus

The most promising application for the apparatus in its current form lies in a return to measurements of ^4He . As discussed in Chapter 1, the data of Kenny and Richards (KR) for $^4\text{He}/\text{Ag}$ show no sign of the increases in heat capacity which accompany solidification on graphite.¹ Moreover, the data are

in good agreement with a model of a 2D noninteracting Bose gas, the first such gas to be observed. The measurements of KR are shown in Fig. 5.1.

Interesting questions about these data have been raised by Taborek.² Taborek argues that the relatively low binding energy of $^4\text{He}/\text{Ag}$ should result in rapid desorption of the ^4He coverages reported by KR by a temperature of 3 K. The argument consists of two parts. In the first, the equilibrium vapor pressure for a given coverage of ^4He is calculated by equating the chemical potential of the film with that of a 3D classical vapor. The second part predicts the desorption rate of a film adsorbed on a substrate suspended in UHV by means of a macroscopic continuum model for the dynamics of thin ^4He films.³ The model treats the adsorbed film as a slab of the bulk liquid which exchanges particles and energy with the vapor above it. This model has been shown to yield good agreement with results for $^4\text{He}/\text{graphite}$ for coverages as low as 1.5 layers. Taborek finds that a binding energy of over 90 K per atom is necessary to explain the stability of the films observed by KR. Since the accepted value of the binding energy for $^4\text{He}/\text{Ag}(111)$ is only 62.5 K, he concludes that the silver surface must have been contaminated.

Taborek's arguments raise questions about the interpretation of the data in KR. The special feature of this experiment is the use of a metal (Ag) substrate with a small binding energy and a small corrugation. A substrate with a stronger binding energy would be more likely to cause solidification of the ^4He film, as is observed on most substrates. However, the fit to the model of the Bose gas is good, and the usual signs of solidification observed on graphite are absent. For comparison, the binding energy of $^4\text{He}/\text{graphite}$ is 143 K. It is possible that the 90 K value estimated by Taborek for the system of KR is still low enough compared to the value on graphite to allow for the dramatic differences in the heat capacity which were observed. Alternatively, it is possible that the fit to the model of the 2D Bose gas is fortuitous.

In this context, it is relevant to note that Bretz *et al.*⁴ have observed a temperature dependence similar to that of the higher coverages in Fig. 5.1 in a study of $^4\text{He}/\text{graphite}$. It can be seen from Fig. 1.2b that the heat capacity of $^4\text{He}/\text{graphite}$ decreases monotonically with decreasing temperature for coverages $n < 0.01 \text{ \AA}^{-2}$ and in a narrow window of coverage near $n = 0.08 \text{ \AA}^{-2}$. Data for low coverages of $^4\text{He}/\text{graphite}$ are shown in Fig. 5.2. The coverage measured for the $^4\text{He}/\text{graphite}$ system has been used to convert

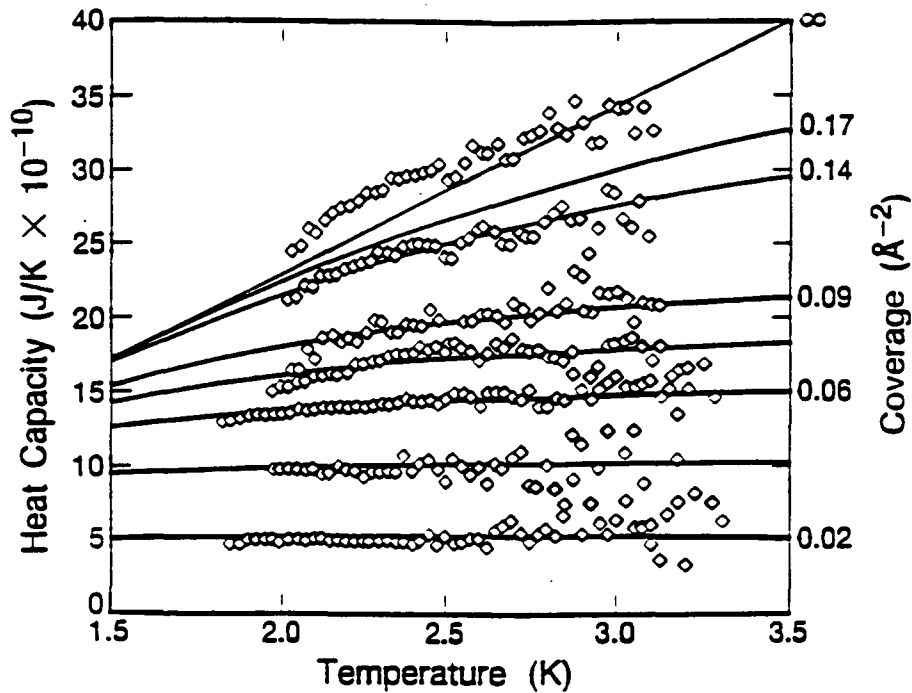


Figure 5.1 Heat capacity for several exposures of $^4\text{He}/\text{Ag}$. The solid lines show the heat capacity of a noninteracting 2D Bose gas for the coverages shown at right. From Kenny and Richards.¹ (These results are the same as those which were shown in Fig. 1.5.)

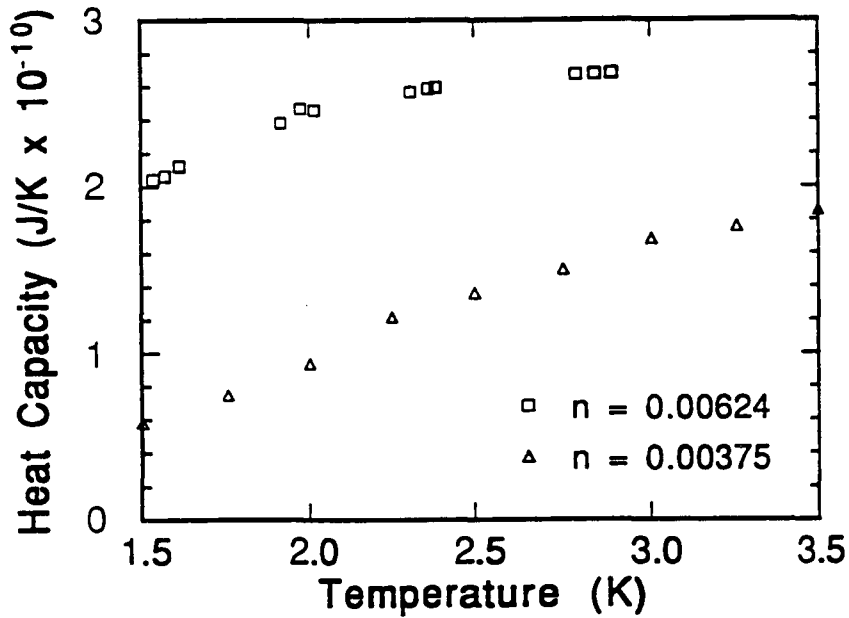


Figure 5.2 Heat capacity of $^4\text{He}/\text{graphite}$ at low coverage. The data are from Bretz *et al.*⁴ and Fig. 1.2b.

specific heats to heat capacities per unit area. These values were then scaled according to the area of the Ag film used for the measurements in Fig. 5.1. The data for the upper curve are from Bretz *et al.*; those for the lower curve were taken from Fig. 1.2b.

The temperature dependence of the upper curve in Fig. 5.2 bears a striking resemblance to the middle curves in Fig. 5.1. For temperatures greater than 2 K, the data of Fig. 5.2 have been shown to agree with calculations for a model which fits the van der Waals equation of state to the high temperature virial coefficients.⁴ The coverages for the ⁴He/graphite data are an order of magnitude smaller than those shown in Fig. 5.1. We note, however, that the coverages listed in Fig. 5.1 are derived from the ideal Bose gas model--not from independent measurements.

Despite the similarity in the temperature dependence, it is clear that there are two fundamental differences between Figs. 5.1 and 5.2: the scale on the heat capacity axis and the coverage dependence. The heat capacity is an order of magnitude smaller in Fig. 5.2, and it does not become independent of temperature as the coverage is decreased. These differences imply that the virial coefficient model is not appropriate for ⁴He/Ag.

In summary, the temperature dependence of the heat capacity observed for high coverages of ⁴He/Ag bears a resemblance to that observed for ⁴He/graphite in two narrow ranges of coverage. However, the data shown in Fig. 5.1 cannot be understood on the basis of the models formulated for ⁴He/graphite. These considerations strengthen the conclusion that the model of the ideal Bose gas provides the best explanation for the data of Fig. 5.1. Further measurements of ⁴He using ac calorimetry are therefore of great interest, both to address the questions raised by Taborek, and to deepen understanding of the similarities and differences between ⁴He/graphite and ⁴He on metals.

The issues of substrate characterization and possible sources of contamination were discussed in the previous chapter. We note here that the nonreproducibility noted in the measurements of H₂ was not evident in the study of ⁴He/Ag, despite the fact that the UHV system was not baked in the latter study. This indicates either that ⁴He is less sensitive to contamination of the surface, or that contamination did not occur during the ⁴He measurements. If the former is true, measurements of H₂ may prove useful

as a test of surface cleanliness which can assist in the interpretation of future data for ^4He .

Measurements of thermal desorption are also possible with the existing apparatus and are expected to be of significant interest. The UHV system is equipped with a quadrupole mass spectrometer (QMS), and a direct line-of-sight between this instrument and the calorimeter can be opened or closed by means of the same rotating shutter used for dosing and evaporation. High background pressures and a significant distance between the calorimeter and the QMS can complicate the detection of molecules desorbed from the calorimeter. Detection of ^4He is particularly challenging since it is the gas with the highest background pressure. However, the implementation of the bake-out procedure has decreased the overall background pressure by a significant amount. Furthermore, a preliminary measurement made prior to the use of bake-outs succeeded in detecting the desorption of H_2 multilayers from the calorimeter. Thus, the prospects for making desorption measurements are encouraging.

Thermal desorption can be used both to check for the presence of contaminants and to measure the coverage of the adsorbate under study. The former requires ramping the temperature to hundreds of kelvins to look for desorption of contaminants such as CO or H_2O . The latter involves ramping the temperature to ~ 4 K for adsorbates such as ^4He or H_2 . It is straightforward to measure relative coverages by integrating the total thermal desorption signal. Measurement of absolute coverages requires calibration of the QMS signal with respect to the signal for a known coverage. If the first layer has an appreciably different binding energy from that of successive layers, as is often the case, an approximate, absolute coverage can be obtained by separately integrating the peak in the spectrum which corresponds to desorption of the monolayer.

Finally, measurements using other adsorbates and substrates can be made with the present apparatus. Most other potential adsorbates are heavier than ^4He and H_2 and are not expected to exhibit phase transitions below 4 K. The melting of Ne monolayers occurs at 13.5 K,⁵ and the transitions for heavier adsorbates are at still higher temperatures. For temperatures below 4 K, these adsorbates are expected to form solids. One effect which can be studied is the crossover from 2D to 3D behavior as the coverage is increased from one monolayer to many. For Debye solids, the temperature dependence

of the heat capacity is expected to change from T^2 to T^3 at this crossover point. The change from T^2 to T^3 behavior in CO multilayers has been observed by Kenny using the present technique.⁶

Of the lighter adsorbates, ^3He is of significant interest. As mentioned in Chapter 1, the imperfect 2D gas phase of ^3He /graphite exhibits distinct differences from that of ^4He /graphite due to the differences between Fermi and Bose statistics. These differences arise through quantum virial coefficient corrections to the behavior of an ideal gas.⁷ In contrast, the temperature dependence of the heat capacity for *noninteracting* particles is the same, independent of statistics.⁷ This behavior is shown by the solid curves in Fig. 5.1. Thus, a comparison of measurements for $^3\text{He}/\text{Ag}$ with the earlier results for $^4\text{He}/\text{Ag}$ is certainly of interest.

Other substrates are also of interest. As discussed in Chapter 1, the extremely weak binding energy of ^4He on the alkali metals is predicted to yield unusual behavior. Absence of solidification and a possible Bose gas phase have been proposed for these systems.^{8,9} Special evaporation boats for depositing films of these highly reactive metals in UHV are commercially available.¹⁰ Because they are highly reactive, it is possible that evaporated films of these metals would be more susceptible to contamination than the noble metals. Also, the extremely low binding energies for ^4He on the alkalis would make the desorption effects predicted by Taborek's analysis even more pronounced.

Adsorption of ^4He on frozen, "pre-plated" layers of H_2 or the noble gases is also of interest. This technique has been used in measurements of heat capacity and third sound. The corrugation of such surfaces is comparable to or greater than that of graphite, but the binding energy is weaker.⁸ In the case of ac calorimetry, heavy rare gases would be the best choice for the pre-plated layer because their higher desorption temperature would make them more stable.

5.3 Extension to Lower Temperatures

The temperature range of the ac calorimeter technique is currently being extended to temperatures as low as 300 mK with the aid of a ^3He refrigerator. The refrigerator is based on a design which was originally devised for astrophysical observations from sounding rockets.¹¹ Hence, it is

compact, self-contained, and requires only electrical connections for operation from a 2 K cold stage.

The refrigerator is mounted on the cold plate of a conventional cryostat. A hole in the wall of the dewar allows access to an evaporation filament and an effusion cell. The hole can be covered by a LHe temperature shutter to reduce the heat load due to thermal radiation. Preliminary measurements indicate that heat capacities as low as 1×10^{-11} J/K can be measured. At a temperature of 800 mK, this value represents approximately 0.25% of the heat capacity of the calorimeter as a whole. This extension of the technique to lower temperatures offers opportunities for a number of exciting measurements.

In the case of H₂, a straightforward extension of the multilayer measurements reported in Chapter 3 is certainly of interest. As can be seen from Figs. 3.2–3.5, the orientational ordering peak falls just below the present temperature range in most of the measurements made to date. With ³He refrigeration, the entire peak and the baseline on both sides will be accessible for a wide range of H₂ coverages. These measurements will make possible a much more detailed comparison between the experimental data and the predictions of finite-size effects. For example, a comparison of the measured and predicted shifts in the temperature of the peak as a function of coverage will be possible.

A search for orientational ordering in H₂ monolayers merits particular attention. At present, the NMR study of ortho-H₂/graphite by Kubik *et al.* constitutes the only experimental observation of this transition.¹² For o-H₂ concentrations of 90% and 77%, they found transitions at 600 mK and 330 mK, respectively. The ortho concentration in n-H₂ is 75%, and enrichment processes for preparing H₂ samples with higher ortho concentrations have been described by Silvera.¹³ Mean field theory calculations for o-H₂ monolayers predict four distinct ordered phases at low temperature, depending on the ratio of the crystal field and the quadrupole-quadrupole interactions.¹⁴ The crystal field experienced by a given H₂ molecule is composed of its van der Waals interactions with neighboring adsorbates and with the substrate. This dependence on the substrate implies that the transition temperature and the ordered phase itself may be different on metallic substrates than on graphite. Hence, measurements on metallic substrates with ac calorimetry are of special interest.

An extension of the results for $^4\text{He}/\text{Ag}$, which were discussed in the previous section, is also clearly of interest. For $T \ll T_0$, where $T_0 = \left(\frac{h^2}{2\pi m g_N k_B} \right) \left(\frac{N}{A} \right)$, the heat capacity of an ideal 2D Bose gas is given by⁷

$$C(T) = \frac{\pi^2}{3} \left(\frac{T}{T_0} \right) N k_B. \quad (5.1)$$

In these expressions, N is the number of bosons, and A is the area. The statistical factor $g_N = 2s + 1$ enters when the nuclear spin s is nonzero. Thus, at low temperature, the heat capacity is linear in T . For the highest finite coverages in Fig. 5.1, the beginning of this linear region is evident near 1.5 K. Observations of a linear temperature dependence for $T < 1.5$ K would provide strong support for the earlier proposal, based on the fit shown in Fig. 5.1, that $^4\text{He}/\text{Ag}$ forms an ideal Bose gas.

It is also possible that the Bose gas interpretation of Fig. 5.1 is correct, but that solidification occurs at lower temperatures. If so, peaks in the heat capacity analogous to those seen on graphite may be observed. Each of the phase boundaries shown in Fig. 1.2 yields a corresponding peak in the heat capacity. None of these boundaries is observed in the data of Fig. 5.1, but it is possible that they have simply shifted to lower temperatures due to the weakening of the ^4He - ^4He and ^4He -substrate interactions. If so, measurements using the new apparatus may discover peaks due to melting or order-disorder transitions. Debye T^2 behavior is observed on graphite for densities in the range 0.08 to 0.12 \AA^{-2} and temperatures below 1.5 K.⁴

Measurements of ^3He at lower temperatures are also of interest. As mentioned in Chapter 1, data for ^3He on graphite are in good agreement with a model of an imperfect gas with quantum virial coefficients appropriate for fermions.^{4, 15} The heat capacity calculated using the second virial coefficient is in quantitative agreement with the data from 4 K to temperatures as low as 0.5 K. From 0.5 to 0.2 K, there is qualitative agreement, but contributions due to higher virial coefficients become important. No effects due to spin-ordering are observed above 0.2 K. A comparison of these data for ^3He on graphite with data for ^3He on metals would be of interest. It has been proposed⁹ that substrates with weak binding energies could allow

delocalization of adsorbed ^4He in the direction perpendicular to the surface, thereby reducing the strength of the ^4He - ^4He interaction. If ^3He - ^3He interactions could be reduced by similar means, it is possible that an ideal Fermi gas could be observed. Thus, the extension of the ac calorimetric technique through the use of ^3He refrigeration opens up possibilities for observing a wide variety of exciting phenomena.

The other extension of the technique which is currently in progress is the development of a quartz-crystal microbalance for making measurements of the coverage. The oscillator is formed by depositing thin metallic films on opposite faces of a thin, AT-cut quartz crystal. These films serve as electrodes which couple the crystal to a resonant drive current in the conventional manner. One of the films also functions as a substrate for measurements of adsorption. The extra mass deposited on the surface of the oscillator causes a proportional decrease in the resonant frequency of the circuit. Such oscillators have been shown to be sensitive and versatile probes of physisorbed films.¹⁶⁻¹⁸

The use of microbalances will provide information on the coverage of an adsorbed film as a function of exposure and temperature. Such information will greatly assist in the interpretation of measurements of the heat capacity. For example, the temperature independent data in Fig. 5.1 are attributed to a classical 2D gas phase with $C/N \approx k_B$. Measurements of the coverage which show that C/N has the expected value would strengthen this interpretation. Ratios far from k_B would indicate that the interpretation must be re-evaluated.

Finally, the addition of a microbalance will allow direct measurements of sticking coefficients. The sticking coefficient is the probability that an incident molecule will be adsorbed on the substrate. Since the flux of molecules from the effusion cell is known, the coverage information from a microbalance determines the sticking coefficient. The study of the adsorption or sticking process is currently an active field of research.¹⁹ Hence, measurements of sticking are of use in interpreting heat capacity data, but they are also of considerable interest in their own right.

5.4 Monolithic Si Calorimeters

The calorimeters currently in use are composite in their construction. That is, the finished calorimeter is assembled from a number of discrete

components, including a substrate, a thermometer, heaters, and electrical leads. Thin layers of silver-filled epoxy are used to attach the thermometer and heaters to the substrate. The bond formed by the epoxy is thin enough to provide a large thermal conductance, yet strong enough to survive repeated thermal cycling. The epoxy is also used to make electrical contacts.

There are two potential disadvantages of this method of construction. One is that the outgassing properties of the epoxy are unknown. The other is that the temperature which such structures are expected to withstand is limited to $\sim 350^{\circ}\text{C}$. This limit is imposed by several of the components. For example, the shear strength of the epoxy decreases at high temperature, and its reliability above 340°C is unknown.²⁰ The resistance of the commercial NiCr heaters becomes unstable above 325°C ,²¹ and the Au contact pads on the NTD thermometers form a eutectic with Ge at 361°C .²²

As discussed in the previous chapter, the nonreproducibility in results obtained on different calorimeters is most likely due to differences in structure or cleanliness of the different substrates. It was also noted that Au films deposited on substrates heated to $\sim 420^{\circ}\text{C}$ produce extremely large, flat, well-oriented crystallites. Therefore, it is important to eliminate potential sources of outgassing, and to develop calorimeters which can be heated to high temperatures.

One way of working toward these goals is to use composite calorimeters with improved components. For example, the electrical contacts to the heaters and thermometer can be made with wire-bonding rather than with epoxy. The heaters and thermometer, with some minor modifications, can be made to withstand temperatures as high as 425°C .²³

A different approach is to utilize microfabrication techniques to make monolithic calorimeters out of silicon. Calorimeters made in this way are currently being used as detectors for x-ray astronomy.²⁴ A diagram of a monolithic Si calorimeter is shown in Fig. 5.3. The central, square section of the calorimeter has dimensions $500\ \mu\text{m} \times 500\ \mu\text{m} \times 10\ \mu\text{m}$. It is suspended by long, thin legs which provide the weak thermal link to the cold stage. The detail of the central section shows resistive thermometers which have been produced through ion implantation. Such techniques eliminate the need for separate thermometers, heaters, and epoxy. Furthermore, structures such as these are known to withstand temperatures as high as 450°C .²⁵ Since both of

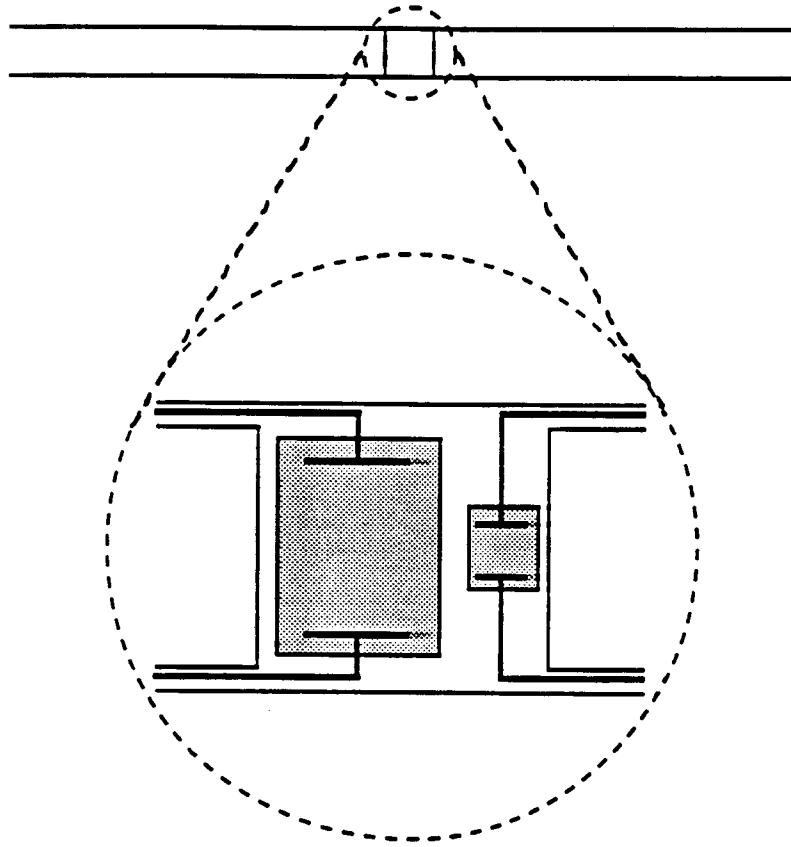


Figure 5.3 Schematic diagram of a monolithic Si calorimeter. The central section is $500\ \mu\text{m} \times 500\ \mu\text{m} \times 10\ \mu\text{m}$ thick, and the support legs are $20\ \mu\text{m} \times 10\ \mu\text{m} \times 3\ \text{mm}$ long. The detail of the central section shows thermistors and conducting lines produced through ion implantation. After McCammon *et al.*²⁴

the goals stated above can be met using monolithic Si calorimeters, they offer an attractive alternative for the next generation of ac calorimeters.

References

- ¹T. W. Kenny and P. L. Richards, *Phys. Rev. Lett.* **64**, 2386 (1990).
- ²P. Taborek, *Phys. Rev. Lett.* **65**, 2612 (1990).
- ³M. Weimer and D. Goodstein, *Phys. Rev. Lett.* **50**, 193 (1983).
- ⁴M. Bretz, J. G. Dash, D. C. Hickernell, E. O. McLean and O. E. Vilches, *Phys. Rev. A* **8**, 1589 (1973).
- ⁵G. B. Huff and J. G. Dash, *J. Low Temp. Phys.* **24**, 155 (1976).
- ⁶T. W. Kenny, Ph.D. thesis, University of California, Berkeley, 1989.
- ⁷J. G. Dash, *Films on Solid Surfaces*, (Academic Press, New York, 1975).
- ⁸E. Cheng, G. Ihm and M. W. Cole, *J. Low Temp. Phys.* **14**, 519 (1989).
- ⁹E. Cheng and M. W. Cole, *Phys. Rev. B* **42**, 3960 (1990).
- ¹⁰Alkali Metal Dispensers, SAES Getters/USA Inc., Colorado Springs, CO.
- ¹¹L. Duband, D. Alsop, A. Lange and P. Kittel, *Advances in Cryogenic Engineering* **35**, 1447 (1990).
- ¹²P. R. Kubik, W. N. Hardy and H. Glattli, *Can. J. Phys.* **63**, 605 (1985).
- ¹³I. F. Silvera, *Rev. Mod. Phys.* **52**, 393 (1980).
- ¹⁴A. B. Harris and A. J. Berlinsky, *Can. J. Phys.* **57**, 1852 (1979).
- ¹⁵R. L. Siddon and M. Schick, *Phys. Rev. A* **9**, 907 (1974).
- ¹⁶J. Krim, Ph.D. thesis, University of Washington, 1984.
- ¹⁷J. Krim, J. G. Dash and J. Suzanne, *Phys. Rev. Lett.* **52**, 640 (1984).
- ¹⁸A. D. Migone, J. Krim, J. G. Dash and J. Suzanne, *Phys. Rev. B* **31**, 7643 (1985).
- ¹⁹Z. W. Gortel and J. Szymanski, *Phys. Lett. A* **147**, 59 (1990).

²⁰Epo-Tek H20E Specifications, Epoxy Technology, Inc., Billerica, MA.

²¹B. LeMar, Technical Assistance, Mini-Systems, Inc., North Attleboro, MA, private communication.

²²J. Beeman, private communication.

²³The contact pad on the NTD thermometer can be made with Al rather than Au. This requires the use of wire-bonding because of the heavy oxide on the Al, but it raises the eutectic point to 425°C. The commercial heaters from Mini Systems can be made with thin films of Ta rather than NiCr. The former are stable up to 425°C, as per Bob Le Mar of Mini Systems.

²⁴D. McCammon, M. Juda, J. Zhang, S. S. Holt, R. L. Kelley, S. H. Moseley and A. E. Szymkowiak, in Proceedings of the 18th International Conference on Low Temperature Physics, Kyoto, Japan, 1987 (Japn. J. Appl. Phys., Tokyo, 1987), Vol. 3, p. 2084. (Japn. J. Appl. Phys. 26 (1987) Suppl. 26-3)

²⁵D. McCammon, private communication.

6. Conclusions

We have further demonstrated the capabilities of the ac calorimetric technique for measuring the heat capacity of adsorbates. This technique is the only technique capable of measuring the heat capacity of adsorbates on evaporated metal films. We have made measurements of para- and normal-H₂ adsorbed on sapphire and evaporated gold substrates. For n-H₂ at a nominal coverage of 25 layers, a peak in the heat capacity is observed at approximately 1.6 K. The peak is due to an orientational ordering transition in a bulk-like phase of the adsorbed H₂. These are the first measurements of the heat capacity due to the orientational ordering of adsorbed H₂.

As the exposure is decreased, the orientational ordering peak is reduced in size and shifts below the minimum of our temperature range. At low exposure, the width of the peak as well as its shift in temperature as a function of exposure provide qualitative evidence for finite-size effects. At higher exposures, the broadening of the peak is dominated by the heterogeneity of the substrate.

Methods have been devised for baking the vacuum system in a manner compatible with the operation of the cold finger at liquid helium temperatures. As part of this effort, epoxy-based heat sinks and other components thought to be sources of excessive outgassing were replaced with new materials better suited to the requirements of ultra-high vacuum. These changes resulted in a major improvement in the background pressure in the chamber and a similarly dramatic improvement in reproducibility. These improvements represent a significant refinement of the ac calorimetric technique.

We have made a careful study of potential sources of heterogeneity in the metallic substrates used in ac calorimeters. Factors likely to contribute to heterogeneity have been identified. Methods for reducing and controlling these sources have been proposed. Prospects for achieving greater control over the preparation of the substrate and a higher level of homogeneity are excellent. Finally, efforts to extend the measurements to lower temperatures are currently in progress. These new measurements will provide a better understanding of the measurements made thus far, and they are expected to produce discoveries of new phenomena as well.

Appendix: Infrared Emission Spectroscopy of CO on Pt(111)

Abstract

We have studied the C=O stretch vibration of bridge-bonded CO on Pt(111) in the temperature range from 225 to 300 K. Our spectra are qualitatively different from those previously reported by Hayden and Bradshaw [Surface Sci. 125 (1983) 787] in that we do not observe the line near 1810 cm^{-1} that they attributed to three-fold bonded CO. We observe only a single line at 1849 cm^{-1} . As the coverage is increased beyond 0.5 monolayer, the linewidth decreases, reaching its minimum value near $\theta = 0.54$. Little change in the frequency or integrated intensity of the line is seen. These observations tend to support "fault line" models for the high coverage structure of CO on Pt(111). The minimum linewidth of the line is $11.5 \pm 0.6 \text{ cm}^{-1}$ for temperatures below 275 K, rising rapidly to $\sim 34 \text{ cm}^{-1}$ at 300 K. This temperature dependence cannot be explained by current models of homogeneous broadening. We attribute it to inhomogeneous broadening associated with an order-disorder transition in the overlayer.

A.1 Introduction

Carbon monoxide on Pt(111) is one of the most intensively studied chemisorption systems. Virtually the full arsenal of experimental techniques has been applied in order to understand its properties, including low energy electron diffraction (LEED),^{1, 2} thermal desorption spectroscopy (TDS),¹⁻⁵ ultraviolet photoelectron spectroscopy (UPS),⁶ and work function measurements.¹ The study of CO on Pt(111) with vibrational spectroscopies has been particularly extensive. There have been several studies using electron energy loss spectroscopy (EELS),^{2, 4, 7-9} as well as a large number of infrared studies, both on recrystallized ribbons¹⁰⁻¹⁴ and on single crystals.^{5, 15-17} Recently this system has also been investigated with inelastic helium scattering.¹⁸ With such a broad experimental background, one might expect that this chemisorption system would hold few surprises. Our infrared study of the C=O stretch vibration of bridge-bonded CO, however, demonstrates that qualitatively different results can be obtained in nominally identical experiments with different samples, for reasons that are not understood.

Electron energy loss spectra of CO on Pt(111) at high coverage consistently show two C=O stretch lines, at frequencies of ~ 1870 and 2110 cm^{-1} . The two lines have comparable intensities. The 2110 cm^{-1} line appears only for $\theta > 0.33$. At $\theta = 0.5$, a $c(4\times 2)$ overlayer is formed, which is believed to comprise equal numbers of bridge-bonded and terminally bonded molecules.^{4, 8, 9, 19}

The IR measurements have been less consistent. The line near 2110 cm^{-1} , attributed to terminal CO, is always observed. The 1870 cm^{-1} line, however, has been observed previously in only three studies,^{5, 14, 15} and only Hayden and Bradshaw⁵ were able to examine it in detail. They studied the line shape as a function of coverage and temperature between 85 and 300 K. Essentially the same behavior was observed for all coverages between 0.45 and 0.55. We will briefly summarize their results for a coverage of $\theta = 0.5$.

At 95 K, a single, rather sharp (13 cm^{-1} FWHM) line was found at 1857 cm^{-1} . As the temperature was increased, a second, broader line appeared, centered near 1810 cm^{-1} . By 300 K, the two features merged into a broad ($>50\text{ cm}^{-1}$ FWHM) line, within which the doublet structure was barely observable. Fig. 1a shows some representative spectra, from their paper. The 1857 cm^{-1} line was assigned to bridge-bonded (two-fold) CO. The 1810 cm^{-1} line was assigned to three-fold coordinated CO, and it was postulated that the energy barrier between the bridge and three-fold sites was low enough to permit thermally activated motion between the two sites. The thermally induced disorder observed with LEED between 250 and 300 K was attributed to the occupation of these three-fold sites.

A similar, though less pronounced doublet structure has been observed by Hayden et al., for CO on Cu(111).²⁰ It has been pointed out that the thermally activated motion between bridge and three-fold sites is equivalent to a dephasing process.^{21, 22} Dephasing has been found^{22, 23} to account for the temperature dependence of the linewidth for bridge-bonded CO on Ni(111) which is expected to be a similar system.

We have reexamined the $1750\text{--}1950\text{ cm}^{-1}$ spectral region, for CO on Pt(111), using infrared emission spectroscopy. Our findings are radically different from those of Hayden and Bradshaw. Throughout the temperature range from 225 to 300 K, we observe only a single symmetric line at 1849 cm^{-1} . We do not observe the line near 1810 cm^{-1} attributed by Hayden and Bradshaw to three-fold coordinated CO. We find that the linewidth of the

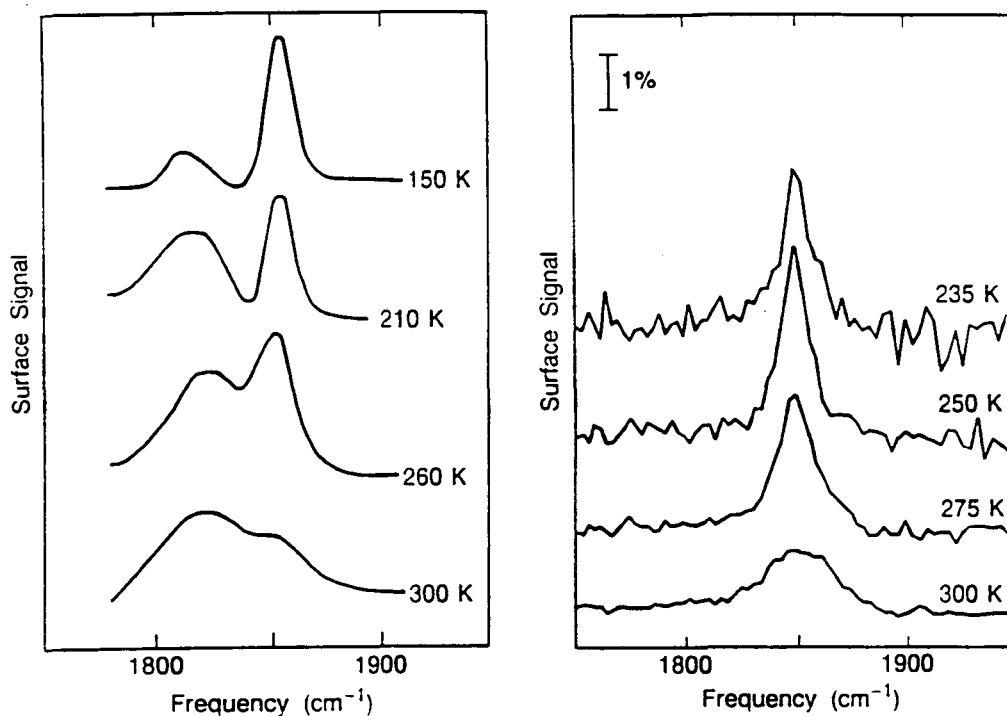


Figure 1 IR spectra of CO on Pt(111) at various temperatures, in the region of the C=O stretch vibration of bridge-bonded CO. (a) As measured by Hayden and Bradshaw.⁵ The line near 1810 cm⁻¹ was attributed to CO bonded in three-fold sites. (b) As measured in the present work. No line near 1810 cm⁻¹ is observed.

1849 cm^{-1} line reaches its minimum value at a coverage significantly above $\theta = 0.5$, where the $c(4 \times 2)$ overlayer is complete. The behavior of the line for $\theta > 0.5$ tends to support the "fault line" models of the high coverage structure of the overlayer. We have also examined the temperature dependence of the linewidth, and we conclude that it is due primarily to inhomogeneous broadening associated with increasing disorder in the overlayer at temperatures above ~ 275 K. The observed temperature dependence is not consistent with any proposed model of homogeneous line-broadening.

A.2 Experimental

The IR emission technique^{24, 25} and our methods of surface preparation and characterization¹⁷ have been fully described elsewhere. We refer the reader to these sources for details. The Pt(111) surface was oriented within 0.5° and contained less than 0.01 monolayer carbon, with no other impurities detectable with a commercial cylindrical mirror Auger spectrometer.

The emission technique relies on thermal radiation from the sample as the only IR source in the system. This method offers significant advantages over reflection-absorption spectroscopy,^{24, 25} but it is not well suited for measurements at low sample temperatures. At the frequencies and temperatures of interest in the present work, the emitted power decreases exponentially with decreasing temperature, according to the Planck law. For this reason, we were able to measure spectra only at temperatures > 225 K.

A.3 Results and discussion

A.3.1 Adsorption sites

Fig. 1b shows IR emission spectra for coverages near $\theta = 0.5$, and temperatures from 225 to 300 K. It is immediately apparent that our results are in qualitative disagreement with those of Hayden and Bradshaw, in that we do not observe the line near 1810 cm^{-1} , attributed to three-fold coordinated CO. Only a single, symmetric line at 1849 cm^{-1} , attributable to bridge-bonded CO, is detected. We have attempted to introduce surface defects by sputtering and have contaminated the surface deliberately with a few percent of a monolayer of carbon, without observing any signal near 1810

cm^{-1} . We have recently learned^{26, 27} that Bradshaw and co-workers have reexamined this spectral region, using the same Pt(111) sample as Hayden and Bradshaw, but a different spectrometer and cleaning procedure. They also find no line near 1810 cm^{-1} . Neither they, nor we, are able to offer an explanation for the discrepancy between these recent observations and the results reported by Hayden and Bradshaw. Evidently the adsorption behavior of CO is so strongly dependent on surface conditions that experiments on different, carefully prepared single crystal samples can show radically different results. It is worth noting in this context that Tobin and Richards¹⁷ found that the linewidth of the molecule-substrate vibration of terminal CO on Pt(111) was very strongly dependent on fine details of the surface condition.

Note added subsequent to publication: Chabal²⁸ has suggested that the line near 1810 cm^{-1} observed by Hayden and Bradshaw may be due to CO adsorbed in two-fold sites at or near steps. The absence of this line in the present work would then be attributed to a lower density of steps on the Pt(111) surface which we have used. Differences in step density can arise from differences in the miscut or the preparation (e.g., sputtering) of the crystal. As noted above, we have deliberately introduced defects through sputtering yet have not observed an increase in signal near 1810 cm^{-1} . The orientation of the Pt(111) crystal was within 0.5° in both the present work and that of Hayden and Bradshaw. This orientation corresponds to a surface with steps one lattice constant in height separated by flat terraces ≥ 100 lattice constants in width. If Chabal's proposal is correct, even this level of miscut can produce qualitative changes in the behavior of the adsorbed CO. Clearly, sample preparation and characterization of unusually high quality would be necessary to test this proposal.

A.3.2 Coverage dependence

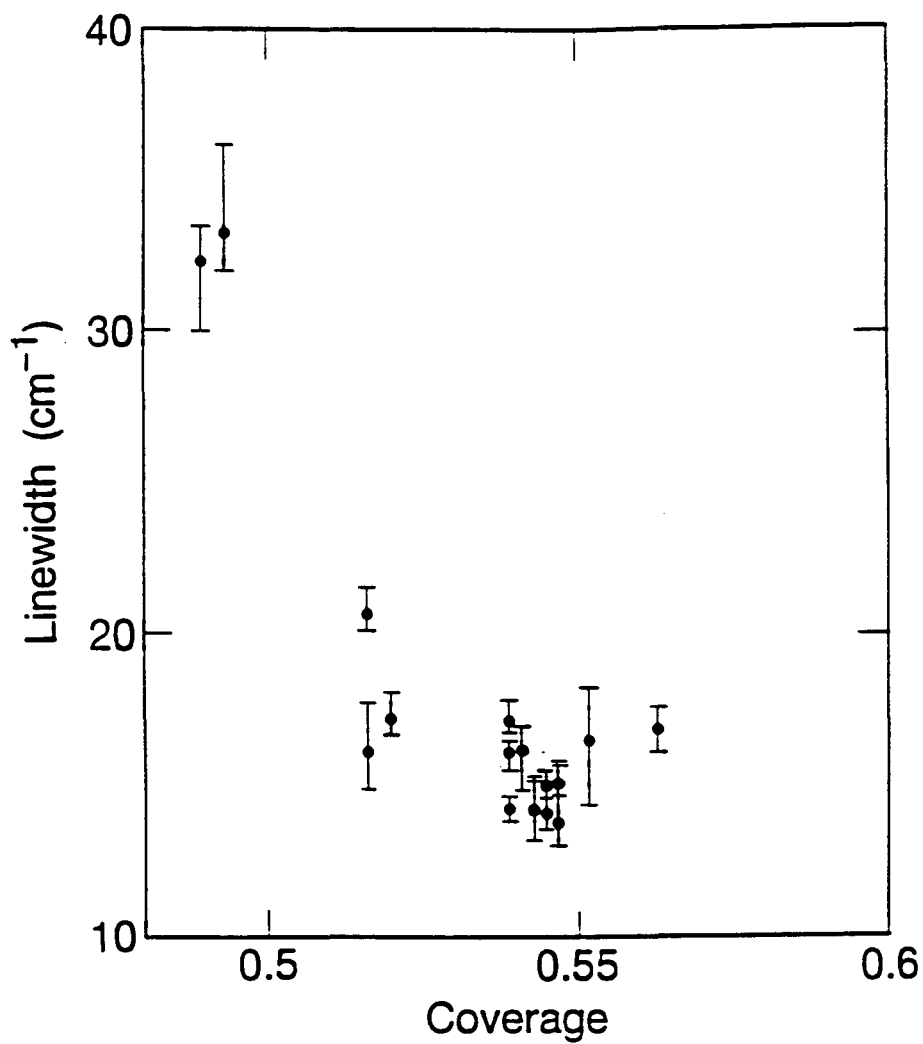
It is well known that adsorbate-adsorbate interactions can give rise to coverage-dependent inhomogeneous broadening.²⁹⁻³² It is therefore essential in a study of vibrational linewidths to control the coverage sufficiently carefully that such effects are minimized. In this section we present measurements of the linewidth of the 1849 cm^{-1} line as a function of coverage. These measurements are necessary to an understanding of the temperature dependence of the linewidth, which we will discuss in the next

section. They also have implications for the structure of the CO overlayer at high coverage.

In Fig. 2 we show the measured linewidth as a function of coverage, for adsorption in the temperature range between 235 and 250 K. The coverage was determined from the CO exposure by means of a calibration curve, which was based on integrated thermal desorption signals. The uncertainty in the absolute coverage is $\sim 10\%$. The calibration curve, and a detailed description of its measurement, have been given elsewhere.¹⁷

It is apparent from Fig. 2 that the minimum linewidth occurs at a coverage of $\theta = 0.54$, which is above the 0.5 monolayer coverage at which the best $c(4 \times 2)$ ordering occurs. This observation is not attributable to uncertainty in the coverage determination. If the LEED pattern is observed at the coverage corresponding to the minimum linewidth, significant elongation of the $(0 \frac{1}{2})$ spots is visible. Conversely, IR measurements at the coverage that gives the best $c(4 \times 2)$ LEED pattern show a significantly larger linewidth. Since it is usually assumed that inhomogeneous broadening will be minimal for a well ordered overlayer, it is surprising that in this case the minimum linewidth occurs at a higher coverage. This observation has implications for the structure of the overlayer at high coverages.

At high coverage, the equilibrium structure will be determined by a balance between interadsorbate repulsion, which favors a quasi-hexagonal structure, and the adsorbate-substrate interaction, which tends to localize the molecules on specific, high-symmetry sites. Two limiting cases have been proposed for the CO overlayer at high coverage ($\theta > 0.5$). The vibrational spectrum in the C=O stretching region can provide a means for distinguishing between the competing models, although it should be kept in mind that intermediate cases are possible. Several authors^{1, 2, 9} have described the structure in terms of a continuous uniaxial compression of the $c(4 \times 2)$ unit cell along the $[110]$ direction. In such a structure, the molecules occupy bridge sites, on-top sites, and many different sites along the line connecting the bridge and on-top sites.⁹ If there were no vibrational coupling between the molecules, and if the vibrational frequency increases monotonically in moving from bridge to on-top sites, one would expect a very broad vibrational spectrum stretching from 1850 cm^{-1} (the vibrational frequency of bridge-bonded CO) to 2100 cm^{-1} (the vibrational frequency of



XBL 868-8917

Figure 2 The linewidth of the bridge-bonded CO vibration as a function of coverage, for temperatures between 235 and 250 K. The minimum occurs at $\theta = 0.54$, which is significantly above the coverage that gives the sharpest $c(4 \times 2)$ LEED pattern.

on-top CO). Vibrational coupling, for example by dipole-dipole coupling, will tend to transfer intensity to the high frequency end of the spectrum, so a single strong line near 2100 cm^{-1} , possibly with a low-intensity tail to lower frequency, is expected. Such spectra are observed at high coverage for CO on Pd(100)³² and for CO on Ru(001).³¹ In both of these systems, it is believed that the CO molecules occupy the full range of possible adsorption sites, yet only a single line is observed in the IR spectrum, with no dramatic changes occurring at the onset of compression. In the case of CO on Pt(111), we would then expect the 1850 cm^{-1} line attributed to bridge-bonded CO to broaden, shift to higher frequency, and lose intensity as the coverage is increased, if the continuous compression model is correct. We do not observe any such dramatic changes in the coverage range studied (up to $\theta = 0.56$).

Avery⁷ and Biberian and Van Hove¹⁹ have proposed "fault line" models, in which all of the molecules remain on high symmetry sites, with high density antiphase boundaries separating locally $c(4\times 2)$ ordered regions. Such a model would predict well-defined lines near 1850 and 2100 cm^{-1} , possibly slightly broadened and/or shifted by dipole-dipole coupling in the high density domain boundaries. This prediction corresponds with our observation that the 1850 cm^{-1} line does not appreciably broaden, shift, or change in intensity as the coverage is increased above $\theta = 0.5$. Hayden and Bradshaw's measurements⁵ of the coverage dependence of the integrated intensities of the bridging and on-top vibrations also supported Avery's fault line model, in which the domain boundaries contain only on-top CO.

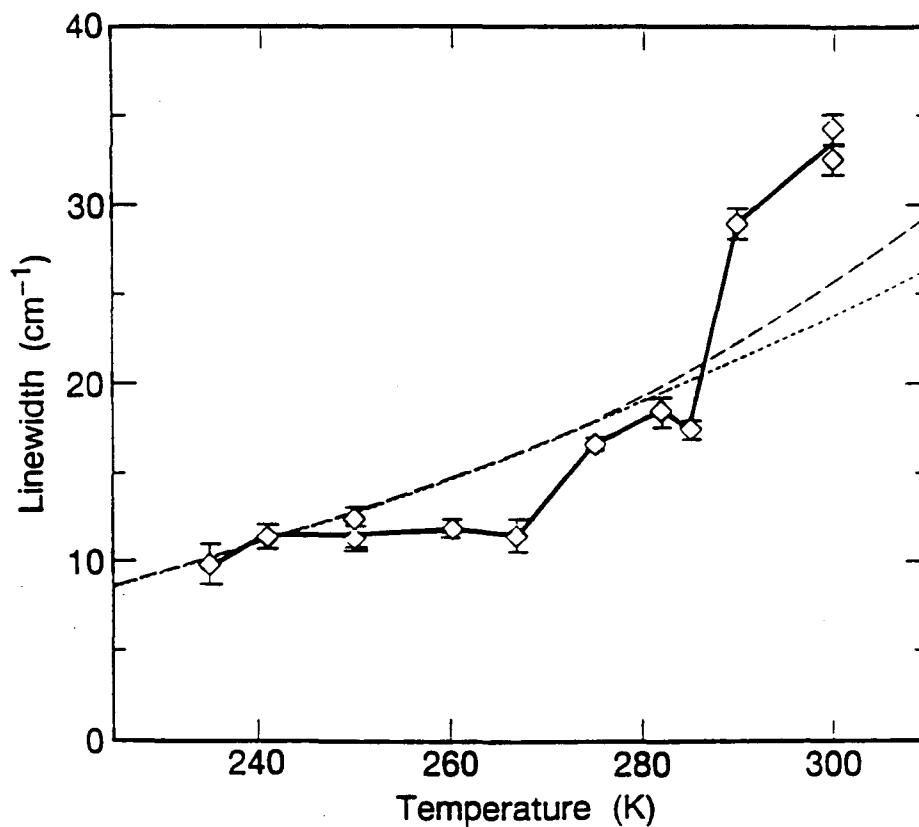
It appears that our vibrational spectra rule out a continuous distribution of adsorption sites, and are consistent with the predictions of fault line models. They do not prove, however, that the CO molecules all remain strictly localized on high symmetry sites. The possibility remains of a compressed structure in which molecules are shifted from high symmetry sites by interadsorbate repulsions, but excessive deviations from the preferred sites are prevented by adsorbate-substrate interactions. The resulting broad distribution of vibrational frequencies, with a gap separating "quasi-bridge-bonded" and "quasi-on-top" species, might not be reflected in the vibrational spectrum because of intensity transfer by dipole-dipole coupling, as mentioned above. More detailed line shape studies including the 2100 cm^{-1} line due to on-top CO and extending to higher coverages might clarify this issue.

A.3.3 Temperature dependence

It is apparent from Fig. 1b that the width of the 1849 cm^{-1} line is strongly temperature-dependent. Measurements of this temperature dependence are of interest because they can provide important clues to the nature of the line-broadening mechanism.^{21, 33} In Fig. 3 we present the linewidth of the 1849 cm^{-1} C=O stretch vibration as a function of temperature. In order to minimize the effects of inhomogeneous broadening, we varied the exposure at each temperature until the linewidth was observed to increase from its minimum value. The optimal exposure varied somewhat with temperature, from 3.5 L at 250 K to 5.0 L at 300 K. The difference is presumably due either to a lower sticking coefficient or to a higher rate of desorption at higher temperatures. The linewidths in Fig. 3 have been corrected for the spectrometer resolution of 7.8 cm^{-1} , which was determined from the angular width of the zero-order diffraction peak and confirmed by measurements of water vapor spectra.

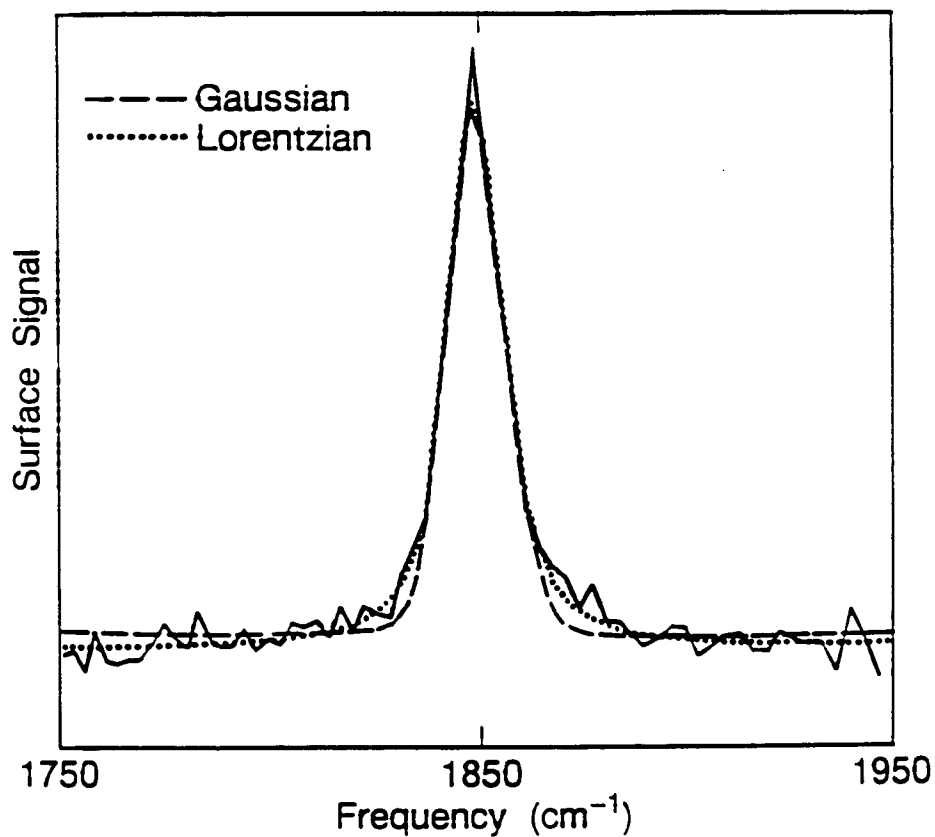
The linewidth seems to be constant at $11.5 \pm 0.6\text{ cm}^{-1}$ at temperatures below 275 K. This value may represent a homogeneous linewidth, caused, for example, by energy relaxation by the excitations of electron-hole pairs. However, it could also represent a residual, temperature-independent inhomogeneous contribution. We have attempted to distinguish these two mechanisms by analyzing the vibrational line shape. Fig. 4 shows the average of four spectra measured at 250 K. The dashed and dotted lines represent best-fit Gaussian and Lorentzian functions, respectively, convolved with the measured instrumental response function. The observed line clearly fits the Lorentzian line shape more closely. This fact suggests that the line is homogeneously broadened. However, there is substantial noise in the spectrum, and the line shape expected for inhomogeneous broadening is not known; there is no strong reason to expect a Gaussian shape.³³ Any conclusion regarding the broadening mechanism must therefore be regarded as very tentative.

At temperatures above 275 K, the linewidth increases sharply, reaching $\sim 34\text{ cm}^{-1}$ at 300 K. We will show below that this increase is largely reversible and cannot be explained by any proposed model of homogeneous broadening. We attribute it to inhomogeneous broadening associated with the reversible order-disorder transition in the $c(4 \times 2)$ overlayer described by Ertl et al.¹ This



XBL 868-8920

Figure 3 The linewidth of the bridge-bonded CO vibration as a function of temperature. The dotted line represents the best fit to a model of dephasing by interaction with other vibrational modes. The dashed line represents the best fit to a model of dephasing by interaction with electron-hole pairs. Neither model adequately fits the data.



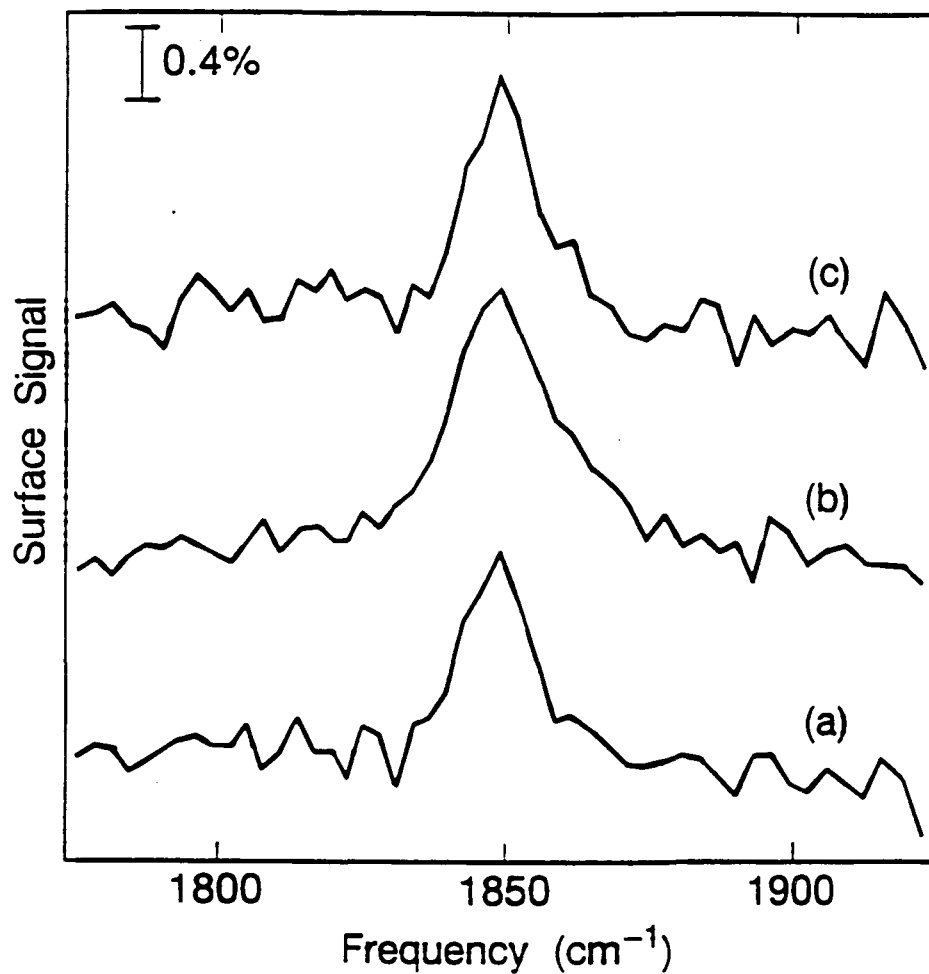
XBL 8611-9036

Figure 4 Line shape analysis of the bridge-bonded CO vibration at 250 K. The solid line represents the average of four separate spectra. The dashed line represents the best fit obtained with a Gaussian function convolved with the measured instrumental response function. The dotted line represents the best fit obtained with a Lorentzian function similarly convolved. The data fit the Lorentzian function more closely.

transition occurs in the temperature range between 275 and 300 K, and is clearly observable with LEED. Our attempts to fit the high-temperature line shapes with Gaussian and Lorentzian functions were inconclusive.

Because of the possibility of desorption, and the strong dependence of the linewidth on coverage, it was necessary to investigate the possibility that the apparent temperature dependence of the linewidth is actually due to coverage variations. The experiment summarized in Fig. 5 rules out such an effect, for temperatures < 281 K. The sample was dosed with 3.5 L CO at 241 K to give a linewidth of $14.1 \pm 0.6 \text{ cm}^{-1}$, as shown in curve a. It was then heated to 281 K, and the spectrum shown as curve b was measured at that temperature, giving a linewidth of $20.2 \pm 1.5 \text{ cm}^{-1}$. Finally, the sample was again cooled to 241 K, and the spectrum shown in curve c was measured. The linewidth was $13.2 \pm 1.1 \text{ cm}^{-1}$, essentially unchanged from its original value. When a similar experiment was performed with sample temperatures of 250 and 300 K, effects due to desorption were observed in addition to reversible temperature-dependent line-broadening. After the sample had been held at 300 K for 30 min, the linewidth at 250 K was 20.3 cm^{-1} – smaller than the 35 cm^{-1} linewidths typically observed at 300 K, but significantly larger than the 14.2 cm^{-1} linewidth measured at 250 K before the sample was heated. After the addition of another 1.0 L at 250 K, the linewidth narrowed again to 14.2 cm^{-1} . It is clear from these measurements that most of the temperature-dependent broadening shown in Fig. 2 is reversible, although desorption becomes significant at the highest temperatures studied ($\sim 300 \text{ K}$).

Three *homogeneous* line-broadening mechanisms have been proposed that are predicted to show a strong temperature dependence:^{21, 33} energy relaxation by multiphonon excitation, dephasing by interaction with molecular or lattice vibrations, and dephasing by interaction with electron-hole pairs. None of the available models for these processes provides an explanation for our data. The multiphonon process should be negligible for the C=O stretch mode, which has a frequency more than nine times the maximum Pt phonon frequency.³⁴ The dephasing process, however, might be expected to be important. As we mentioned above, the linewidth of the C=O stretch vibration of bridge-bonded CO on Ni(111) has been attributed to dephasing by interaction with another molecular vibration.^{22, 23} This process is characterized by an approximately exponential temperature dependence. It has also been suggested that dephasing by electron-hole pairs, which is



XBL 868-8918

Figure 5 Spectra showing the reversibility of the temperature-dependent line-broadening. (a) Spectrum of 3.5 L CO ($\theta = 0.54$) at 241 K. (b) Spectrum measured at 281 K after dosing at 241 K. (c) Spectrum measured after cooling sample back to 241 K.

characterized by a T^4 dependence, could explain the data for CO on Ni(111).³⁵ The linewidth of the C=O stretch mode of terminally bonded CO on Ru(100) has also been attributed to vibrational dephasing.³⁶

In the present case of bridge bonded CO on Pt(111), the observed temperature dependence is inconsistent with the proposed dephasing models. The dephasing model of Persson and co-workers^{22, 36} predicts the variation of both linewidth and the vibrational frequency with temperature. Within the experimental error of approximately $\pm 1 \text{ cm}^{-1}$, we observe no change in the vibrational frequency over the temperature range studied. The dotted line in Fig. 3 represents the best fit of this model to our linewidth data, subject to our experimental limit on the frequency shift. The essentially exponential dependence predicted by the model is clearly incapable of fitting the abrupt change in the linewidth that we observe. The T^4 dependence predicted electron-hole pair dephasing³⁵ is equally unsuccessful in fitting the data; the best fit is shown as the dashed line. A temperature-independent contribution to the linewidth was included in both models, but in each case the best fit was achieved when the value of that contribution was zero. It is possible that more complicated dephasing models – including coupling to more than one vibrational mode, for example, or incorporating a more realistic model of the coupling to the metal electrons – could fit the observed temperature dependence. In the absence of a well-justified basis for assuming some such many-parameter model, however, and in view of the observed order-disorder transition, it is more judicious to conclude that the observed broadening is inhomogeneous.

A.4 Summary

In summary, we have studied the C=O stretch vibration of bridge-bonded CO on Pt(111) in the temperature range from 225 to 300 K. We find that the minimum linewidth occurs for a coverage > 0.5 monolayer. The behavior of the line at coverages > 0.5 tends to support "fault line" models of the high coverage structure. Our spectra are *qualitatively* different from those of Hayden and Bradshaw⁵ in that we observe no line near 1810 cm^{-1} . We observe a single line at 1849 cm^{-1} . The width of the line at the optimal coverage is $11.5 \pm 0.6 \text{ cm}^{-1}$ for temperatures below 275 K, rising rapidly to $\sim 34 \text{ cm}^{-1}$ at 300 K. This temperature dependence cannot be explained by current models of homogeneous broadening. We attribute it to inhomogeneous

broadening associated with an order-disorder transition in the overlayer. We are not able to determine conclusively whether the temperature-independent linewidth at temperatures < 275 K is homogeneous or inhomogeneous, although examination of the line shape tends to favor a homogeneous broadening mechanism.

References

- ¹G. Ertl, M. Neumann and K. M. Streit, *Surface Sci.* **64**, 393 (1977).
- ²H. Steininger, S. Lehwald and H. Ibach, *Surface Sci.* **123**, 264 (1982).
- ³D. M. Collins and W. E. Spicer, *Surface Sci.* **69**, 85 (1977).
- ⁴H. Hopster and H. Ibach, *Surface Sci.* **77**, 109 (1978).
- ⁵B. E. Hayden and A. M. Bradshaw, *Surface Sci.* **125**, 787 (1983).
- ⁶D. M. Collins and W. E. Spicer, *Surface Sci.* **69**, 114 (1977).
- ⁷N. R. Avery, *J. Chem. Phys.* **74**, 4202 (1981).
- ⁸H. Froitzheim, H. Hopster, H. Ibach and S. Lehwald, *Appl. Phys.* **13**, 147 (1977).
- ⁹A. M. Baro and H. Ibach, *J. Chem. Phys.* **71**, 4812 (1979).
- ¹⁰R. A. Shigeishi and D. A. King, *Surface Sci.* **58**, 379 (1976).
- ¹¹A. Crossley and D. A. King, *Surface Sci.* **68**, 528 (1977).
- ¹²R. A. Shigeishi and D. A. King, *Surface Sci.* **75**, L397 (1978).
- ¹³A. Crossley and D. A. King, *Surface Sci.* **95**, 131 (1980).
- ¹⁴M. D. Baker and M. A. Chesters, in *Vibrations at Surfaces*, edited by R. Caudana, J.-M. Gilles and A. A. Lucas (Plenum, New York, 1982), p. 289.
- ¹⁵H.-J. Krebs and H. Lüth, *Appl. Phys.* **14**, 337 (1977).
- ¹⁶K. Horn and J. Pritchard, *J. Phys. (Paris)* **38**, C4 (1977).
- ¹⁷R. G. Tobin and P. L. Richards, *Surface Sci.* **179**, 387 (1987).
- ¹⁸A. M. Lahee, J. P. Toennies and C. Woll, *Surface Sci.* **177**, 371 (1986).
- ¹⁹J. P. Biberian and M. A. V. Hove, *Surface Sci.* **138**, 361 (1984).

- ²⁰B. E. Hayden, K. Kretzschmar and A. M. Bradshaw, *Surface Sci.* **155**, 553 (1985).
- ²¹J. W. Gadzuk and A. C. Luntz, *Surface Sci.* **144**, 429 (1984).
- ²²B. N. J. Persson and R. Ryberg, *Phys. Rev. Lett.* **54**, 2119 (1985).
- ²³M. Trenary, K. J. Uram, F. Bozso and J. T. Yates, *Surface Sci.* **146**, 269 (1984).
- ²⁴S. Chiang, R. G. Tobin and P. L. Richards, *J. Vac. Sci. Tech. A* **2**, 1069 (1984).
- ²⁵P. L. Richards and R. G. Tobin, in Vibrational Spectroscopy of Molecules on Surfaces, edited by J. T. Yates, Jr. and T. E. Madey (Plenum, New York, 1987), p. 417.
- ²⁶A. M. Bradshaw, private communication.
- ²⁷M. Tüshaus, E. Schweizer, P. Hollins and A. M. Bradshaw, *J. El. Spec. Rel. Phen.* **44**, 305 (1987).
- ²⁸Y. J. Chabal, *Surface Sci. Reports* **8**, 211 (1988).
- ²⁹B. N. J. Persson and R. Ryberg, *Phys. Rev. B* **24**, 6954 (1981).
- ³⁰R. G. Tobin, S. Chiang, P. A. Thiel and P. L. Richards, *Surface Sci.* **140**, 393 (1984).
- ³¹H. Pfnür, D. Menzel, F. M. Hoffmann, A. Ortega and A. M. Bradshaw, *Surface Sci.* **93**, 431 (1980).
- ³²A. Ortega, F. M. Hoffmann and A. M. Bradshaw, *Surface Sci.* **119**, 79 (1982).
- ³³R. G. Tobin, *Surface Sci.* **183**, 226 (1987).
- ³⁴R. Ohrlich and W. Drexel, in Proc. Symposium on Neutron Inelastic Scattering, Copenhagen, Vol. 1, edited by (International Atomic Energy Agency, Vienna, 1968), p. 203.
- ³⁵H. Morawitz, *Phys. Rev. Lett.* **58**, 2778 (1987).
- ³⁶B. N. J. Persson, F. M. Hoffmann and R. Ryberg, *Phys. Rev. B* **34**, 2266 (1986).

LAWRENCE BERKELEY LABORATORY
UNIVERSITY OF CALIFORNIA
TECHNICAL INFORMATION DEPARTMENT
BERKELEY, CALIFORNIA 94720